UC Berkeley
UC Berkeley Electronic Theses and Dissertations

Title
Nonlinear optical studies of aqueous interfaces, polymers, and nanowires

Permalink
https://escholarship.org/uc/item/78c5g5t8

Author
Onorato, Robert Michael

Publication Date
2010

Peer reviewed|Thesis/dissertation

eScholarship.org Powered by the California Digital Library
University of California

Nonlinear optical studies of aqueous interfaces, polymers, and nanowires

by

Robert Michael Onorato

A dissertation submitted in partial satisfaction of the

requirements for the degree of

Doctor of Philosophy

in

Chemistry

in the

Graduate Division

of the

University of California, Berkeley

Committee in charge:

Professor Richard J. Saykally, Chair
Professor Ronald C. Cohen
Professor Michael Manga

Spring 2010

Nonlinear optical studies of aqueous interfaces, polymers, and nanowires

© 2010

by Robert Michael Onorato

Abstract

Probing aqueous interfaces via UV second harmonic generation

by

Robert Michael Onorato

Doctor of Philosophy in Chemistry

University of California, Berkeley

Professor Richard J. Saykally, Chair

Understanding the structure and composition of aqueous interfaces is one of the most important current problems in modern science. Aqueous interfaces are ubiquitous in Nature, ranging from aerosols to cellular structures. Aerosol chemistry is presently the most significant unknown factor in predicting climate change, and an understanding of the chemistry that occurs at aerosol interfaces would significantly improve climate models. Similarly, the nature of aqueous biological interfaces has a profound effect on the structure and function of proteins and other biological structures. Despite the importance of these problems, aqueous interfaces remain incompletely understood due to the challenges of experimentally probing them.

Recent experimental and theoretical results have firmly established the existence of enhanced concentrations of selected ions at the air/water interface. In this dissertation, I use an interface-specific technique, UV second harmonic generation (SHG), to further investigate the adsorption of ions to the air/water interface and to extend the study of ion adsorption towards more biologically relevant systems, alcohol/water interfaces.

In Chapter 2, I describe resonant UV-SHG studies of the strongly chaotropic thiocyanate ion adsorbed to the interface formed by water and a monolayer of dodecanol, wherein the Gibbs free energy of adsorption was determined to be -6.7 ± 1.1 and -6.3 ± 1.8 kJ/mol for sodium and potassium thiocyanate, respectively, coincident with the value determined for thiocyanate at the air/water interface. Interestingly, at concentrations near and above 4 M, the resonant SHG signal increases discontinuously, indicating a structural change in the interfacial region.

Recent experimental and theoretical work has demonstrated that the adsorption of bromide is particularly important for chemical reactions on atmospheric aerosols, including the depletion of ozone. In Chapter 3, UV-SHG resonant with the bromide charge-transfer-to-solvent band and a Langmuir adsorption model are used to determine the affinity of bromide for both the air/water and dodecanol/water interfaces in the molar concentration regime. The Gibbs free energy of adsorption for the former is determined to be -1.4 kJ/mol with a lower 90% confidence limit of -4.1 kJ/mol. For the dodecanol/water interface the data are best fit with a Gibbs free energy of +8 kJ/mol with an estimated a lower limit of -4 kJ/mol.

Adsorption of ions to the air/water interface in the millimolar regime is a particularly interesting phenomenon. In Chapter 4, the affinity of sodium chloride and sodium bromide to the air/water interface is probed by UV-SHG. Both salts exhibit a strong adsorption, with free energies greater than -20 kJ/mol. Interestingly, sodium chloride exhibits a stronger affinity for the interface than does sodium iodide, which was previously studied by Poul Peterson. This is counter to both experimental and theoretical results for higher concentrations. It has been predicted that ion adsorption is dictated by strong and opposing electrostatic and entropic forces. The change in order of ion interfacial affinity can be explained by relatively small changes in these forces at different concentrations and ionic strengths.

In Chapters 5 and 6, other work using nonlinear optical techniques is described. Coherent anti-Stokes Raman scattering microscopy is a promising tool for chemically selective imaging based on molecular vibrations. While CARS is currently used as a biological imaging tool, many variations are still being developed, perhaps the most important being multiplex CARS microscopy. Multiplex CARS has the advantage of comparing images based on different molecular vibrations without changing the excitation wavelengths. In Chapter 5, I demonstrate both high spectral and spatial resolution multiplex CARS imaging of polymer films using a simple scheme for chirped CARS with a spectral bandwidth of 300 cm^{-1}.

In Chapter 6, the nonlinear optical properties of $KNbO_3$ nanowires are studied. Using SHG and sum frequency generation, efficient nonlinear optical frequency conversion is demonstrated in single $KNbO_3$ nanowires that act as optical waveguides, yielding a coherent tunable subwavelength light source.

For Madeline

Table of Contents

Chapter 1: Introduction

1.1 Salts and the aqueous interface……1
1.2 Nonlinear optical spectroscopy……4

Chapter 2: Adsorption of thiocyanate ions to the dodecanol/water interface characterized by UV second harmonic generation

2.1 Introduction……... 12
2.2 Experimental methods……... 13
2.3 SHG and the Langmuir adsorption model……13
2.4 Dodecanol/water structure……14
2.5 Results and discussion……... 15
2.6 Conclusions……... 20

Chapter 3: Measurement of bromide ion affinities for the air/water and dodecanol/water interfaces at molar concentrations by UV-SHG spectroscopy

3.1 Introduction……... 25
3.2 Experimental methods……... 26
3.3 The air/water interface……...27
3.4 The dodecanol/water interface……...30
3.5 Conclusions……... 33

Chapter 4: Halides strongly adsorb to the air/water interface of millimolar aqueous solutions

4.1 Introduction……... 38
4.2 Experimental methods……... 38
4.3 A Langmuir adsorption model……...39
4.4 Results and discussion……... 39
4.5 Conclusions……... 42
4.6 Future SHG work……...43

Chapter 5: Chirped-CARS microscopy

5.1 The CARS technique ……... 49
5.2 Chirped-CARS……...51
5.3 Experimental methods……... 54
5.4 Results and discussion……... 55

Chapter 6: Nonlinear optical studies of $KNbO_3$ nanowires

6.1 Introduction……... 67
6.2 Experimental design……... 67
6.3 Results……... 67
6.4 Future outlook……... 70

Acknowledgements

First and foremost, I would like to thank Rich. His infectious enthusiasm for science and the freedom that he granted me to pursue my own path were exactly what I wanted from an advisor. One of Rich's greatest traits is that he continually has new ideas; evaluating these ideas and choosing which ones to pursue has been an excellent learning experience.

Next I would like to thank the Saykally group, especially the members of the "femto lab." Kelly, Poul, Paul, and Abigail were the ones who first welcomed me to the group, and have since moved on. I especially appreciate Kelly with whom I worked closely for his help and friendship. Along the way I have worked with Naoki, Soo-Chang, and Neil. It was a learning experience to see Neil dissect physical problems. Dale and Greg continue on at Berkeley. Sharing ideas, frustrations, and every so often progress with Dale has been integral to my work and success since moving to the SHG project. I would also like to thank Yuri for the collaboration on our nanowire work.

Finally, I would like to thank my family for providing me with the opportunities that led me to Berkeley. My parents did everything I could of asked in raising me to be successful, and I cannot thank them enough. Madeline has provided endless support and has lived with me through the ups and downs of my graduate career.

The work presented here was supported by the National Science Foundation, NASA, the Industrial Technology Research Institute, and the College of Chemistry.

Chapter 1

Introduction

1.1 Salts and the aqueous interface

Water covers more than 70 percent of the Earth's surface and comprises more than 60 percent of the human body. Water is not only ubiquitous, but it exhibits many interesting properties due to its unusual hydrogen bonding structure.[1] As a result, water has been the subject of particularly intense scientific study. Not only is the physical nature of water important, but understanding the behavior of aqueous solutions and more specifically the interfaces formed by aqueous solutions is essential to both atmospheric chemistry and biology, as well as the energy sciences and electrochemistry. The ocean surface covers an area greater than 10^{14} square meters, and the structure and composition of this enormous interface, in addition to the interfaces formed by water aerosol in the atmosphere, govern much of the Earth's chemistry. The transport of ions through biological interfaces regulates vital bodily functions, while the interaction of ions with proteins modulates their structure and function.

It was previously conventional wisdom that inorganic ions were generally repelled from the air/water interface. Onsager and Samaras[2] used the method of images,[3] modeling ions as point charges and the interface as a discontinuous intersection of two continuous dielectrics, to describe the "image force" repelling ions from the air/water interface. Their conclusion was supported by surface tension measurements, wherein the water surface tension increased with salt concentration, indicating that ions were, indeed, repelled from the interface.[4-8] In opposition to this general picture that ions are repelled from the air/water interface, Jones and Ray found a minimum in the surface tension for 13 inorganic salts near 1 mM concentrations.[9-13]

Recently, experiments motivated by atmospheric chemistry have forced a reevaluation of ion adsorption to the air/water interface. Hu et al.[14] found that the uptake of molecular chlorine and bromine by aqueous sodium chloride and bromide solutions could not be explained without the presence of interfacial chloride and bromide ions. Work by Finlayson-Pitts et al.[15-17] further emphasized the potential importance of the interfacial chemistry of chloride and bromide salts as well as nitrate and sulfate salts to atmospheric reactions. Bromide, for example, reacts with ozone forming molecular bromine and leading to ozone depletion.[17] An enhanced surface bromide concentration may be part of an explanation for the strong correlation of ozone with molecular bromine in the arctic[18-20] and at mid-latitudes.[21-26] Meanwhile, theoretical studies of water clusters containing halides predicted that ions are preferentially solvated at the surface of large water clusters,[27, 28] and vibrational spectroscopy of small clusters ($n \leq 3$) indicated that the balance of ion solvation and hydrogen bond formation shifts towards hydrogen bonds for the larger halides.[29-31]

These studies ignited experimental efforts to confirm the presence of inorganic ions at the air/water interface and to quantify their relative affinities. Two studies were published in quick succession, using vibrational sum frequency generation (VSFG), a second-order nonlinear process that is inherently surface specific, as an indirect probe of the surface structure of aqueous solutions of fluoride, chloride, bromide, and iodide in the molar concentration regime by measuring their effects on the OH stretching vibrations of water.[32, 33] The reported spectra of these halide solutions are similar. Liu et al. concluded that bromide and iodide exhibit enhanced concentration at the surface relative to the bulk,[32] while Raymond et al. interpreted their results as indicating fluoride to be a "structure maker" and chloride, bromide, and iodide to be "structure

breakers."[33] Second harmonic generation (SHG), another surface sensitive second-order nonlinear process, was used by Petersen et al. to demonstrate the surface enhancement of iodide in the millimolar concentration range[34] and azide in the molar concentration regime.[35] Depth profiling via x-ray photoelectron spectroscopy also confirmed a relative concentration enhancement of bromide and iodide in the interface.[36] These initial experimental results were further supported by theoretical work. Dang et al. reported preferential adsorption of iodide to the liquid/vapor interface using both polarizable and non-polarizable models.[37] Meanwhile, molecular dynamics (MD) simulations by Jungwirth and Tobias indicated that the surface affinity of halides correlated with the ion polarizability.[38]

Experimental efforts have continued to further quantify the nature ion adsorption to the air/water interface. Surface tension measurements analyzed with a single-ion partitioning model determined coefficients of relative adsorption affinity.[39, 40] Electrospray ionization mass spectrometry results corroborated these relative affinities.[41] For example, the surface tension and electrospray ionization results both found the following sequence of ion interfacial affinity: SCN^- > I^- > NO_3^- > Br^-. There have been a number of recent resonant SHG studies to directly probe ions at the interface via their charge-transfer-to-solvent (CTTS) transitions, which lie deep in the ultraviolet. The concentration of ferrocyanide is enhanced relative to the bulk at low concentrations.[42] The presence of the halides,[43, 44] nitrate,[45] and thiocyanide[46] were also confirmed at the interface using SHG. For the first time, VSFG was used to directly probe an anion at the interface, using the thiocyanide C≡N stretching mode.[47, 48] XPS measurements addressed an atmospherically relevant system, a mixed solution of bromide and chloride, demonstrating that bromide is strongly enhanced at the interface relative to chloride.[49] A recent MD simulation by Noah-Vanhoucke and Geissler allowed the interfacial surface to deform.[50] They found that this adjustment made a significant change to the driving forces of ion interfacial adsorption, However, they find it difficult to make quantitative predictions because the large and opposing electrostatic and entropic forces nearly cancel at the interface, making any energetic gain at the interface relatively small and uncertain. While a full explanation is still being developed, it is now clear that many inorganic ions are not only *present* at the air/water interface, but that some are *preferentially adsorbed*.

Another dimension of the developing description of aqueous interfaces is whether the pH of the pure water interface is basic or acidic. This has been a hotly debated and divisive topic, as is clear from the recent comment[51] and response[52] to a review of the topic,[53] which were closely accompanied by articles titled simply *Water surface is acidic*[54] and *The surface of neat water is basic*.[55]

Much of the experimental evidence for a basic interface is from macroscopic colloid and bubble experiments. In an emulsion of oil in water, hydroxide must be added in order to maintain a constant pH.[56] This indicates that hydroxide is adsorbed to the oil droplet interface, requiring the addition of base to maintain the pH of the aqueous bulk. Bubbles and oil droplets in water respond as though they are negatively charged in an electric field, leading to the conclusion that hydroxide is adsorbed.[57-59] Using similar methodology, an isoelectric point near pH 4 has been determined.[60] In an attempt to justify these findings, Gray-Weale and Beattie argue that hydroxide suppresses correlations between water molecules, wherein the energetic cost can be minimized when hydroxide resides at the interface.[61]

In contrast to these findings, simulations and experiments probing the microscopic nature of the water surface have predicted an enhanced concentration of hydronium, but not hydroxide, at the interface. One model treats hydronium as a "defect" in the water structure because it has

three hydrogen bond donating sites and only one acceptor site.[62] It is therefore preferable for hydronium to adsorb to the interface where it will not disrupt the hydrogen bond network as strongly. Using SHG, Petersen and Saykally concluded that hydronium is present at the interface by noting an increased concentration enhancement of iodide for hydroiodic acid in comparison to sodium iodide in the molar bulk concentration regime.[46] Here, the electro-neutrality of the interface was invoked to explain that an increase in iodide is due to adsorption of hydronium, whereas the sodium ion is not strongly adsorbed to the interface. They also ruled out a strong hydroxide adsorption at molar bulk concentrations using SHG.[63] In a collaborative work, molecular dynamics simulations predicted surface concentration enhancement of hydronium and depletion of hydroxide, while VSFG of the –OH stretching region indicated the presence of hydronium at the interface.[64] Another VSFG study also demonstrated the strong effects of hydronium at the surface, while the effects of hydroxide were much weaker.[65] More recent phase-sensitive VSFG studies have confirmed the presence of hydronium at the interface, but also indicate adsorption of hydroxide.[66, 67] Recently, using photoelectron spectroscopy, the surface concentration of hydroxide was determined to increase linearly with bulk sodium hydroxide concentration, while molecular dynamics simulations of various concentrations of sodium hydroxide all exhibited surface depletion of hydroxide.[68]

This increased focus on interfacial chemistry has also served to fuel renewed investigations of Hofmeister effects. In 1888, Hofmeister ordered a series of salts by how effectively they solubilized egg whites.[69] Similar sequences appear regarding effects on other properties, such as surface tension, hydrocarbon solubility, and protein stability across various fields from biochemistry to colloid chemistry.[70-72] For some time it was commonly thought that Hofmeister effects were caused by the degree of order induced by the added ions on the water structure. Recent work has debunked this idea. Omta et al. used femtosecond pump-probe spectroscopy to demonstrate that the orientational correlation time of water is not changed in the presence of salt beyond the first solvation shell.[73] Cappa et al. used x-ray absorption spectroscopy of halides to similarly demonstrate that the hydrogen bond network is not significantly affected beyond the first solvation shell.[4] Raman spectroscopy in combination with Monte Carlo simulations demonstrated that the change in Raman spectrum with the addition of halide salts to water is due to the electric field of the ions altering the spectral features and not due to the structure of water becoming more or less ordered.[74] In light of these and other studies,[75] the focus of work on the Hofmeister series has shifted towards understanding the interactions of specific ions with macromolecular interfaces and with other hydrated charge sites, such as protein backbones.

A comparison of iodide adsorption to an air/butanol/water interface[76] was made to previous results at the air/water interface,[36] finding that the observed surface concentration enhancement of iodide is suppressed. Ion adsorption to a macromolecular layer on water, including both hydrophobic and hydrophilic moieties, was studied by VSFG, indicating a Hofmeister-like series of ion adsorption affinity. Ninham et al. have incorporated polarizability of the ions in the description of ions into a theoretical model based on electrical double-layer van der Waals forces,[77, 78] and have predicted ion specific adsorption to micelles[79], among other specific-ion effects.[80-82] Jungwirth et al. have also made important contributions to the modeling of Hofmeister effects.[83-86, 53, 87] Notably, they have predicted different locations and mechanisms of adsorption for fluoride and iodide to a hydrophobic sphere with point charges on its surface[85] and found that ion adsorption to proteins leads to increased protein-protein interactions.[84] Ion adsorption to hydrophobic regions of macromolecules is similar to the adsorption of ions to the

air/water interface, and the study of these interfaces has accordingly been converging into one effort.

Much progress has recently been made in understanding the adsorption of ions to aqueous interfaces, but significant work remains, including the development of a complete description of the mechanism. As Wolfgang Pauli put it, "God made the bulk; surfaces were invented by the Devil."

1.2 Nonlinear optical spectroscopy

The interaction of light with matter changes the instantaneous polarization of the material. In the case of linear spectroscopy, this change has a direct dependence on the electric field of the light. Nonlinear optics utilizes the smaller but sometimes significant response of the material that depends on higher orders of the electric field. The polarization of a material $P(t)$ can be expanded as a power series:

$$P(t) = P^{(1)}(t) + P^{(2)}(t) + P^{(3)}(t) + ... \qquad [1]$$

Here $P^{(1)}(t)$ is the first-order polarization, $P^{(2)}(t)$ is the second-order polarization, etc. The polarization can be rewritten as the product of a molecular response constant, $\chi^{(n)}$, and the dependence on the electric field:

$$P(t) = \chi^{(1)}E(t) + \chi^{(2)}E^2(t) + \chi^{(3)}E^3(t) + ... \qquad [2]$$

$\chi^{(2)}$ is called the second-order nonlinear susceptibility, and generally involves three electric fields. The polarization of three electric fields involved in second order processes are commonly labeled as i, for photons at the frequency of the material response, j and k, for the incident photons. The response of the material can be different for each polarization combination, and therefore $\chi^{(2)}_{ijk}$ is a 27 element tensor. Due to the dependence on higher orders of the electric field, work utilizing the nonlinear optical response is generally performed with lasers of high peak electric field. Pulsed lasers are, therefore, a natural choice of light source.

Second-order nonlinear processes most generally result from the interaction of two input photons with frequencies, ω_1 and ω_2. The second-order response of the material occurs at either the sum of the frequency of these two photons, $\omega_3 = \omega_1 + \omega_2$, or the difference of the frequency, $\omega_3 = |\omega_1 - \omega_2|$. These two processes are commonly called sum frequency generation and difference frequency generation. A variation on sum frequency is second harmonic generation, where the frequencies ω_1 and ω_2 are degenerate.

Nonlinear processes can be resonantly enhanced when the frequency of one photon or the sum the two photon frequencies are close to an electronic or molecular transition frequency. In the case of sum frequency, one frequency is often tuned to a vibrational stretching mode of the material being probed,

$$\chi^{(2)}_{SFG} \propto \frac{1}{\omega_M - \omega_{IR} - i\Gamma_M}. \qquad [3]$$

Here ω_M is the molecular frequency, in this case of a vibrational motion, and ω_{IR} is the frequency of one of the photons. Γ_M is the lifetime of the molecular vibration. It is clear that the denominator will become small and the molecular response will be large when ω_M and ω_{IR} are similar. Further details about nonlinear optical interactions can be found in the texts of Shen, Boyd, and Mukamel.[88-90]

Second-order nonlinear techniques are ideally suited to the study of interfaces because they are sensitive to broken inversion symmetry. In the case of centro-symmetric media, there is no second order response in the dipole approximation. This can be shown mathematically by

defining an inversion operator, $\hat{i}$. Inversion of the nonlinear susceptibility returns the same tensor because the medium is centro-symmetric,

$$\hat{i}\chi^{(2)}_{ijk} = \chi^{(2)}_{-i-j-k} = \chi^{(2)}_{ijk}. \quad [4]$$

Inversion of the electric field changes the sign of the electric field,

$$\hat{i}(E_{j,k}) = E_{-j,-k} = -E_{j,k}. \quad [5]$$

Inversion of the second-order polarization also changes the sign,

$$\hat{i}\left(P^{(2)}_i = \chi^{(2)}_{ijk}E_jE_k\right) = -P^{(2)}_i. \quad [6]$$

However, the inverted the second-order polarization is the same as the product of [4] and the square of [5],

$$\chi^{(2)}_{ijk}(-E_j)(-E_k) = P^{(2)}_i, \quad [7]$$

It has been shown that $-P^{(2)}_i = P^{(2)}_i$, which necessitates that the second-order polarization is equal to zero for centro-symmetric media. Therefore, second-order nonlinear optical techniques can be used to selectively probe an interface.

In Chapters 2, 3, and 4, second harmonic generation two-photon resonant with the CTTS band of aqueous anions will be used as a direct probe of ions at the liquid interface. Chapter 2 establishes that thiocyanide is preferentially adsorbed to the dodecanol/water interface, and Chapter 3 reports on the behavior of bromide at both the air/water and dodecanol/water interfaces in the molar concentration range. Chapter 4 presents evidence that chloride and bromide have strong affinities to the air/water interface in the millimolar concentration range. In Chapter 5, a novel variant of a third-order nonlinear optical technique, chirped-coherent anti-Stokes Raman spectroscopy, is presented as a high spectral and spatial resolution microscopy technique. Chapter 6 summarizes experiments characterizing the nonlinear optical properties of nanowires for the purpose of frequency conversion.

1.3 References

1. F. Franks; Plenum Press: New York, New York, 1972-1982.
2. L. Onsager and N. N. T. Samaras, "Surface tension of Debye-Huckel electrolytes." *Journal of Chemical Physics.* 528-536, (1934).
3. D. J. Griffiths *Introduction to Electrodynamics*; 3rd ed.; Prentice Hall, Inc.: Upper Saddle River, New Jersey, 1999.
4. N. L. Jarvis and M. A. Scheiman, "Surface Potentials of Aqueous Electrolyte Solutions." *Journal of Physical Chemistry.* **72**, 74-&, (1968).
5. B. E. Conway, "State of Water and Hydrated Ions at Interfaces." *Advances in Colloid and Interface Science.* **8**, 91-211, (1977).
6. P. K. Weissenborn and R. J. Pugh, "Surface-Tension and Bubble Coalescence Phenomena of Aqueous-Solutions of Electrolytes." *Langmuir.* **11**, 1422-1426, (1995).
7. P. K. Weissenborn and R. J. Pugh, "Surface tension of aqueous solutions of electrolytes: Relationship with ion hydration, oxygen solubility, and bubble coalescence." *Journal of Colloid and Interface Science.* **184**, 550-563, (1996).
8. A. W. Adamson *Physical Chemistry of Surfaces*; 6th ed.; Wiley: New York, New York, 1999.
9. G. Jones and W. A. Ray, "The surface tension of solutions." *Journal of the American Chemical Society.* **57**, 957-958, (1935).
10. G. Jones and W. A. Ray, "The surface tension of solutions of electrolytes as a function of the concentration I A differential method for measuring relative surface tension." *Journal of the American Chemical Society.* **59**, 187-198, (1937).
11. G. Jones and W. A. Ray, "The Surface Tension of Solutions of Electrolytes as a Function of the Concentration II*." *Journal of the American Chemical Society.* **63**, 288-294, (1941).
12. G. Jones and W. A. Ray, "The surface tension of solutions of electrolytes as a function of the concentration. III. Sodium chloride." *Journal of the American Chemical Society.* **63**, 3262-3263, (1941).
13. G. Jones and W. A. Ray, "The surface tension of solutions of electrolytes as a function of the concentration. IV. Magnesium sulfate." *Journal of the American Chemical Society.* **64**, 2744-2745, (1942).
14. J. H. Hu, Q. Shi, P. Davidovits, D. R. Worsnop, M. S. Zahniser and C. E. Kolb, "Reactive Uptake of Cl2(G) and Br2(G) by Aqueous Surfaces as a Function of Br- and I- Ion Concentration - the Effect of Chemical-Reaction at the Interface." *Journal of Physical Chemistry.* **99**, 8768-8776, (1995).
15. E. M. Knipping, M. J. Lakin, K. L. Foster, P. Jungwirth, D. J. Tobias, R. B. Gerber, D. Dabdub and B. J. Finlayson-Pitts, "Experiments and Simulations of Ion-Enhanced Interfacial Chemistry on Aqueous NaCl Aerosols." *Science.* **288**, 301-306, (2000).
16. A. Laskin, D. J. Gaspar, W. H. Wang, S. W. Hunt, J. P. Cowin, S. D. Colson and B. J. Finlayson-Pitts, "Reactions at interfaces as a source of sulfate formation in sea-salt particles." *Science.* **301**, 340-344, (2003).
17. S. W. Hunt, M. Roeselova, W. Wang, L. M. Wingen, E. M. Knipping, D. J. Tobias, D. Dabdub and B. J. Finlayson-Pitts, "Formation of Molecular Bromine from the Reaction of Ozone with Deliquesced NaBr Aerosol: Evidence for Interface Chemistry." *The Journal of Physical Chemistry A.* **108**, 11559-11572, (2004).

18. G. A. Impey, P. B. Shepson, D. R. Hastie, L. A. Barrie and K. G. Anlauf, "Measurements of photolyzable chlorine and bromine during the Polar sunrise experiment 1995." *Journal of Geophysical Research-Atmospheres.* **102**, 16005-16010, (1997).
19. K. L. Foster, R. A. Plastridge, J. W. Bottenheim, P. B. Shepson, B. J. Finlayson-Pitts and C. W. Spicer, "The role of Br-2 and BrCl in surface ozone destruction at polar sunrise." *Science.* **291**, 471-474, (2001).
20. C. W. Spicer, R. A. Plastridge, K. L. Foster, B. J. Finlayson-Pitts, J. W. Bottenheim, A. M. Grannas and P. B. Shepson, "Molecular halogens before and during ozone depletion events in the Arctic at polar sunrise: concentrations and sources." *Atmospheric Environment.* **36**, 2721-2731, (2002).
21. R. R. Dickerson, K. P. Rhoads, T. P. Carsey, S. J. Oltmans, J. P. Burrows and P. J. Crutzen, "Ozone in the remote marine boundary layer: A possible role for halogens." *Journal of Geophysical Research-Atmospheres.* **104**, 21385-21395, (1999).
22. I. Nagao, K. Matsumoto and H. Tanaka, "Sunrise ozone destruction found in the sub-tropical marine boundary layer." *Geophysical Research Letters.* **26**, 3377-3380, (1999).
23. I. E. Galbally, S. T. Bentley and C. P. Meyer, "Mid-latitude marine boundary-layer ozone destruction at visible sunrise observed at Cape Grim, Tasmania, 41 degrees 5." *Geophysical Research Letters.* **27**, 3841-3844, (2000).
24. V. Matveev, M. Peleg, D. Rosen, D. S. Tov-Alper, K. Hebestreit, J. Stutz, U. Platt, D. Blake and M. Luria, "Bromine oxide - ozone interaction over the Dead Sea." *Journal of Geophysical Research-Atmospheres.* **106**, 10375-10387, (2001).
25. J. Stutz, R. Ackermann, J. D. Fast and L. Barrie, "Atmospheric reactive chlorine and bromine at the Great Salt Lake, Utah." *Geophys. Res. Lett.* **29**, 1380, (2002).
26. U. Friess, J. Hollwedel, G. König-Langlo, T. Wagner and U. Platt, "Dynamics and chemistry of tropospheric bromine explosion events in the Antarctic coastal region." *J. Geophys. Res.* **109**, D06305, (2004).
27. S. J. Stuart and B. J. Berne, "Effects of polarizability on the hydration of the chloride ion." *Journal of Physical Chemistry.* **100**, 11934-11943, (1996).
28. S. J. Stuart and B. J. Berne, "Surface curvature effects in the aqueous ionic solvation of the chloride ion." *Journal of Physical Chemistry A.* **103**, 10300-10307, (1999).
29. P. Ayotte, C. G. Bailey, G. H. Weddle and M. A. Johnson, "Vibrational spectroscopy of small Br-center dot(H2O)(n) and I-center dot(H2O)(n) clusters: Infrared characterization of the ionic hydrogen bond." *Journal of Physical Chemistry A.* **102**, 3067-3071, (1998).
30. P. Ayotte, S. B. Nielsen, G. H. Weddle, M. A. Johnson and S. S. Xantheas, "Spectroscopic observation of ion-induced water dimer dissociation in the X-center dot(H2O)(2) (X = F, Cl, Br, I) clusters." *Journal of Physical Chemistry A.* **103**, 10665-10669, (1999).
31. P. Ayotte, G. H. Weddle and M. A. Johnson, "An infrared study of the competition between hydrogen-bond networking and ionic solvation: Halide-dependent distortions of the water trimer in the X-center dot(H2O)(3), (X = Cl, Br, I) systems." *Journal of Chemical Physics.* **110**, 7129-7132, (1999).
32. D. F. Liu, G. Ma, L. M. Levering and H. C. Allen, "Vibrational Spectroscopy of aqueous sodium halide solutions and air-liquid interfaces: Observation of increased interfacial depth." *Journal of Physical Chemistry B.* **108**, 2252-2260, (2004).

33. E. A. Raymond and G. L. Richmond, "Probing the molecular structure and bonding of the surface of aqueous salt solutions." *Journal of Physical Chemistry B.* **108**, 5051-5059, (2004).
34. P. B. Petersen, J. C. Johnson, K. P. Knutsen and R. J. Saykally, "Direct experimental validation of the Jones-Ray effect." *Chemical Physics Letters.* **397**, 46-50, (2004).
35. P. B. Petersen and R. J. Saykally, "Confirmation of enhanced anion concentration at the liquid water surface." *Chemical Physics Letters.* **397**, 51-55, (2004).
36. S. Ghosal, J. C. Hemminger, H. Bluhm, B. S. Mun, E. L. D. Hebenstreit, G. Ketteler, D. F. Ogletree, F. G. Requejo and M. Salmeron, "Electron spectroscopy of aqueous solution interfaces reveals surface enhancement of halides." *Science.* **307**, 563-566, (2005).
37. L. X. Dang and T.-M. Chang, "Molecular Mechanism of Ion Binding to the Liquid/Vapor Interface of Water." *The Journal of Physical Chemistry B.* **106**, 235-238, (2001).
38. P. Jungwirth and D. J. Tobias, "Ions at the air/water interface." *Journal of Physical Chemistry B.* **106**, 6361-6373, (2002).
39. L. M. Pegram and M. T. Record, "Partitioning of atmospherically relevant ions between bulk water and the water/vapor interface." *Proceedings of the National Academy of Sciences of the United States of America.* **103**, 14278-14281, (2006).
40. L. M. Pegram and M. T. Record, "Hofmeister Salt Effects on Surface Tension Arise from Partitioning of Anions and Cations between Bulk Water and the Air-Water Interface." *J. Phys. Chem. B.* **111**, 5411-5417, (2007).
41. J. Cheng, C. D. Vecitis, M. R. Hoffmann and A. J. Colussi, "Experimental anion affinities for the air/water interface." *Journal of Physical Chemistry B.* **110**, 25598-25602, (2006).
42. P. B. Petersen and R. J. Saykally, "Adsorption of ions to the surface of dilute electroyte solutions: The Jones-Ray effect revisited." *Journal of the American Chemical Society.* **127**, 15446-15452, (2005).
43. P. B. Petersen and R. J. Saykally, "Probing the interfacial structure of aqueous electrolytes with femtosecond second harmonic generation spectroscopy." *Journal of Physical Chemistry B.* **110**, 14060-14073, (2006).
44. P. B. Petersen and R. J. Saykally, "On the nature of ions at the liquid water surface." *Annual Review of Physical Chemistry.* **57**, 333-364, (2006).
45. D. E. Otten, P. B. Petersen and R. J. Saykally, "Observation of nitrate ions at the air/water interface by UV-second harmonic generation." *Chemical Physics Letters.* **449**, 261-265, (2007).
46. P. B. Petersen and R. J. Saykally, "Evidence for an enhanced hydronium concentration at the liquid water surface." *Journal of Physical Chemistry B.* **109**, 7976-7980, (2005).
47. P. Viswanath and H. Motschmann, "Oriented thiocyanate anions at the air-electrolyte interface and its implications on interfacial water - A vibrational sum frequency spectroscopy study." *Journal of Physical Chemistry C.* **111**, 4484-4486, (2007).
48. P. Viswanath and H. Motschmann, "Effect of interfacial presence of oriented thiocyanate on water structure." *Journal of Physical Chemistry C.* **112**, 2099-2103, (2008).
49. S. Ghosal, M. A. Brown, H. Bluhm, M. J. Krisch, M. Salmeron, P. Jungwirth and J. C. Hemminger, "Ion Partitioning at the Liquid/Vapor Interface of a Multicomponent Alkali Halide Solution: A Model for Aqueous Sea Salt Aerosols." *Journal of Physical Chemistry A.* **112**, 12378-12384, (2008).

50. J. Noah-Vanhoucke and P. L. Geissler, "On the fluctuations that drive small ions toward, and away from, interfaces between polar liquids and their vapors." *Proceedings of the National Academy of Sciences of the United States of America.* **106**, 15125-15130, (2009).
51. J. K. Beattie, "Comment on Autoionization at the surface of neat water: is the top layer pH neutral, basic, or acidic? by R. Vacha, V. Buch, A. Milet, J. P. Devlin and P. Jungwirth, Phys. Chem. Chem. Phys., 2007, 9, 4736." *Physical Chemistry Chemical Physics.* **10**, 330-331, (2008).
52. R. Vacha, V. Buch, A. Milet, J. P. Devlin and P. Jungwirth, "Response to Comment on Autoionization at the surface of neat water: is the top layer pH neutral, basic, or acidic? by J. K. Beattie, Phys. Chem. Chem. Phys., 2007, 9, DOI : 10.1039/b713702h." *Physical Chemistry Chemical Physics.* **10**, 332-333, (2008).
53. R. Vacha, D. Horinek, M. L. Berkowitz and P. Jungwirth, "Hydronium and hydroxide at the interface between water and hydrophobic media." *Physical Chemistry Chemical Physics.* **10**, 4975-4980, (2008).
54. V. Buch, A. Milet, R. Vacha, P. Jungwirth and J. P. Devlin, "Water surface is acidic." *Proceedings of the National Academy of Sciences of the United States of America.* **104**, 7342-7347, (2007).
55. J. K. Beattie, A. N. Djerdjev and G. G. Warr, "The surface of neat water is basic." *Faraday Discussions.* **141**, 31-39, (2009).
56. J. K. Beattie and A. M. Djerdjev, "The pristine oil/water interface: Surfactant-free hydroxide-charged emulsions." *Angewandte Chemie-International Edition.* **43**, 3568-3571, (2004).
57. A. Graciaa, G. Morel, P. Saulner, J. Lachaise and R. S. Schechter, "The Zeta-Potential of Gas-Bubbles." *Journal of Colloid and Interface Science.* **172**, 131-136, (1995).
58. A. Graciaa, P. Creux, C. Dicharry and J. Lachaise, "Measurement of the zeta potential of oil drops with the spinning tube zetameter." *Journal of Dispersion Science and Technology.* **23**, 301-307, (2002).
59. J. K. Beattie, "The intrinsic charge on hydrophobic microfluidic substrates." *Lab on a Chip.* **6**, 1409-1411, (2006).
60. M. Takahashi, "xi potential of microbubbles in aqueous solutions: Electrical properties of the gas-water interface." *Journal of Physical Chemistry B.* **109**, 21858-21864, (2005).
61. A. Gray-Weale and J. K. Beattie, "An explanation for the charge on water's surface." *Physical Chemistry Chemical Physics.* **11**, 10994-11005, (2009).
62. M. K. Petersen, S. S. Iyengar, T. J. F. Day and G. A. Voth, "The hydrated proton at the water liquid/vapor interface." *Journal of Physical Chemistry B.* **108**, 14804-14806, (2004).
63. P. B. Petersen and R. J. Saykally, "Is the liquid water surface basic or acidic? Macroscopic vs. molecular-scale investigations." *Chemical Physics Letters.* **458**, 255-261, (2008).
64. M. Mucha, T. Frigato, L. M. Levering, H. C. Allen, D. J. Tobias, L. X. Dang and P. Jungwirth, "Unified molecular picture of the surfaces of aqueous acid, base, and salt solutions." *Journal of Physical Chemistry B.* **109**, 7617-7623, (2005).
65. T. L. Tarbuck, S. T. Ota and G. L. Richmond, "Spectroscopic studies of solvated hydrogen and hydroxide ions at aqueous surfaces." *Journal of the American Chemical Society.* **128**, 14519-14527, (2006).

66. C. Tian, N. Ji, G. A. Waychunas and Y. R. Shen, "Interfacial Structures of Acidic and Basic Aqueous Solutions." *J. Am. Chem. Soc.* **130**, 13033-13039, (2008).
67. C. S. Tian and Y. R. Shen, "Structure and charging of hydrophobic material/water interfaces studied by phase-sensitive sum-frequency vibrational spectroscopy." *Proceedings of the National Academy of Sciences of the United States of America.* **106**, 15148-15153, (2009).
68. B. Winter, M. Faubel, R. Vacha and P. Jungwirth, "Behavior of hydroxide at the water/vapor interface." *Chemical Physics Letters.* **474**, 241-247, (2009).
69. F. Hofmeister, *Arch. Exptl. Pathol. Pharmakol.* **24**, 247-260, (1888).
70. K. D. Collins and M. W. Washabaugh, "The Hofmeister Effect and the Behavior of Water at Interfaces." *Quarterly Reviews of Biophysics.* **18**, 323-422, (1985).
71. M. G. Cacace, E. M. Landau and J. J. Ramsden, "The Hofmeister series: salt and solvent effects on interfacial phenomena." *Quarterly Reviews of Biophysics.* **30**, 241-277, (1997).
72. W. Kunz, P. Lo Nostro and B. W. Ninham, "The present state of affairs with Hofffieister effects." *Current Opinion in Colloid & Interface Science.* **9**, 1-18, (2004).
73. A. W. Omta, M. F. Kropman, S. Woutersen and H. J. Bakker, "Negligible Effect of Ions on the Hydrogen-Bond Structure in Liquid Water." *Science.* **301**, 347-349, (2003).
74. J. D. Smith, R. J. Saykally and P. L. Geissler, "The Effects of Dissolved Halide Anions on Hydrogen Bonding in Liquid Water." *J. Am. Chem. Soc.* **129**, 13847-13856, (2007).
75. Y. Zhang and P. S. Cremer, "Interactions between macromolecules and ions: the Hofmeister series." *Current Opinion in Chemical Biology Model systems / Biopolymers.* **10**, 658-663, (2006).
76. M. J. Krisch, R. D'Auria, M. A. Brown, D. J. Tobias, J. C. Hemminger, M. Ammann, D. E. Starr and H. Bluhm, "The effect of an organic surfactant on the liquid-vapor interface of an electrolyte solution." *Journal of Physical Chemistry C.* **111**, 13497-13509, (2007).
77. B. W. Ninham and V. Yaminsky, "Ion binding and ion specificity: The Hofmeister effect and Onsager and Lifshitz theories." *Langmuir.* **13**, 2097-2108, (1997).
78. M. Boström, D. R. M. Williams and B. W. Ninham, "Specific Ion Effects: Why DLVO Theory Fails for Biology and Colloid Systems." *Physical Review Letters.* **87**, 168103, (2001).
79. M. Bostrom, D. R. M. Williams and B. W. Ninham, "Ion specificity of micelles explained by ionic dispersion forces." *Langmuir.* **18**, 6010-6014, (2002).
80. M. Bostrom, D. R. M. Williams and B. W. Ninham, "Surface tension of electrolytes: Specific ion effects explained by dispersion forces." *Langmuir.* **17**, 4475-4478, (2001).
81. M. Bostrom, D. R. M. Williams and B. W. Ninham, "Specific Ion Effects: Why the Properties of Lysozyme in Salt Solutions Follow a Hofmeister Series." *Biophys. J.* **85**, 686-694, (2003).
82. M. Bostrom, W. Kunz and B. W. Ninham, "Hofmeister effects in surface tension of aqueous electrolyte solution." *Langmuir.* **21**, 2619-2623, (2005).
83. P. Jungwirth and B. Winter, "Ions at aqueous interfaces: From water surface to hydrated proteins." *Annual Review of Physical Chemistry.* **59**, 343-366, (2008).
84. M. Lund and P. Jungwirth, "Ion specific protein assembly and hydrophobic surface forces." *Physical Review Letters.* **100**, (2008).
85. M. Lund, R. Vacha and P. Jungwirth, "Specific Ion Binding to Macromolecules: Effects of Hydrophobicity and Ion Pairing." *Langmuir.* **24**, 3387-3391, (2008).

86. M. Lund, L. x. c. Vrbka and P. Jungwirth, "Specific Ion Binding to Nonpolar Surface Patches of Proteins." *J. Am. Chem. Soc.* **130**, 11582-11583, (2008).
87. N. Vlachy, B. Jagoda-Cwiklik, R. Vacha, D. Touraud, P. Jungwirth and W. Kunz, "Hofmeister series and specific interactions of charged headgroups with aqueous ions." *Advances in Colloid and Interface Science.* **146**, 42-47, (2009).
88. Y. R. Shen *The principles of nonlinear optics*; J. Wiley: New York, NY, 1984.
89. S. Mukamel *Principles of nonlinear optical spectroscopy*; Oxford University Press: New York, NY, 1995.
90. R. W. Boyd *Nonlinear Optics*; 2nd ed.; Elsevier: San Diego, CA, 2003.

Chapter 2:

Adsorption of thiocyanate ions to the dodecanol/water interface characterized by UV second harmonic generation

2.1 Introduction

Recent experimental and theoretical results have firmly established the existence of enhanced concentrations of selected ions at the air/water interface. Ion adsorption to aqueous interfaces involving complex organic molecules is relevant to biology in connection with the familiar but incompletely understood Hofmeister effects. The Hofmeister series, first described in 1888 in terms of salt-dependent effects on the aqueous solubility of proteins,[1] appears in fields ranging from biochemistry to colloid chemistry.[2-4] More than a century after Hofmeister's work, there is still no comprehensive molecular explanation for these macroscopic ion-selective effects, despite numerous published studies and models. Interfacial effects are currently believed to be the predominant source of the Hofmeister phenomena,[2, 3, 5] and recent studies have confirmed that long-range solvation effects play a minimal role, as the water hydrogen bonding structure is generally not significantly affected beyond the first hydration shell of aqueous monovalent ions.[6-8]

The interfacial affinities of various anions for a protein-like/water interface have been shown to follow a Hofmeister series in studies by Chen et al. using vibrational sum frequency spectroscopy (VSFS),[9] demonstrating that stronger interfacial affinities correlate with "salting-in" of proteins. Using surface tension measurements, Pegram and Record have found similar results for the air-water interface.[10, 11] Collins has proposed the "law of matching water affinities" to explain Hofmeister effects, which utilizes ion hydration strength to explain ion-specific interactions.[12] Jungwirth et al. have recently performed a number of simulations investigating the relation between the Hofmeister series and specific-ion interactions with various model and chemical interfaces.[13-19] In one of these studies, ions at opposite ends of the Hofmeister anion series, fluoride and iodide, exhibit two different mechanisms of adsorption to a model macromolecule.[15] The weakly hydrated iodide ions preferentially adsorb to hydrophobic surfaces, while the strongly hydrated fluoride ions adsorb via an electrostatic interaction to regions of positive charge. Using x-ray photoelectron spectroscopy (XPS), Krisch et al. found the iodide surface concentration enhancement at the air/liquid interface of a butanol and water mixture to be less than that of a pure aqueous solution.[20]

It is clearly of interest to establish the affinities of such simple ions for the chemical moieties that exist at aqueous interfaces with proteins and other biologically relevant complex molecules, such as fatty acids, polyglycerides, and lipids. Herein we describe our investigations of selective adsorption of the thiocyanate anion, positioned at the extreme of the Hofmeister "structure breaker" anion series, to a long-chain alcohol/water interface. The presence of thiocyanate ions at the interface comprising a monolayer of dodecanol with water is probed via charge-transfer-to-solvent (CTTS) resonant SHG, and the Gibbs free energy of surface adsorption is determined using a Langmuir adsorption model. The effect of cation identity is also assessed by comparing adsorption from NaSCN and KSCN solutions. Interfacial adsorption of thiocyanate has been the focus of many recent experimental studies, and we compare our new results to those recently obtained for the air/water[21-23] and macromolecule/water[9] interfaces.

2.2 Experimental

The laser system has been described in detail previously [24]. Briefly, a home-built Ti:sapphire oscillator seeds a regenerative amplifier (Spectra-Physics Spitfire). The amplified pulses pump an OPA (Quantronix TOPAS) generating the visible light used as the fundamental beam (1 kHz, 2 μJ, ~100 fs) for SHG generation. A motorized variable neutral density filter is used to modulate the fundamental beam power during the course of the experiment. A beam splitter is used to direct <10% of the fundamental beam intensity to a photodiode as a relative measure of the power applied to the sample surface. The remaining fundamental light is focused on the sample surface with a 10 cm lens at 60° relative to the surface normal with p-polarization. For an isotropic surface with the plane of incidence defined as the xz-plane, the symmetry of the system dictates that the only non-zero $\chi^{(2)}$ elements accessed by p-polarized incident light are $\chi^{(2)}_{zzz}$, $\chi^{(2)}_{zxx}$, and $\chi^{(2)}_{xzx} = \chi^{(2)}_{xxz}$. Therefore, all generated SHG is p-polarized. The SHG light is collimated by a 10 cm fused-Si lens and separated from the fundamental beam through the use of three dichroic mirrors and a monochromator (PI Acton, Spectra Pro SP-2155) before being collected by a solar-blind PMT (Hammamatsu, R7154PHA).

The modulated power of each pulse of the fundamental beam, R, is measured by the photodiode and binned into groups of $R^2 \pm \Delta$. The average number of photons, $\bar{k}$, collected per laser pulse is much less than one, and the PMT is used as a photon counter. The number of laser pulses where zero photons are detected, $N^{k=0}_{pulses}$, is counted, and assuming Poisson statistics for the distribution of photons detected in a given shot, the expectation value for the number of photons in a given fundamental power bin, $R^2 \pm \Delta$, can be evaluated as

$$\langle k \rangle = -\ln\left[\frac{N^{k=0}_{pulses}}{N^{total}_{pulses}}\right]_{R^2 \pm \Delta} . \qquad [2.1]$$

Since SHG is a second-order process, plotting this value versus R^2 provides a linear relationship. The slope of the resulting line, determined by a variance-weighted least-squares fit, is taken as the system response, proportional to $\left|\chi^{(2)}_{system}\right|^2$. This also provides an inherent confirmation that the SHG signal exhibits the correct second-order power dependence.

All glassware was cleaned using Nochromix dissolved in concentrated sulfuric acid and rinsed with 18.2 MΩ water (Millipore MilliQ). Solutions were made with 18.2 MΩ water, NaSCN (Sigma-Aldrich, >99.99% metals basis), and KSCN (Sigma-Aldrich, >99.0%), which were used without further purification. An alcohol monolayer was prepared on the solution surface by floating a 1-dodecanol (Sigma-Aldrich, 98%) crystal on the solution surface, as described by Casson et al [25]. All samples were prepared and measured at room temperature.

2.3 SHG and the Langmuir adsorption model

SHG spectroscopy of CTTS bands has recently been used to determine the affinity of several anions (thiocyanate,[21] azide,[26] iodide,[27, 24] ferrocyanaide,[28] and hydroxide[29]) for the air/water interface. In these and the current experiments, the fundamental beam in the visible region of the spectrum is two-photon resonant with the CTTS band located in the deep UV, providing a direct probe for selected anions. Since SHG is a second-order nonlinear optical technique, under the dipole approximation SHG is only generated when the system does not exhibit centro-symmetric symmetry and is therefore interface specific for the dodecanol/water

system. For this reason, it is a useful technique for probing the interface of complex molecules with water.

The SHG intensity can be written

$$I_{SHG} = \left|\chi^{(2)}_{system}\right|^2 I^2_{fundamental}, \qquad [2.2]$$

where the system response, $\chi^{(2)}_{system}$, can be partitioned into contributions due to the solvent, in this case the dodecanol/water interface, and contributions due to the solute:

$$\chi^{(2)}_{system} = \chi^{(2)}_{solvent} + \chi^{(2)}_{solute}. \qquad [2.3]$$

The dodecanol/water response is non-resonant, and therefore will be a purely real quantity. In the case of CTTS SHG, the solute response is the product of the number of surface anions in the laser focus, N_S, and the orientationally averaged hyperpolarizability,

$$\chi^{(2)}_{solute} = N_S \left\langle \beta \right\rangle_{orientation}. \qquad [2.4]$$

The application of a Langmuir adsorption model to SHG of ions at an interface has been described in detail previously[26, 24] and is only described briefly here. Since the system response is proportional to the number of anions at the interface, a Langmuir model may be used to determine the affinity of the anions for the interface. The system response can be parameterized as

$$\left|\chi^{(2)}_{system}\right|^2 = \left|A + (B + iC)N_S\right|^2. \qquad [2.5]$$

Here A represents the non-resonant solvent response and B and C represent the real and imaginary components of the solute response.

A Langmuir model is applied here by dividing the solution into bulk and surface domains for which an equilibrium equation can be written describing the exchange of surface and bulk species,

$$S_S + N_B \rightleftharpoons S_B + N_S, \qquad [2.6]$$

where S is one solvent molecule and X_B and X_S reside in the bulk and surface partitions, respectively. In this formulation it is assumed that the solvent and solute exchange in a 1:1 ratio. This model also presumes that all interfacial adsorption sites are equivalent and always occupied by either a solvent or solute molecule, implying two things in the dodecanol/water case. First, the model is only valid up to one monolayer of surface adsorption by the ion. Second, interactions between neighboring adsorption sites must be negligible.

Manipulation of the Langmuir model provides the following expression for the number of surface ions in terms of the bulk concentrations of the solvent and solute:

$$N_S = \frac{N_S^{\max}[N_B]}{[N_B] + [S_B]\exp\left[\Delta G_{ads}/RT\right]}. \qquad [2.7]$$

Here, $N_S^{\max} = S_S + N_S$ and represents the total number of surface sites, and ΔG_{ads} is the Gibbs free energy of solute adsorption to the interface. Inserting [2.7] into [2.5] and allowing the B and C parameters of [2.5] to include $N_S^{\max}$ provides the equation used to fit the data. The data are fit such that at different wavelengths the parameters A, B, and C are independent, while ΔG_{ads} is fit to all the wavelengths simultaneously.

2.4 Dodecanol/water structure

The intrinsic structure of the long-chain alcohol/water interface is well-understood. The surface area of a 1-dodecanol molecule on the water surface is ~20 Å^2.[30, 31] X-ray studies have

confirmed that the alcohol chains stand nearly vertically on the water surface.[32, 33] Hence, the OH terminus of dodecanol is able to form hydrogen bonds with water or to contribute to the hydration shell of an adsorbed anion. VSFS has been used to determine that *gauche* defects of the aliphatic chain are very rare below the 2D phase transition temperature (T_m(2D)), which for 1-dodecanol is 39.1°C.[34, 25, 31]

T_m(2D) of dodecanol on pure water and on a 20% by weight solution of KBr agreed within error.[30] This implies that any bromide ions at the interface, which have been predicted to preferentially adsorb to the air/water interface,[35, 36] do not penetrate into the dodecanol layer. Similarly, VSFS of the CH region of another macromolecule, poly-(N-isoproylacrylamide) (PNIPAM), on D_2O was the same for pure water and numerous 1 M salt solutions, including NaSCN.[9] Since VSFS is sensitive to number density and orientational changes, both the concentration and orientation were invariant to salt addition. Therefore, it is assumed that interfacial adsorption of thiocyanate at the dodecanol/water interface does not disrupt the concentration or orientation of the dodecanol monolayer.

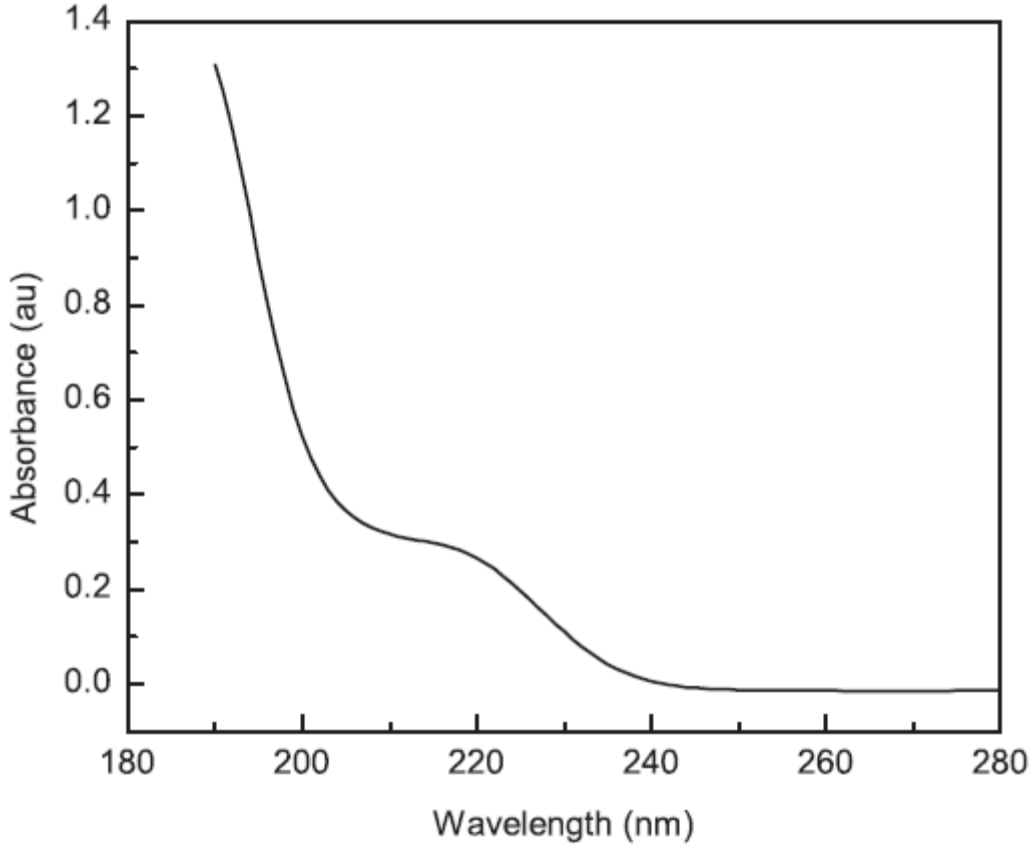

Figure 2.1. UV absorption spectrum of aqueous sodium thiocyanate.

2.5 Results and Discussion

The bulk aqueous CTTS absorption spectrum of NaSCN is presented in Figure 2.1. The SHG spectrum at the dodecanol/water interface is likely shifted from that of the bulk aqueous solution due to the different environment presented by the interfacial region, as observed for other anions at the air/water interface.[37]

The SHG intensities of NaSCN and KSCN at the dodecanol/water interface are plotted in Figure 2.2 for a series of wavelengths as a function of bulk concentration. The SHG intensity is normalized such that it is unity for the dodecanol/water interface with no dissolved salt. The non-resonant signal due to the intrinsic dodecanol/water interface is approximately four times greater than that of neat water. The SHG intensity clearly increases with anion concentration, indicating that thiocyanate is present at the water/dodecanol interface, since the structure of the dodecanol monolayer has been shown to remain invariant upon salt addition.[30, 9] The two-photon resonance with the CTTS band at 205 nm provides a significant signal enhancement relative to the weakly resonant signal at 230 nm and non-resonant signal at 266 nm. The signal enhancement, defined here as $\left(I_{SHG}^{205}-1\right)/\left(I_{SHG}^{266}-1\right)$, fluctuates at low concentrations, but above 1 M the enhancement factor is 7.9 ± 1.2. The NaSCN and KSCN data are remarkably similar, despite effects due to the different cations. For each wavelength nearly all common concentration data points lie within their relative errors, as previously found for ions at the air/water interface.[24] The only significant exception occurs above 4 M concentrations (henceforth concentrations ≥ 4 M will be referred to as high concentration), where the SHG intensity for NaSCN is greater than that of KSCN for both on- and off-resonant wavelengths.

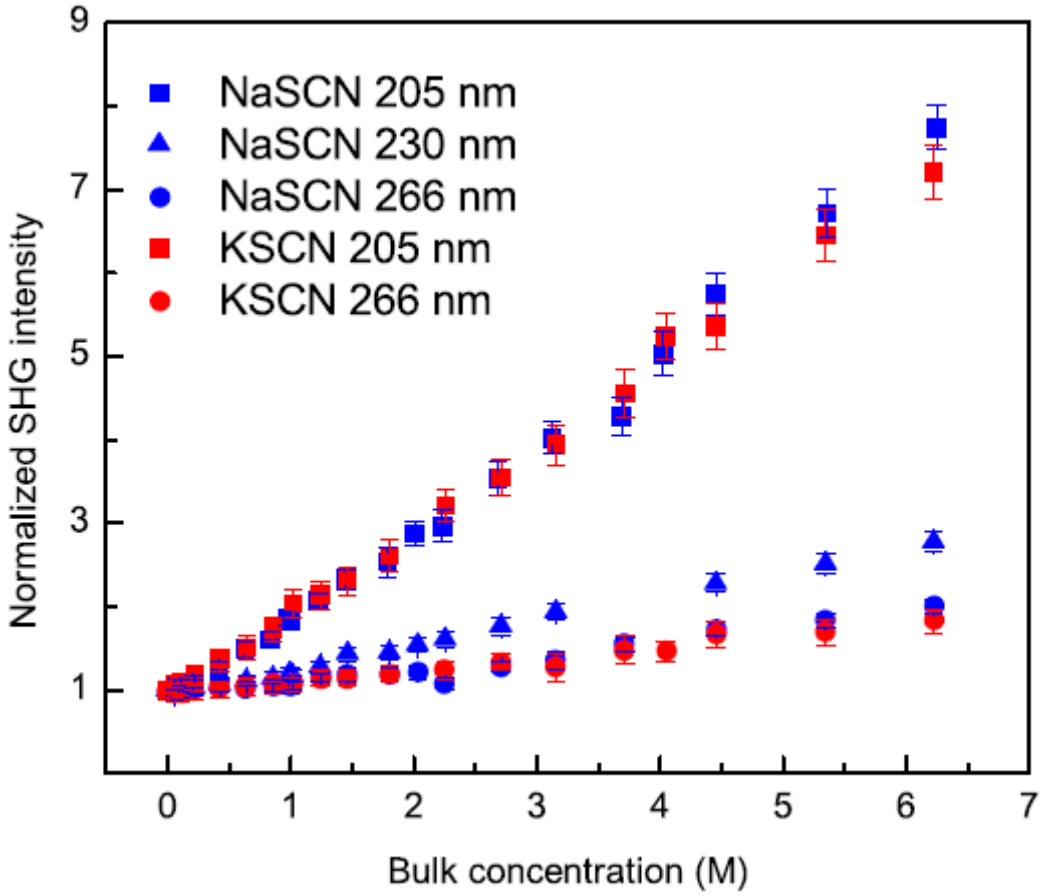

Figure 2.2. SHG response for NaSCN and KSCN solutions plotted as a function of bulk concentration. The wavelengths 205 nm, 230 nm, and 266 nm represent resonant, weakly-resonant, and non-resonant responses, respectively. The error bars are one standard deviation.

At 266 nm, the SHG intensity increases with concentration despite being far from any expected resonance. Similar behavior for non-resonant SHG of sodium halide salts has been attributed to a thickening of the interfacial layer (defined as the region exhibiting broken inversion symmetry) with increasing concentration.[38] However, this assumes that both the ions and their solvation shells are symmetric, and therefore do not contribute to the SHG signal. The hydration shell of thiocyanate will not be symmetric as the ion itself is asymmetric. Moreover, molecular dynamics simulations have shown that thiocyanate is not expected to be well-hydrated at the air/water interface,[21] and this may also be the case at the alcohol/water interface. Therefore, the non-resonant increase in SHG signal with increasing thiocyanate concentration originates from the local alteration of the interfacial hydrogen bonding structure by thiocyanate as well as from any change in interfacial thickness.

Inspection of the data for both NaSCN and KSCN reveals that there is a salient kink in the SHG intensity at high concentrations (see Figure 2.3). The SHG intensity at high concentrations is greater than extrapolation of the lower concentration data would predict based on the Langmuir adsorption model. Therefore, the Langmuir fits shown in Figure 2.3 only include the data at concentrations below the onset of this kink. The fit parameters are shown in Table 2.1; the errors are one standard deviation.

Table 1. Langmuir fit parameters[a]

	wavelength (nm)	B	C	ΔG_{ads} (kJ/mol)
NaSCN all data	205	3.2 ± 1.5	2.1 ± 1.8	-4.5 ± 0.9
	230	1.0 ± 0.5	1.6 ± 0.4	
	266	0.1 ± 0.2	1.9 ± 0.3	
NaSCN molarity < 4	205	1.0 ± 0.8	2.6 ± 0.3	-6.7 ± 1.1
	230	0.1 ± 0.2	1.8 ± 0.3	
	266	0.0 ± 0.2	1.2 ± 0.3	
KSCN molarity < 4[b]	205	1.7 ± 1.7	1.8 ± 1.4	-6.3 ± 1.8
	266	0.1 ± 0.2	1.1 ± 0.4	

[a] Parameter A is equal to one within 1% error in all cases. [b] KSCN fit of the full concentration range does not converge.

The Langmuir fit parameters for the entire concentration range are also included in Table 2.1 for NaSCN. Comparing the relative errors of the fit parameters of the truncated and full data sets, especially parameter *C* for 205 nm, indicates that including the high concentration SHG intensity in the Langmuir fit is not appropriate. The Langmuir fit of the entire concentration range of KSCN does not converge, serving as further evidence of the divergence from Langmuir conditions at high concentrations.

The Gibbs free energy of adsorption of the thiocyanate ion to the surface was found to be -6.7 ± 1.1 kJ/mol for NaSCN and -6.3 ± 1.8 kJ/mol for KSCN using the truncated data sets. Interestingly, despite different interfacial structures, the thiocyanate affinity at the dodecanol/water interface is within experimental error of that determined for NaSCN at the

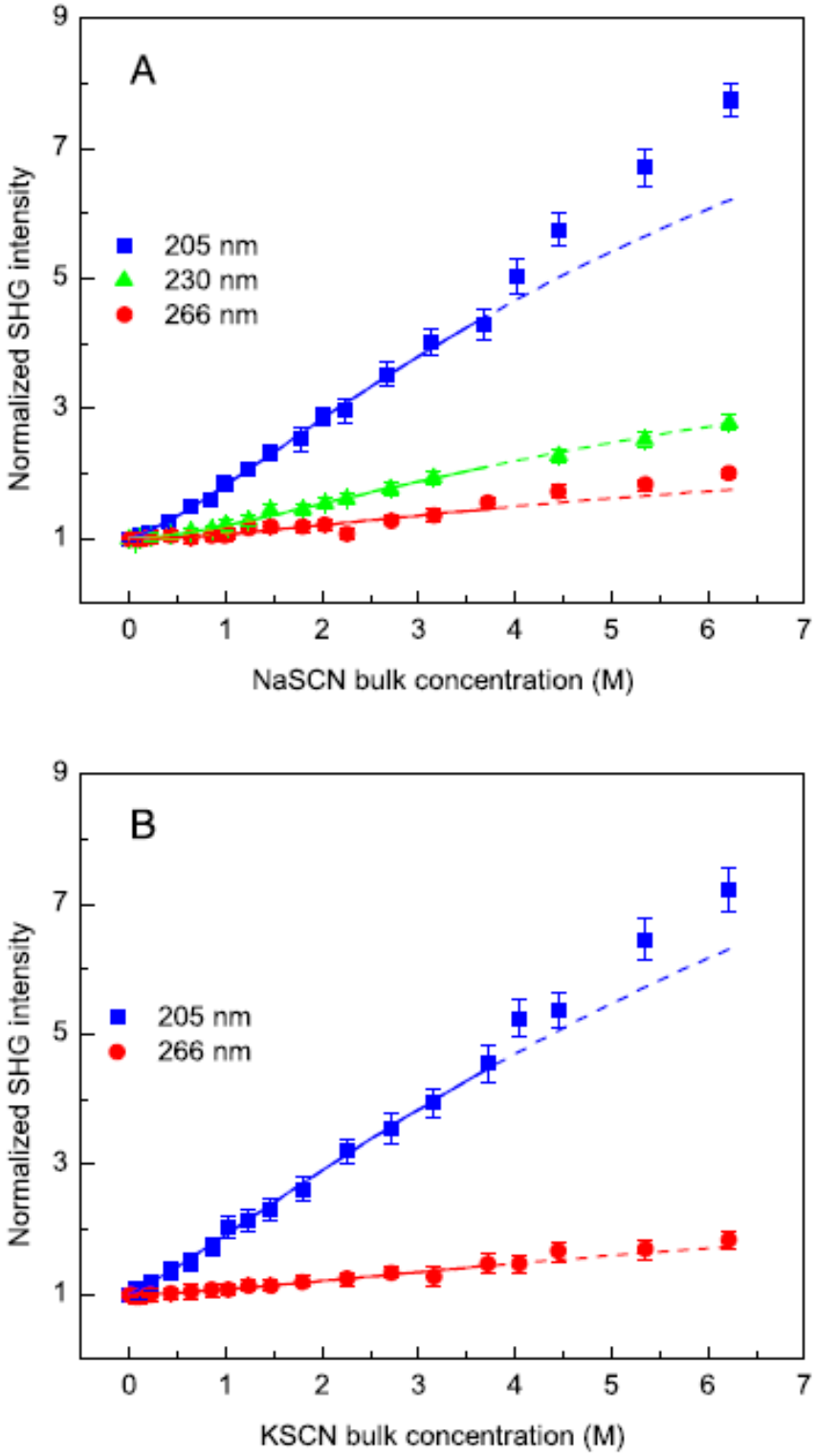

Figure 2.3. SHG response for NaSCN (a) and KSCN (b) solutions and the corresponding Langmuir fits. The fits only include concentrations less than 4 M. The high concentration data are shown and the Langmuir fits are continued as dotted lines to illustrate the divergence from the fits of the high concentration data. The error bars are one standard deviation.

air/water interface, -7.5 ± 0.1 kJ/mol.[21] Adsorption of thiocyanate to the air/water interface was previously found by directly probing thiocyanate via VSFS, but no thermodynamic data were reported.[22, 23]

Whether the agreement between the air/water and dodecanol/water interfaces is coincidental or the adsorption mechanism is relatively unchanged between the two interfaces remains an interesting question. Weakly hydrated ions have been shown to adsorb to air/water and hydrophobic/water interfaces by both experiment[39, 40, 10, 11] and theory,[41, 13, 15] presumably due to hydrophobic effects, resulting in minimal disruption of the strong hydrogen bonding interactions of water. However, since the structure of the surfactant is unchanged by the presence of ions in similar systems[30, 9] and the dodecanol layer is part of the hydrogen bond network at the interface, the energetic preference of ions for the interface due to hydrophobic exclusion may be less than at the air/water interface. This difference could be counteracted by the relative image charge repulsions of thiocyanate at the air/water interface and the dodecanol/water interface. The image charge repulsion at the dodecanol/water interface is weaker since the dielectric constant of dodecanol is greater than that of air.

The presence of ions at the air/alcohol/water interface was previously investigated by XPS.[20] In that study the photoelectron kinetic energy was varied to probe different depths of a 1-butanol and water solution deliquesced on a potassium iodide crystal. The authors conclude that the surface-enhanced concentration previously observed at the air/water interface[42] is suppressed at the air/butanol/water interface, as evidenced by a flattening of the ratio of iodide to potassium as a function of escape depth. This would appear to be in contrast with the results presented here, albeit with a different anion. However, the nature of the two interfaces makes direct comparisons difficult. The air/solution interface comprising butanol and water is characterized by a non-uniform layer of loosely packed butanol, whereas the air/solution interface comprising dodecanol and water is a rigid monolayer. Furthermore, the manner in which the interface is probed is quite different for XPS and SHG. In XPS the depth into the solution that is probed is determined by the photoelectron kinetic energy, while SHG probes regions characterized by broken inversion symmetry. Moreover, XPS measures relative concentrations, and our work reports Gibbs free energies of adsorption. The concentration and the Gibbs free energy are related in our model through the number of surface adsorption sites, which will vary depending on the system.

Another study of a macromolecule/water interface investigated thiocyanate at the PNIPAM/water interface with VSFS.[9] Their work used a different formulation of the Langmuir model, but analysis of their data with the Langmuir formulation used here yields a ΔG_{ads} of approximately -18 kJ/mol. The stronger adsorption to the PNIPAM/water interface is likely due to the presence of strongly polar amide moieties at the interface.

The fractional surface coverage of thiocyanate ions can be calculated from the Gibbs free energy by dividing Equation [2.7] by $N_S^{\max}$. The surface coverage versus bulk concentration is plotted in Figure 2.4. As the bulk concentration of thiocyanate ions is increased, the surface concentration eventually becomes large enough that ion-ion interactions cannot be neglected. The breakdown of the Langmuir model for this system occurs when the thiocyanate surface coverage is approximately half of the number of surface sites. At this bulk concentration the ratio of all ions (including both anions and cations) to water molecules is ~1:6. Not only will there be repulsion between surface anions, but ion pairing of the cation and anion will also occur. It is therefore not surprising that the Langmuir model breaks down in this regime, but it is striking that the transition from Langmuir to non-Langmuir conditions appears to be so sharp. This is indicative of a structural change at the interface. Although the nature of the structural change is

not clear from this work, it could be a change in the interfacial water structure, a second thiocyanate adsorption site in the interfacial layer, or a disruption of the dodecanol monolayer structure.

In most of the previous surface sensitive spectroscopic studies of thiocyanate, concentrations above 4 M have not been investigated.[21, 9, 22] However, Viswanath et al.[23] included concentrations up to 5 M in their direct VSFS study of thiocyanate at the air/water interface, finding that the oscillator strength, indicative of the surface anion density, leveled off at and above 3 M concentrations. Further study of this interesting interfacial structural change is of considerable interest.

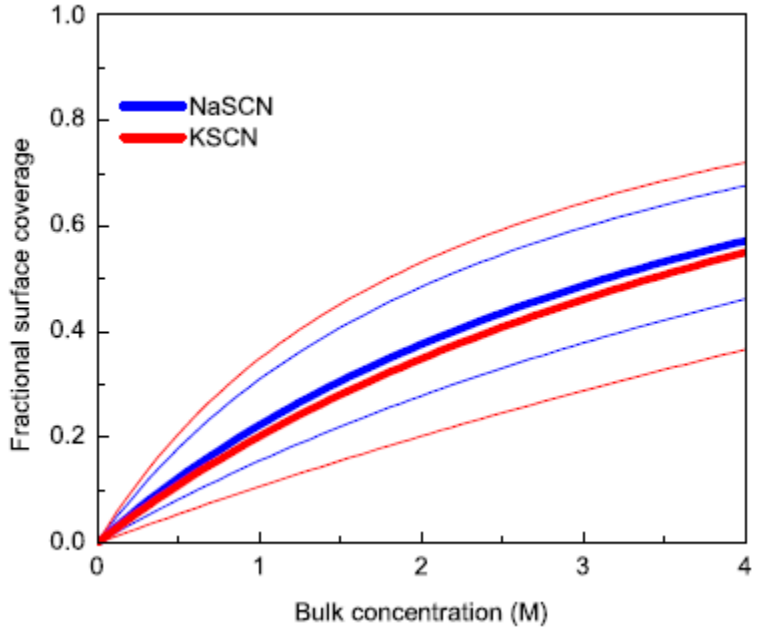

Figure 2.4. Predicted fractional surface coverage of NaSCN and KSCN as a function of bulk concentration (bold lines). The narrow lines represent the error, one standard deviation.

2.6 Conclusions

The prevailing explanation for the Hofmeister series invokes specific ion interactions at the macromolecule/water interface[12, 5, 9, 13-19]. In order to experimentally assess more complex issues, such as protein solubility and enzyme inhibition the interactions of ions with specific and relevant chemical moieties must be understood. Here we report the study of anion adsorption to the interface formed by a monolayer of a long-chain alcohol and water, using resonant CTTS SHG of the strongly chaotropic thiocyanate ion. A Langmuir analysis shows that thiocyanate exhibits an enhanced interfacial concentration relative to that of the bulk. Cation identity has a minimal effect on the affinity of thiocyanate for the interface, since the surface affinities of thiocyanate for NaSCN and KSCN solutions were identical within error. These results are relevant to water/lipid interfaces, for example, since thiocyanate would now be expected to preferentially adsorb to OH rich cell walls. However, such interfaces are obviously more complex than an alcohol monolayer, and a more thorough understanding is clearly necessary. At high concentrations the increase in SHG signal with concentration is discontinuously greater than predicted by extrapolating lower concentrations, indicating an apparent change in the interfacial

structure. High concentration analysis may be more relevant to physiological systems, since ions often have large apparent concentrations due to confinement by other structures.

Understanding the general mechanisms of surface adsorption involves a balance of competing forces, including hydrophobic exclusion effects, image charge repulsion, and direct interactions between the ion and the adsorbent. Varying the identity of both the ion and the liquid-liquid interface in future SHG studies can provide further insight on these interactions.

2.7 References

1. F. Hofmeister, *Arch Exp Pathol Pharmakol.* **24**, 247-260, (1888).
2. K. D. Collins and M. W. Washabaugh, "The Hofmeister effect and the behaviour of water at interfaces." *Quarterly Reviews of Biophysics.* **18**, 323-422, (1985).
3. M. G. Cacace, E. M. Landau and J. J. Ramsden, "The Hofmeister series: salt and solvent effects on interfacial phenomena." *Quarterly Reviews of Biophysics.* **30**, 241-277, (1997).
4. W. Kunz, P. Lo Nostro and B. W. Ninham, "The present state of affairs with Hofffieister effects." *Current Opinion in Colloid & Interface Science.* **9**, 1-18, (2004).
5. Y. Zhang and P. S. Cremer, "Interactions between macromolecules and ions: the Hofmeister series." *Current Opinion in Chemical Biology Model systems / Biopolymers.* **10**, 658-663, (2006).
6. A. W. Omta, M. F. Kropman, S. Woutersen and H. J. Bakker, "Negligible Effect of Ions on the Hydrogen-Bond Structure in Liquid Water." *Science.* **301**, 347-349, (2003).
7. C. D. Cappa, J. D. Smith, K. R. Wilson, B. M. Messer, M. K. Gilles, R. C. Cohen and R. J. Saykally, "Effects of Alkali Metal Halide Salts on the Hydrogen Bond Network of Liquid Water." *Journal of Physical Chemistry B.* **109**, 7046-7052, (2005).
8. J. D. Smith, R. J. Saykally and P. L. Geissler, "The Effects of Dissolved Halide Anions on Hydrogen Bonding in Liquid Water." *J. Am. Chem. Soc.* **129**, 13847-13856, (2007).
9. X. Chen, T. Yang, S. Kataoka and P. S. Cremer, "Specific ion effects on interfacial water structure near macromolecules." *Journal of the American Chemical Society.* **129**, 12272-12279, (2007).
10. L. M. Pegram and M. T. Record, "Partitioning of atmospherically relevant ions between bulk water and the water/vapor interface." *Proceedings of the National Academy of Sciences.* **103**, 14278-14281, (2006).
11. L. M. Pegram and M. T. Record, "Hofmeister Salt Effects on Surface Tension Arise from Partitioning of Anions and Cations between Bulk Water and the Air-Water Interface." *J. Phys. Chem. B.* **111**, 5411-5417, (2007).
12. K. D. Collins, "Ions from the Hofmeister series and osmolytes: effects on proteins in solution and in the crystallization process." *Methods Macromolecular Crystallization.* **34**, 300-311, (2004).
13. M. Lund and P. Jungwirth, "Ion specific protein assembly and hydrophobic surface forces." *Physical Review Letters.* **100**, (2008).
14. M. Lund and P. Jungwirth, "Patchy proteins, anions and the Hofmeister series." *Journal of Physics-Condensed Matter.* **20**, 494218, (2008).
15. M. Lund, R. Vacha and P. Jungwirth, "Specific Ion Binding to Macromolecules: Effects of Hydrophobicity and Ion Pairing." *Langmuir.* **24**, 3387-3391, (2008).
16. M. Lund, L. x. c. Vrbka and P. Jungwirth, "Specific Ion Binding to Nonpolar Surface Patches of Proteins." *J. Am. Chem. Soc.* **130**, 11582-11583, (2008).
17. J. Heyda, T. Hrobarik and P. Jungwirth, "Ion-Specific Interactions between Halides and Basic Amino Acids in Water." *J Phys Chem A.* **113**, 1969-1975, (2009).
18. P. E. Mason, C. E. Dempsey, L. Vrbka, J. Heyda, J. W. Brady and P. Jungwirth, "Specificity of Ion-Protein Interactions: Complementary and Competitive Effects of Tetrapropylammonium, Guanidinium, Sulfate, and Chloride Ions." *Journal of Physical Chemistry B.* **113**, 3227-3234, (2009).

19. N. Vlachy, B. Jagoda-Cwiklik, R. Vácha, D. Touraud, P. Jungwirth and W. Kunz, "Hofmeister series and specific interactions of charged headgroups with aqueous ions." *Advances in Colloid and Interface Science.* **146**, 42-47, (2009).
20. M. J. Krisch, R. D'Auria, M. A. Brown, D. J. Tobias, C. Hemminger, M. Ammann, D. E. Starr and H. Bluhm, "The Effect of an Organic Surfactant on the Liquid-Vapor Interface of an Electrolyte Solution." *The Journal of Physical Chemistry C.* **111**, 13497-13509, (2007).
21. P. B. Petersen, R. J. Saykally, M. Mucha and P. Jungwirth, "Enhanced concentration of polarizable anions at the liquid water surface: SHG spectroscopy and MD simulations of sodium thiocyanide." *Journal of Physical Chemistry B.* **109**, 10915-10921, (2005).
22. P. Viswanath and H. Motschmann, "Oriented thiocyanate anions at the air-electrolyte interface and its implications on interfacial water - A vibrational sum frequency spectroscopy study." *Journal of Physical Chemistry C.* **111**, 4484-4486, (2007).
23. P. Viswanath and H. Motschmann, "Effect of interfacial presence of oriented thiocyanate on water structure." *Journal of Physical Chemistry C.* **112**, 2099-2103, (2008).
24. P. B. Petersen and R. J. Saykally, "Probing the interfacial structure of aqueous electrolytes with femtosecond second harmonic generation spectroscopy." *Journal of Physical Chemistry B.* **110**, 14060-14073, (2006).
25. B. D. Casson, R. Braun and C. D. Bain, "Phase transitions in monolayers of medium-chain alcohols on water studied by sum-frequency spectroscopy and ellipsometry." *Faraday Discussions.* 209-229, (1996).
26. P. B. Petersen and R. J. Saykally, "Confirmation of enhanced anion concentration at the liquid water surface." *Chemical Physics Letters.* **397**, 51-55, (2004).
27. P. B. Petersen, J. C. Johnson, K. P. Knutsen and R. J. Saykally, "Direct experimental validation of the Jones-Ray effect." *Chemical Physics Letters.* **397**, 46-50, (2004).
28. P. B. Petersen and R. J. Saykally, "Adsorption of ions to the surface of dilute electroyte solutions: The Jones-Ray effect revisited." *Journal of the American Chemical Society.* **127**, 15446-15452, (2005).
29. P. B. Petersen and R. J. Saykally, "Is the liquid water surface basic or acidic? Macroscopic vs. molecular-scale investigations." *Chemical Physics Letters.* **458**, 255-261, (2008).
30. B. D. Casson and C. D. Bain, "Determination of the optical properties of monolayers on water." *Langmuir.* **13**, 5465-5469, (1997).
31. S. Z. Can, D. D. Mago, O. Esenturk and R. A. Walker, "Balancing Hydrophobic and Hydrophilic Forces at the Water/Vapor Interface: Surface Structure of Soluble Alcohol Monolayers." *The Journal of Physical Chemistry C.* **111**, 8739-8748, (2007).
32. A. Renault, J. F. Legrand, M. Goldmann and B. Berge, "Surface Diffraction Studies of 2d Crystals of Short Fatty Alcohols at the Air-Water-Interface." *Journal De Physique II.* **3**, 761-766, (1993).
33. J. F. Legrand, A. Renault, O. Konovalov, E. Chevigny, J. Als-Nielsen, G. Grübel and B. Berge, "X-ray grazing incidence studies of the 2D crystallization of monolayers of 1-alcohols at the air-water interface." *Thin Solid Films.* **248**, 95-99, (1994).
34. R. Braun, B. D. Casson and C. D. Bain, "A Sum-Frequency Study of the 2-Dimensional Phase-Transition in a Monolayer of Undecanol on Water." *Chemical Physics Letters.* **245**, 326-334, (1995).

35. P. Jungwirth and D. J. Tobias, "Molecular Structure of Salt Solutions: A New View of the Interface with Implications for Heterogeneous Atmospheric Chemistry." *The Journal of Physical Chemistry B.* **105**, 10468-10472, (2001).
36. L. X. Dang, "Computational Study of Ion Binding to the Liquid Interface of Water." *The Journal of Physical Chemistry B.* **106**, 10388-10394, (2002).
37. H. Wang, E. Borguet and K. B. Eisenthal, "Generalized Interface Polarity Scale Based on Second Harmonic Spectroscopy." *The Journal of Physical Chemistry B.* **102**, 4927-4932, (1998).
38. H. T. Bian, R. R. Feng, Y. Y. Xu, Y. Guo and H. F. Wang, "Increased interfacial thickness of the NaF, NaCl and NaBr salt aqueous solutions probed with non-resonant surface second harmonic generation (SHG)." *Physical Chemistry Chemical Physics.* **10**, 4920-4931, (2008).
39. M. Washabaugh and K. Collins, "The systematic characterization by aqueous column chromatography of solutes which affect protein stability." *J. Biol. Chem.* **261**, 12477-12485, (1986).
40. J. Cheng, C. D. Vecitis, M. R. Hoffmann and A. J. Colussi, "Experimental anion affinities for the air/water interface." *Journal of Physical Chemistry B.* **110**, 25598-25602, (2006).
41. A. Kalra, N. Tugcu, S. M. Cramer and S. Garde, "Salting-In and Salting-Out of Hydrophobic Solutes in Aqueous Salt Solutions." *The Journal of Physical Chemistry B.* **105**, 6380-6386, (2001).
42. S. Ghosal, J. C. Hemminger, H. Bluhm, B. S. Mun, E. L. D. Hebenstreit, G. Ketteler, D. F. Ogletree, F. G. Requejo and M. Salmeron, "Electron Spectroscopy of Aqueous Solution Interfaces Reveals Surface Enhancement of Halides." *Science.* **307**, 563-566, (2005).

Chapter 3

Measurement of bromide ion affinities for the air/water and dodecanol/water interfaces at molar concentrations by UV-SHG spectroscopy

3.1 Introduction

The adsorption of monovalent inorganic ions to interfaces formed by aqueous solutions with air, hydrocarbons, surfactants, and proteins is a phenomenon of central interest to broad areas of science.[1, 2] For example, halides at the interfaces of aqueous aerosols appear to play an important role in atmospheric chemistry.[3, 4] In particular, interfacially adsorbed bromide appears to be actively involved in ozone depletion. The rate of reaction of interfacial bromide with ozone is at least comparable to and may be much greater than the corresponding rate in the bulk.[5] Measurements of molecular bromine, a product of this reaction, correlate with ozone depletion in the Arctic[6-8] and at mid-latitudes.[9-14] Moreover, the adsorption of aqueous ions to hydrophobic and hydrophilic groups of biomolecules affects many biological processes. Hofmeister famously sequenced a number of salts in terms of how effectively they solubilize egg white protein,[15] and it is generally agreed that Hofmeister effects are caused by ion-protein interactions,[16-18] but a complete description of the mechanism remains elusive.

Recent work has firmly established the existence of enhanced concentrations of specific ions at the air/water interface.[19-22] Image charge repulsion, an electrostatic force driving ions away from the interface, has long been invoked to explain surface tension results indicating that the interface is largely devoid of inorganic ions.[23] Although it is now clear that this description of the interface is incorrect for many ions, this electrostatic force is still an important component of a mechanistic explanation. Molecular dynamics (MD) simulations have suggested that large anion polarizability leads to surface adsorption,[22] but experimentally the two properties do not appear to be entirely correlated,[24] A "law of matching water affinities" has been suggested, wherein ions of similar hydration strength tend to bind together as contact ion pairs.[25] MD simulations have shown a tendency for weakly solvated anions to adsorb to hydrophobic regions, while smaller, strongly solvated anions prefer to adsorb to a positive charge, implying that multiple adsorption mechanisms are involved in ion-protein interactions. Another recent MD study finds that when the surface plane is allowed to distort an energy minimum can exist for an ion at a polar liquid/vapor interface, originating from a competition between strong and opposing electrostatic and entropic forces.[26] This theory demonstrates that the presence and magnitude of the energy minimum is strongly dependent on the size and charge of the ion, but the near-cancellation of the driving forces makes it difficult to use simulations to reliably predict details of specific ion adsorption.

While the adsorption mechanism is not yet clearly understood, numerous experimental methods have been used to assess ion adsorption to aqueous interfaces. Surface tension measurements have quantified relative affinities of a large selection of ions at the air/water interface.[27, 28] Electrospray ionization mass spectrometry was used to assess trends in ionic properties of ions that were ejected from water droplets.[24] A depth profile of relative halide concentration has been measured using x-ray photoelectron spectroscopy (XPS) by varying the photoelectron kinetic energy, finding that the concentration of bromide is enhanced at the air/water interface, while chloride is not.[21, 29] XPS has also demonstrated that the iodide concentration is enhanced at the air/water interface, but that the effect is suppressed at the butanol/water interface.[21, 30]

Second-order nonlinear spectroscopy studies comprise a large subset of experimental work at aqueous interfaces, as it is inherently sensitive to broken inversion symmetry at both the macroscopic and microscopic scales. Vibrational sum frequency generation (VSFG) experiments probing the –OH stretching region at the air/water interface have indicated enhanced surface concentrations of bromide and iodide,[19] but recently the development of phase-sensitive VSFG has called the interpretation of previous VSFG experiments into question.[31, 32] Phase-sensitive VSFG has been used to characterize the interface of basic and acidic solutions, as well as that of sodium iodide.[33] VSFG has also been used to directly measure the vibrational spectrum of thiocyanide at an air/water interface.[34, 35] A Hofmeister-like series was established using VSFG for ion adsorption to a macromolecule/water interface.[36] Non-resonant second harmonic generation (SHG) has been used to postulate that the interfacial thickness, the depth of broken inversion symmetry, increases linearly with salt concentration.[37] The presence of ions at the air/water[20, 38-40, 22, 41-43] and alcohol/water[44] interfaces has been directly confirmed via resonant SHG.

In this paper the adsorption of the weakly chaotropic bromide anion to both the air/water interface and an alcohol/water interface is addressed using UV SHG. Like VSFG, SHG, is a second-order nonlinear process that is interface specific due to symmetry considerations. The charge-transfer-to-solvent (CTTS) band of the anion, located deep in the UV, is utilized as a two-photon resonance to both enhance the SHG signal and to selectively probe the anion. A modified Langmuir adsorption model is used to determine the Gibbs free energy of ion adsorption to the interface, and these interfacial affinities are put into context by comparing with other relevant studies.

3.2 Experimental Methods

A. Experimental Details. All glassware was cleaned using Nochromix dissolved in concentrated sulfuric acid and rinsed with 18.2 MΩ water (Millipore MilliQ A10). Solutions were made with 18.2 MΩ water and NaBr (Sigma-Aldrich, >99.0%) which was baked in a tube furnace under nitrogen at 500°C for eight hours. NaBr used without further purification yielded different results than baked NaBr, which is likely due to organic contaminants.[37] Some solutions were also filtered using a polyvinylidene fluoride filter (Millipore GVWP01300) that was thoroughly rinsed with water and an all glass filter assembly; these solutions behaved similarly to those that were not filtered. The alcohol monolayer was prepared on the solution surface by floating a 1-dodecanol (Sigma-Aldrich, 98%) crystal on the solution surface, as described by Casson et al.[45] All samples were prepared and measured at room temperature.

The laser system has been described in detail previously.[38] Briefly, a regenerative amplifier (Spectra-Physics Spitfire, 1 kHz, 100 fs) seeded by a home-built Ti:sapphire oscillator is used to pump an optical parametric amplifier (OPA, Quantronix TOPAS). The tunable output of the OPA is used as the fundamental beam. The fundamental intensity is continuously modulated by a motorized neutral density filter. Less than 10% of the modulated fundamental is directed to a photodiode as a reference pulse energy measurement. The p-polarized fundamental is focused onto the sample surface at an angle of incidence of 60° relative to the surface normal. The pulse energy density at the interface is less than 0.3 $J \cdot cm^{-2}$ per pulse. The p-polarized SHG light is collected in the reflection geometry and separated from the fundamental with a series of dichroic mirrors and a monochromator (PI Acton, Spectra Pro SP-2155) before being detected by a solar-blind PMT (Hammamatsu, R7154PHA). The observed signal intensities are on the order of 0.01 photons per pulse.

As SHG is a second order process, the signal intensity is proportional to the square of the fundamental intensity,

$$I_{SHG} = \left|\chi^{(2)}_{effective}\right|^2 I^2_{fundamental} \qquad [3.1]$$

where, $\chi^{(2)}_{effective}$ is the observed second-order nonlinear susceptibility of the system. The reference pulse energy (R) is binned into groups of $R^2 \pm \Delta$, and the number of pulses where zero photons are detected, $N^{k=0}_{pulses}$, is counted. Poisson statistics are assumed for the distribution of SHG photons detected for each pulse, and the average number of photons for a given $R^2 \pm \Delta$ bin can be evaluated as

$$\langle k \rangle = -\ln\left[\frac{N^{k=0}_{pulses}}{N^{total}_{pulses}}\right]_{R^2 \pm \Delta} . \qquad [3.2]$$

Plotting this value versus R^2 provides a linear relationship. The slope of the resulting line, determined by a variance-weighted least-squares fit, is taken as the system response constant, proportional to $\left|\chi^{(2)}_{effective}\right|^2$. This also provides an inherent confirmation that the SHG signal exhibits the correct second-order power dependence.

B. Surface Adsorption Model. In order to determine thermodynamic quantities from the SHG signal an of aqueous solution interface, a modified Langmuir adsorption model is used. The model used here has been described in detail elsewhere[38, 41, 44] and an overview is given here. The solution is partitioned into interfacial and bulk regions, and is assumed to obey the equilibrium expression

$$S_S + N_B \rightleftharpoons S_B + N_S . \qquad [3.3]$$

S_i is the solvent species and N_i is the solute species, while the subscripts $i = B$ and S indicate that the species resides in the bulk and surface partitions, respectively.

The effective nonlinear susceptibility can be separated into the solvent and the solute contributions, each with complex phase and is parameterized as

$$\left|\chi^{(2)}_{effective}\right|^2 = \left|A + (B + iC)N_S\right|^2 \qquad [3.4]$$

where the relative phase of the response of the neat solvent, A, is defined such it is entirely real. The molecular response parameters of the solute species, B and C, can grow large when in resonance with the CTTS band. This effective molecular response is governed by the effective hyperpolarizability, a third rank tensor averaged over molecular orientations.

The number density of surface solute species can be written in terms of the bulk solute concentration:

$$N_S = \frac{N_S^{\max}[N_B]}{[N_B] + [H_2O]/K} . \qquad [3.5]$$

Here $N_S^{\max}$ is the number of surface sites and $K = \exp\left[-\Delta G_{ads}/RT\right]$. ΔG_{ads} is the Gibbs free energy change of replacing an interfacial solvent species with a solute species. This if the concentration dependence of the SHG signal is measured this free energy can be determined by a fit of parameters A, B, and C.

3.3 The Air/water Interface

The bromide CTTS absorption maximum in the bulk is centered near 200 nm.[46] The SHG signal is plotted as a function of bulk sodium bromide concentration in Figure 3.1a for SHG

wavelengths of 265 nm and 193 nm for the air/water interface. The SHG response is normalized such that the response of neat water is unity. Note that the concentration range spans from 6 mM to 7 M concentrations, and that at both 193 nm and 265 nm the response at 6 mM is less than that of neat water, indicative of destructive interference between the water response and the bromide response at low concentrations (discussed in a future publication). The observed SHG signal is weak relative to a similar ion, iodide; the maximum SHG response of bromide is just twice that of water, whereas for iodide it is 12 times the water response.

A valuable comparison is a non-resonant SHG study by Wang et al.[37] For bromide, chloride, and fluoride they find that the non-resonant signal (SHG = 400 nm) increases linearly with salt concentration, ascribing this to thickening of the interfacial region. The 265 nm data presented here can be fit quite reasonably with a linear model, indicating that this wavelength is non-resonant. However, the 193nm data do not fit to a linear model; the data are clearly super-linear. We thus conclude that the 193 nm data exhibit a weak resonant enhancement.

The CTTS band of surface bromide anions could be shifted from its known bulk value,[47] explaining the weakness of the SHG response at 193 nm. Previous SHG studies at the air/water interface found a small red shift of the surface CTTS band relative to the bulk spectrum,[41] which would indicate a shift away from 193 nm for bromide. However, the SHG response of 7 M (nearly saturated) NaBr was measured at 205 nm and 210 nm, and both were found to be in between the response at 193 nm and 265 nm (see Table 3.1). Therefore, it is unlikely that such a shift in the CTTS band is the cause of the weakness of the observed SHG signal.

Table 3.1.

Wavelength (nm)	Normalized SHG response
193	2.07
205	1.84
210	1.84
265	1.76

The strength of the effective hyperpolarizability may also explain the weak bromide response. Bromide, being a smaller and less polarizable ion than iodide, will have a smaller effective hyperpolarizability and thus a weaker SHG response. Measurements of the Hyper-Rayleigh scattering (HRS) of a 5 M aqueous sodium bromide solution has indicated that the magnitude of the bromide hyperpolarizability is relatively small, supporting the suggestion that the weak response may simply be due to a relatively weak chromophore.[37] For comparison, the SHG response of both bromide and iodide are weak relative to thiocyanide ($SHG_{max} \approx 200$ times water). As thiocyanide exhibits broken inversion symmetry on the molecular scale, it has a much larger effective hyperpolarizability than the spherical halides. The relatively weak effective hyperpolarizability of bromide in comparison to iodide may be further exasperated by the solvation structures of these ions at the interface. MD simulations show that bromide ions are less exposed, or better solvated, at the interface than iodide.[48, 49] In such a case we can envision that the symmetry of the more-desolvated iodide ion will be broken more severely than that of the bromide, even if the molecular response would otherwise be equal. Therefore, the interfacial structure may enhance the response of iodide more than that of bromide without any net difference in number density.

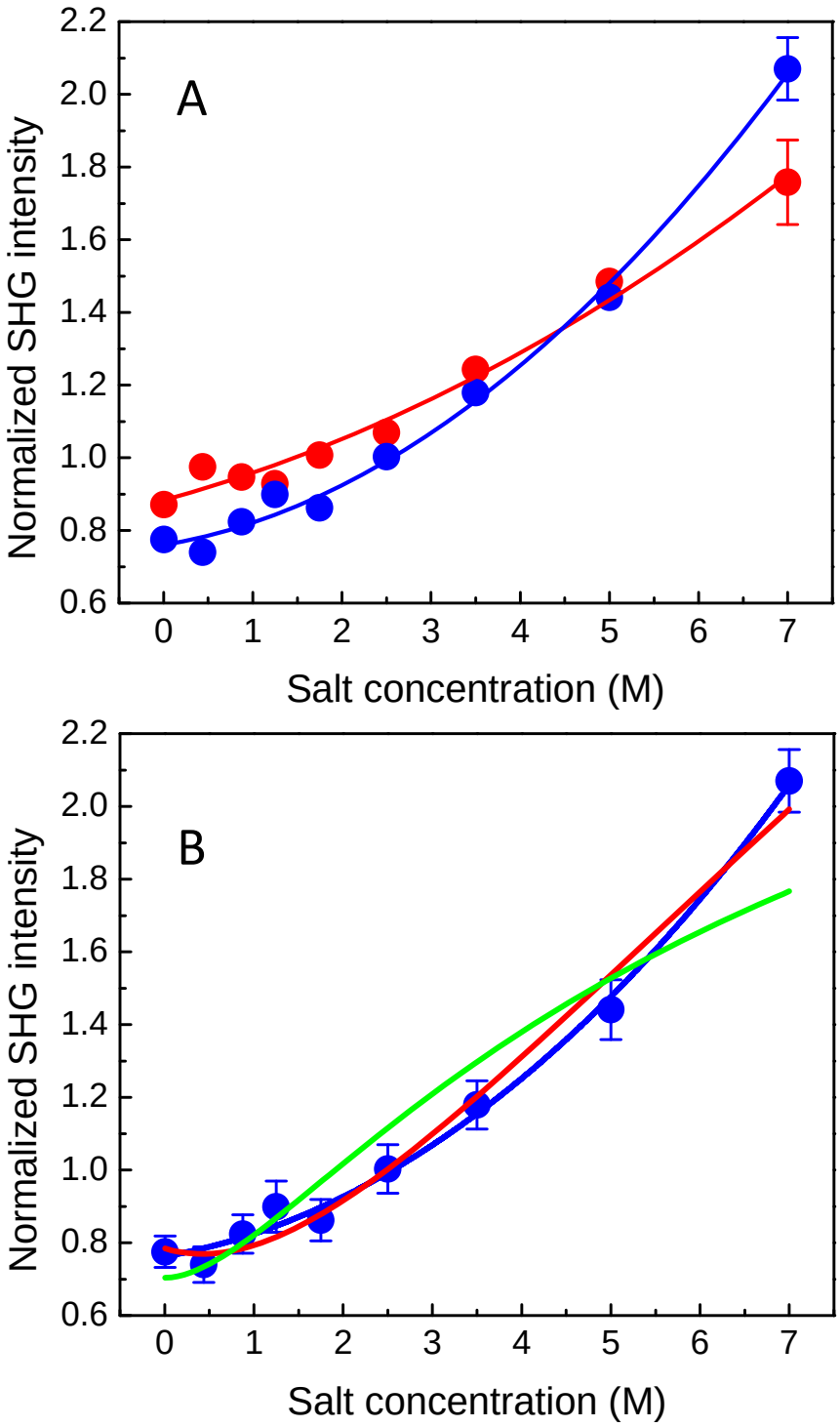

Figure 3.1. (a) The SHG intensity (• 193 nm and • 265 nm) of bromide at the air/water interface normalized to the neat water response as a function of concentration. The lines are the Langmuir isotherm fit to the data. The concentration ranges from 6 mM to 7 M. (b) A comparison of Langmuir isotherm fits to the data (only • 193 nm is pictured) with the free energy of adsorption unconstrained, ΔG_{ads} = -1.4 kJ/mol (—), and constrained to values of -4 (—) and -7 kJ/mol (—). The -4 kJ/mol fit approximates the data, but the data are not well-represented by the -7 kJ/mol fit.

Finally, the number of ions at the interface may explain the weaker SHG signal of bromide. For the molar concentration regime the Langmuir isotherm fit to the bromide data gives an equilibrium constant, K = 1.8 ± 2, corresponding to a free energy of -1.4 kJ/mol. However, discussing the associated error in the latter is problematic since a negative equilibrium constant is non-physical. Therefore, the positive limit for the free energy cannot be determined from these data. The inability to determine a positive limit is a manifestation of the simple model used and has been discussed previously.[42] The negative limit of the free energy can be calculated, however, yielding a 90% confidence limit of $\Delta G_{ads} \geq$ -4.1 kJ/mol. Figure 3.1b shows the Langmuir isotherm fits at 193 nm when the free energy is constrained to -4 and -7 kJ/mol in comparison to the unconstrained fit and the experimental data. The -4 kJ/mol fit appears to be reasonable, considering the data and the associated error; however, the -7 kJ/mol fit does not match the experiment. This agrees well with the above calculated lower limit for the free energy. The free energy of iodide adsorption was previously determined to be consistent with both -3.3 and 0 kJ/mol, although no finite limits were given.[41] Based on these results, the relative number of surface bromide and iodide ions cannot be determined.

Previously, the adsorption of thiocyanide,[22] nitrate,[42] iodide,[41] and hydroxide[43] to the air/water interface were also studied by UV SHG for concentrations in the molar regime. The reported lower limit, best fit, and upper limit of the Gibbs free energy are reported in Table 3.2. Based on these results, it is not possible to order the free energies of these ions beyond noting that thiocyanide is the most strongly adsorbed. Compiling the results from other experimental techniques by Pegram and Record,[28] Cheng et al.,[24] and Ghosal et al.[21] yields the following sequence in order of decreasing interfacial affinity: $SCN^- > I^- > NO_3^- > Br^- > OH^-$. While not explicitly supporting this sequence, the SHG data can be considered consistent with these results.

Table 3.2.

anion	lower limit	ΔG_{ads} (kJ/mol)	upper limit	reference
SCN^-	-7.6	-7.5	-7.4	19
I^-	-3.3*	NA	0*	43
NO_3^-	-2	15	NA	39
Br^-	-4.1	-1.4	NA	
OH^-	-4	NA	NA	44

* the lower and upper limits are not statistically determined in this case. The data were said to bein agreement with either energy, and the actual limits are likely larger.

3.4 The Dodecanol/water Interface

The structure of the dodecanol/water interface has been well characterized. The dodecanol molecules are tightly packed with a surface area of 20 Å/molecule[50] while the aliphatic chains stand nearly vertical.[51, 52] This surface structure is largely unaffected by the presence of salt.[50] This leaves the hydroxyl terminus free to interact with the solvent via hydrogen bonding or to explicitly contribute to the solvation shell of an anion approaching the interfacial plane. VSFG demonstrated that there is little evidence of non-hydrogen bonded –OH groups at the alcohol/water interface.[53]

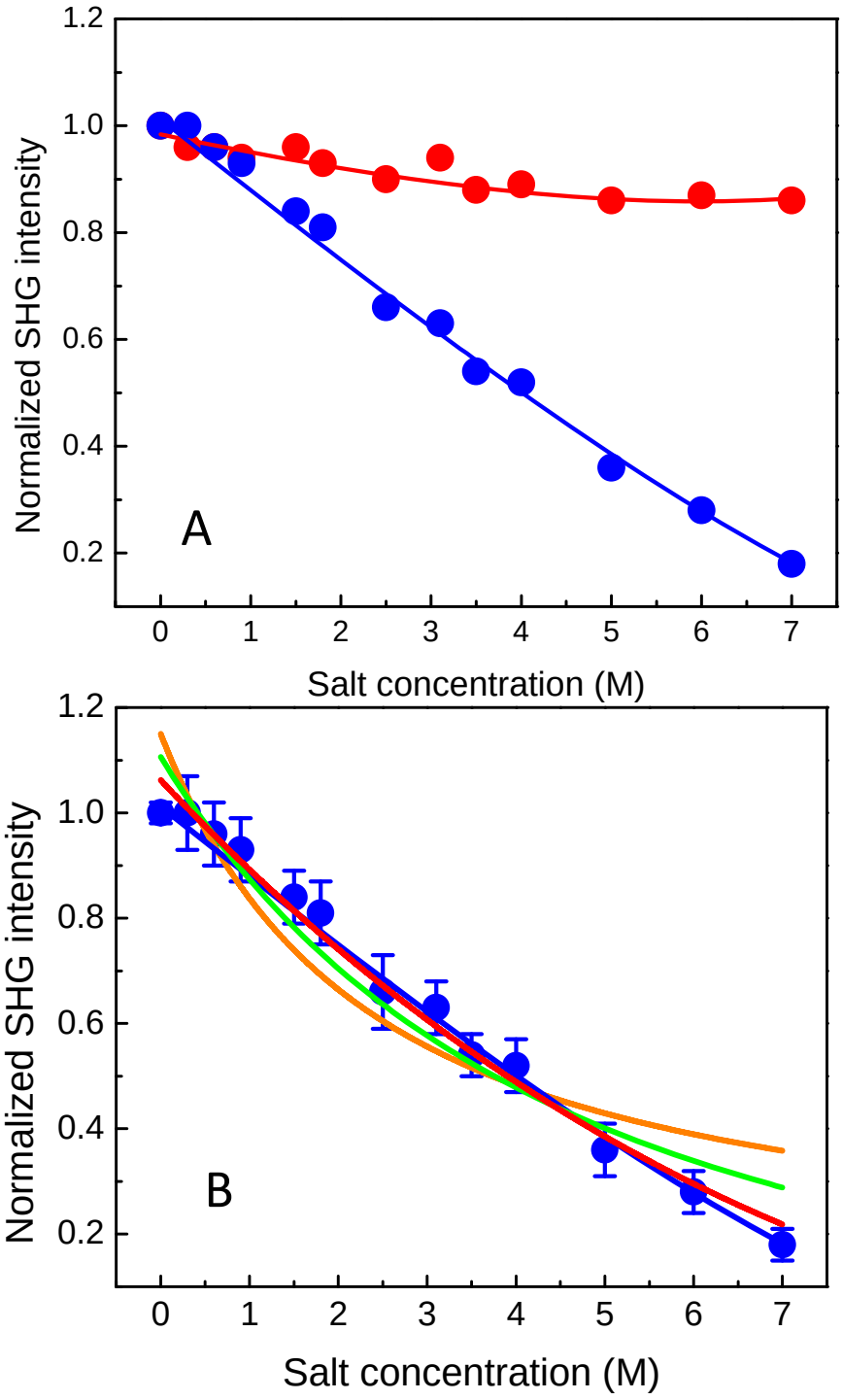

Figure 3.2. (a) The SHG intensity (• 193 nm and • 265 nm) of bromide at the dodecanol/water interface normalized to the water/dodecanol response as a function of concentration. The lines are the Langmuir isotherm fit to the data. The concentration ranges from 0 M to 7 M. (b) A comparison of Langmuir isotherm fits to the data (only • 193 nm is pictured) with the free energy of adsorption unconstrained, ΔG_{ads} = 8 kJ/mol (—), and constrained to values of -2 (—), -4 (—), and -7 kJ/mol (—). The -2 kJ/mol fit reasonably approximates the data, but the data is not well-represented by the -4 or -10 kJ/mol fits.

The SHG response of bromide at the dodecanol/water interface is out of phase with the water/dodecanol response, and thus initially decreases as a function of increasing concentration (see Figure 3.2a). The ratio of the non-resonant SHG response at the dodecanol/water interface and the air/water interface is 3.2 to 1 at both 193 nm and 265 nm, demonstrating a significantly stronger resonant enhancement of the SHG signal at the dodecanol/water interface than at the air/water interface. Calculating the resonant enhancement as

$$\delta = \frac{\Delta SHG_{193}}{\Delta SHG_{265}} \quad , \qquad [3.6]$$

where ΔSHG is the change in SHG from the lowest to highest concentration, the enhancement factor is nearly six at the dodecanol/water interface, but only 1.5 at the air/water interface.

There are two potential explanations for the increased resonant response. First, different interfacial structures may yield different effective hyperpolarizabilities, as discussed earlier. However, in this case the contribution of the hydroxyl group of dodecanol to the solvation shell of interfacial bromide may present a different local environment to the ion than at the air/water interface. If the spherical shape of bromide is deformed more on average at the dodecanol/water interface than at the air/water interface, the correspondingly larger effective hyperpolarizability could explain the stronger resonant response.

The second possibility is that there are simply more bromide ions at the interface. This would indicate either that bromide is adsorbed more strongly, that there are more surface sites at the dodecanol/water interface, or some combination of both. The model used here does not explicitly establish the number of surface sites, so only the relative affinity of bromide for the two interfaces can be directly compared.

The Langmuir isotherm fit shown in Figure 3.2a yields a free energy of +8 kJ/mol. The uncertainty is large, and constraining the free energy to the lower limit of the uncertainty does not reproduce the shape of the data. Instead, a lower limit is estimated by plotting isotherms fitting the data with the free energy constrained to a specific value and judging the fidelity to the data. Similar to the air/water interface data, an upper limit cannot be determined. Decreasing the free energy near -4 kJ/mol, the isotherms progress from closely approximating the data to no longer reproducing the shape of the data. Isotherms are plotted for representative free energies in Figure 3.2b. Therefore, we estimate a lower limit of -4 kJ/mol to the free energy. Similar to its behavior at the air/water interface, bromide does not have a strong affinity for the dodecanol/water interface at molar bulk concentrations.

Based on the results presented here, it cannot be concluded whether the bromide interfacial affinity is greater for the air/water interface or the dodecanol/water interface. Considering the forces that determine the extent of surface adsorption, it is not clear to which interface stronger adsorption would be predicted. One of the major forces driving ions to the interface is the entropy gain due to hydrophobic exclusion of the ion. At the dodecanol/water interface this force is weaker because even ions at the interface disrupt the hydrogen bonding network. However, the electrostatic force associated with image charge repulsion, the major force inhibiting ion adsorption, should also be weaker at the dodecanol/water interface, since the dispersion forces of the alkyl chains can screen the ionic charges from their images much better than the low-dielectric vapor. A recent MD simulation addressing ion adsorption at the air/water interface emphasized the importance of interfacial flexibility on interfacial ion adsorption.[26] This is particularly interesting, considering that the dodecanol/water interface will be considerably less easily deformed than the air/water interface.

The adsorption of thiocyanide to both the air/water[22] and dodecanol/water[44] interfaces can also be considered. Thiocyanide adsorbed to both interfaces more strongly than bromide, -7.5 kJ/mol in the case of air/water and -6.7 kJ/mol in the case of dodecanol/water. Similar to bromide, the difference in the affinity of thiocyanide to the air/water and dodecanol/water interfaces is within the error of the measurement. In contrast to the bromide results, the maximum thiocyanide SHG response is an order of magnitude weaker at the dodecanol/water interface (20 times water) than at the air/water interface (200 times water). The effective hyperpolarizability is strongly dependent on the orientation of the ions at the interface. As thiocyanide is not spherically symmetric, it is likely that the average ion orientation is different at aqueous interfaces with vapor and dodecanol. Since the strength of adsorption is similar for thiocyanide at the air/water and dodecanol/water interfaces, the change in average ion orientation and possibly fewer surface sites must account for the weaker SHG signal at the dodecanol/water interface.

Another experimental technique has also been used to compare ion interfacial affinities to air/water and alcohol/water interfaces. XPS depth profiling of potassium iodide indicates a weaker concentration enhancement of iodide at the air/butanol/water interface than at the air/water interface.[21, 30] The dodecanol/water interface is much more rigid than the butanol/water interface, generally presenting the hydrophilic –OH to the liquid. The butanol exposes a much greater proportion of hydrophobic sites to water at the interface, so the experiments are not directly comparable. It would be interesting to compare a SHG study of iodide at the dodecanol/water interface to these XPS results and to compare an XPS study of bromide and thiocyanide to the SHG results.

3.5 Conclusions

The structure of a liquid interface exerts a strong effect on the observed SHG response of adsorbed anions. Bromide exhibits only a very weak resonant response at the air/water interface, but the response is significantly stronger at the alcohol/water interface. Both the number of ions at the interface and their effective hyperpolarizability are expected to contribute to this effect, but more detailed conclusions cannot be made.

At molar concentrations the bromide anion shows at most a weak affinity for both the air/water and alcohol/water interfaces at molar concentrations. Using a modified Langmuir adsorption model, the lower 90% confidence limit of the Gibbs free energy of adsorption is -4.1 kJ/mol at the air/water interface with a best fit of -1.4 kJ/mol. Similarly, at the dodecanol/water interface the lower limit is near -4 kJ/mol, but with a best fit of +8 kJ/mol. No upper limit to the free energy could be determined for either interface. Measuring the full CTTS spectrum via SHG would allow for a more detailed understanding of ion adsorption. However, under the current experimental arrangement acquiring a detailed spectrum for a range of concentrations is prohibitively time-consuming. Regardless of its actual surface affinity, bromide ions are clearly present in detectable numbers at both the air/water and surfactant/water interfaces, consistent with atmospheric studies that indicate a high concentration of reactive halides at aqueous droplet interfaces.

3.6 References

1. P. B. Petersen and R. J. Saykally, "On the nature of ions at the liquid water surface." *Annual Review of Physical Chemistry.* **57**, 333-364, (2006).
2. P. Jungwirth and B. Winter, "Ions at aqueous interfaces: From water surface to hydrated proteins." *Annual Review of Physical Chemistry.* **59**, 343-366, (2008).
3. J. H. Hu, Q. Shi, P. Davidovits, D. R. Worsnop, M. S. Zahniser and C. E. Kolb, "Reactive Uptake of Cl2(G) and Br2(G) by Aqueous Surfaces as a Function of Br- and I- Ion Concentration - the Effect of Chemical-Reaction at the Interface." *Journal of Physical Chemistry.* **99**, 8768-8776, (1995).
4. E. M. Knipping, M. J. Lakin, K. L. Foster, P. Jungwirth, D. J. Tobias, R. B. Gerber, D. Dabdub and B. J. Finlayson-Pitts, "Experiments and Simulations of Ion-Enhanced Interfacial Chemistry on Aqueous NaCl Aerosols." *Science.* **288**, 301-306, (2000).
5. S. W. Hunt, M. Roeselova, W. Wang, L. M. Wingen, E. M. Knipping, D. J. Tobias, D. Dabdub and B. J. Finlayson-Pitts, "Formation of Molecular Bromine from the Reaction of Ozone with Deliquesced NaBr Aerosol: Evidence for Interface Chemistry." *The Journal of Physical Chemistry A.* **108**, 11559-11572, (2004).
6. G. A. Impey, P. B. Shepson, D. R. Hastie, L. A. Barrie and K. G. Anlauf, "Measurements of photolyzable chlorine and bromine during the Polar sunrise experiment 1995." *Journal of Geophysical Research-Atmospheres.* **102**, 16005-16010, (1997).
7. K. L. Foster, R. A. Plastridge, J. W. Bottenheim, P. B. Shepson, B. J. Finlayson-Pitts and C. W. Spicer, "The role of Br-2 and BrCl in surface ozone destruction at polar sunrise." *Science.* **291**, 471-474, (2001).
8. C. W. Spicer, R. A. Plastridge, K. L. Foster, B. J. Finlayson-Pitts, J. W. Bottenheim, A. M. Grannas and P. B. Shepson, "Molecular halogens before and during ozone depletion events in the Arctic at polar sunrise: concentrations and sources." *Atmospheric Environment.* **36**, 2721-2731, (2002).
9. R. R. Dickerson, K. P. Rhoads, T. P. Carsey, S. J. Oltmans, J. P. Burrows and P. J. Crutzen, "Ozone in the remote marine boundary layer: A possible role for halogens." *Journal of Geophysical Research-Atmospheres.* **104**, 21385-21395, (1999).
10. I. Nagao, K. Matsumoto and H. Tanaka, "Sunrise ozone destruction found in the sub-tropical marine boundary layer." *Geophysical Research Letters.* **26**, 3377-3380, (1999).
11. I. E. Galbally, S. T. Bentley and C. P. Meyer, "Mid-latitude marine boundary-layer ozone destruction at visible sunrise observed at Cape Grim, Tasmania, 41 degrees 5." *Geophysical Research Letters.* **27**, 3841-3844, (2000).
12. V. Matveev, M. Peleg, D. Rosen, D. S. Tov-Alper, K. Hebestreit, J. Stutz, U. Platt, D. Blake and M. Luria, "Bromine oxide - ozone interaction over the Dead Sea." *Journal of Geophysical Research-Atmospheres.* **106**, 10375-10387, (2001).
13. J. Stutz, R. Ackermann, J. D. Fast and L. Barrie, "Atmospheric reactive chlorine and bromine at the Great Salt Lake, Utah." *Geophys. Res. Lett.* **29**, 1380, (2002).
14. U. Friess, J. Hollwedel, G. König-Langlo, T. Wagner and U. Platt, "Dynamics and chemistry of tropospheric bromine explosion events in the Antarctic coastal region." *J. Geophys. Res.* **109**, D06305, (2004).
15. F. Hofmeister, *Arch. Exptl. Pathol. Pharmakol.* **24**, 247-260, (1888).
16. K. D. Collins and M. W. Washabaugh, "The Hofmeister Effect and the Behavior of Water at Interfaces." *Quarterly Reviews of Biophysics.* **18**, 323-422, (1985).

17. M. G. Cacace, E. M. Landau and J. J. Ramsden, "The Hofmeister series: salt and solvent effects on interfacial phenomena." *Quarterly Reviews of Biophysics.* **30**, 241-277, (1997).
18. Y. Zhang and P. S. Cremer, "Interactions between macromolecules and ions: the Hofmeister series." *Current Opinion in Chemical Biology Model systems / Biopolymers.* **10**, 658-663, (2006).
19. D. F. Liu, G. Ma, L. M. Levering and H. C. Allen, "Vibrational Spectroscopy of aqueous sodium halide solutions and air-liquid interfaces: Observation of increased interfacial depth." *Journal of Physical Chemistry B.* **108**, 2252-2260, (2004).
20. P. B. Petersen, J. C. Johnson, K. P. Knutsen and R. J. Saykally, "Direct experimental validation of the Jones-Ray effect." *Chemical Physics Letters.* **397**, 46-50, (2004).
21. S. Ghosal, J. C. Hemminger, H. Bluhm, B. S. Mun, E. L. D. Hebenstreit, G. Ketteler, D. F. Ogletree, F. G. Requejo and M. Salmeron, "Electron spectroscopy of aqueous solution interfaces reveals surface enhancement of halides." *Science.* **307**, 563-566, (2005).
22. P. B. Petersen, R. J. Saykally, M. Mucha and P. Jungwirth, "Enhanced concentration of polarizable anions at the liquid water surface: SHG spectroscopy and MD simulations of sodium thiocyanide." *Journal of Physical Chemistry B.* **109**, 10915-10921, (2005).
23. L. Onsager and N. N. T. Samaras, "Surface tension of Debye-Huckel electrolytes." *Journal of Chemical Physics.* 528-536, (1934).
24. J. Cheng, C. D. Vecitis, M. R. Hoffmann and A. J. Colussi, "Experimental anion affinities for the air/water interface." *Journal of Physical Chemistry B.* **110**, 25598-25602, (2006).
25. K. D. Collins, "Ions from the Hofmeister series and osmolytes: effects on proteins in solution and in the crystallization process." *Methods.* **34**, 300-311, (2004).
26. J. Noah-Vanhoucke and P. L. Geissler, "On the fluctuations that drive small ions toward, and away from, interfaces between polar liquids and their vapors." *Proceedings of the National Academy of Sciences of the United States of America.* **106**, 15125-15130, (2009).
27. L. M. Pegram and M. T. Record, "Partitioning of atmospherically relevant ions between bulk water and the water/vapor interface." *Proceedings of the National Academy of Sciences of the United States of America.* **103**, 14278-14281, (2006).
28. L. M. Pegram and M. T. Record, "Hofmeister Salt Effects on Surface Tension Arise from Partitioning of Anions and Cations between Bulk Water and the Air-Water Interface." *J. Phys. Chem. B.* **111**, 5411-5417, (2007).
29. S. Ghosal, M. A. Brown, H. Bluhm, M. J. Krisch, M. Salmeron, P. Jungwirth and J. C. Hemminger, "Ion Partitioning at the Liquid/Vapor Interface of a Multicomponent Alkali Halide Solution: A Model for Aqueous Sea Salt Aerosols." *Journal of Physical Chemistry A.* **112**, 12378-12384, (2008).
30. M. J. Krisch, R. D'Auria, M. A. Brown, D. J. Tobias, J. C. Hemminger, M. Ammann, D. E. Starr and H. Bluhm, "The effect of an organic surfactant on the liquid-vapor interface of an electrolyte solution." *Journal of Physical Chemistry C.* **111**, 13497-13509, (2007).
31. V. Ostroverkhov, G. A. Waychunas and Y. R. Shen, "New Information on Water Interfacial Structure Revealed by Phase-Sensitive Surface Spectroscopy." *Physical Review Letters.* **94**, 046102, (2005).
32. N. Ji, V. Ostroverkhov, C.-Y. Chen and Y.-R. Shen, "Phase-Sensitive Sum-Frequency Vibrational Spectroscopy and Its Application to Studies of Interfacial Alkyl Chains." *J. Am. Chem. Soc.* **129**, 10056-10057, (2007).

33. C. S. Tian and Y. R. Shen, "Sum-frequency vibrational spectroscopic studies of water/vapor interfaces." *Chemical Physics Letters.* **470**, 1-6, (2009).
34. P. Viswanath and H. Motschmann, "Oriented thiocyanate anions at the air-electrolyte interface and its implications on interfacial water - A vibrational sum frequency spectroscopy study." *Journal of Physical Chemistry C.* **111**, 4484-4486, (2007).
35. P. Viswanath and H. Motschmann, "Effect of interfacial presence of oriented thiocyanate on water structure." *Journal of Physical Chemistry C.* **112**, 2099-2103, (2008).
36. X. Chen, T. Yang, S. Kataoka and P. S. Cremer, "Specific ion effects on interfacial water structure near macromolecules." *Journal of the American Chemical Society.* **129**, 12272-12279, (2007).
37. H. T. Bian, R. R. Feng, Y. Y. Xu, Y. Guo and H. F. Wang, "Increased interfacial thickness of the NaF, NaCl and NaBr salt aqueous solutions probed with non-resonant surface second harmonic generation (SHG)." *Physical Chemistry Chemical Physics.* **10**, 4920-4931, (2008).
38. P. B. Petersen and R. J. Saykally, "Confirmation of enhanced anion concentration at the liquid water surface." *Chemical Physics Letters.* **397**, 51-55, (2004).
39. P. B. Petersen and R. J. Saykally, "Adsorption of ions to the surface of dilute electroyte solutions: The Jones-Ray effect revisited." *Journal of the American Chemical Society.* **127**, 15446-15452, (2005).
40. P. B. Petersen and R. J. Saykally, "Evidence for an enhanced hydronium concentration at the liquid water surface." *Journal of Physical Chemistry B.* **109**, 7976-7980, (2005).
41. P. B. Petersen and R. J. Saykally, "Probing the interfacial structure of aqueous electrolytes with femtosecond second harmonic generation spectroscopy." *Journal of Physical Chemistry B.* **110**, 14060-14073, (2006).
42. D. E. Otten, P. B. Petersen and R. J. Saykally, "Observation of nitrate ions at the air/water interface by UV-second harmonic generation." *Chemical Physics Letters.* **449**, 261-265, (2007).
43. P. B. Petersen and R. J. Saykally, "Is the liquid water surface basic or acidic? Macroscopic vs. molecular-scale investigations." *Chemical Physics Letters.* **458**, 255-261, (2008).
44. R. M. Onorato, D. E. Otten and R. J. Saykally, "Adsorption of thiocyanate ions to the dodecanol/water interface characterized by UV second harmonic generation." *Proceedings of the National Academy of Sciences.* **106**, 15176-15180, (2009).
45. B. D. Casson, R. Braun and C. D. Bain, "Phase transitions in monolayers of medium-chain alcohols on water studied by sum-frequency spectroscopy and ellipsometry." *Faraday Discussions.* 209-229, (1996).
46. M. J. Blandamer and M. F. Fox, "Theory and applications of charge-transfer-to-solvent spectra." *Chem. Rev.* **70**, 59-93, (1970).
47. H. F. Wang, E. Borguet and K. B. Eisenthal, "Generalized interface polarity scale based on second harmonic spectroscopy." *Journal of Physical Chemistry B.* **102**, 4927-4932, (1998).
48. P. Jungwirth and D. J. Tobias, "Ions at the air/water interface." *Journal of Physical Chemistry B.* **106**, 6361-6373, (2002).
49. P. Jungwirth and D. J. Tobias, "Specific Ion Effects at the Air/Water Interface." *Chem. Rev.* **106**, 1259-1281, (2006).

50. B. D. Casson and C. D. Bain, "Determination of the optical properties of monolayers on water." *Langmuir.* **13**, 5465-5469, (1997).
51. A. Renault, J. F. Legrand, M. Goldmann and B. Berge, "Surface Diffraction Studies of 2d Crystals of Short Fatty Alcohols at the Air-Water-Interface." *Journal De Physique II.* **3**, 761-766, (1993).
52. J. F. Legrand, A. Renault, O. Konovalov, E. Chevigny, J. Alsnielsen, G. Grubel and B. Berge, "X-Ray Grazing-Incidence Studies of the 2d Crystallization of Monolayers of 1-Alcohols at the Air-Water-Interface." *Thin Solid Films.* **248**, 95-99, (1994).
53. C. D. Stanners, Q. Du, R. P. Chin, P. Cremer, G. A. Somorjai and Y.-R. Shen, "Polar ordering at the liquid-vapor interface of n-alcohols (C1-C8)." *Chemical Physics Letters.* **232**, 407-413, (1995).

Chapter 4

Halides strongly adsorb to the air/water interface of millimolar aqueous solutions

4.1 Introduction

The presence of high concentrations of halide anions at the vapor interface of aqueous solutions has been recently established by both theory and experiment.[1-9] This is contrary to the model of Onsager and Samaras, posited in 1934, that invokes the method of images in predicting that the interface is primarily devoid of ions.[10] Less than one year later, Jones and Ray measured a minimum in the surface tension of potassium chloride, indicating a surface excess at low concentrations.[11] In that and four later publications, they demonstrated surface tension minima in the millimolar regime of 13 inorganic salts.[12-15] The effect appeared to be dependent on both the anion and the cation. Langmuir disputed their results as an experimental artifact,[16] but Dole and Swartout used a method that would not exhibit this artifact to measure the surface tension, and also found a minimum for potassium chloride.[17] Despite subsequent efforts to both support and debunk the Jones-Ray effect, it had remained a largely unexplained anomaly until the current resurgence of interest in inorganic ions at aqueous interfaces.

Dating back to the early 1990s, laboratory experiments and theoretical studies predicted that bromide and chloride ions at aqueous interfaces play an important role in atmospheric chemistry.[18, 1, 2] Meanwhile, ground-level and atmospheric measurements of molecular bromine, a byproduct of the reaction of bromide with ozone, show a correlation with ozone depletion.[19-27] This incited a flourish of experimental and theoretical work characterizing the presence of inorganic ions to aqueous interfaces, as reviewed elsewhere.[28, 29] Notably, the presence of halides at the interface has been demonstrated via vibrational sum-frequency generation (VSFG),[3, 5] second harmonic generation (SHG),[4, 8] x-ray photoelectron spectroscopy (XPS),[6, 9] and electrospray ionization mass spectrometry.[7] Generally, it appears that halide affinity for the interface increases with increasing ionic radii.

Most of this work has been carried out at high concentrations (~1 M) and only a few have sampled the low concentration regime necessary to address the enigmatic Jones-Ray effect. SHG of sodium and potassium iodide solutions indicated a strong affinity for the interfacial region.[4] These salts were not among the 13 Jones-Ray salts, but another alkali halide, cesium iodide, did exhibit a minimum in surface tension.[13] Another Jones-Ray salt, potassium ferrocyanide also has been shown to have a strong affinity for the interface at low concentrations via SHG.[30]

Despite the recent interest in ion adsorption to aqueous interfaces, the adsorption of ions to the air/water interface, especially at low concentrations, remains incompletely understood. In this chapter, the adsorption of sodium bromide and sodium chloride to the air/water interface of aqueous solutions of millimolar concentration is addressed via UV charge-transfer-to-solvent (CTTS) SHG. A modified Langmuir model is used to determine Gibbs free energies of adsorption to the interface, and the relative anion affinities are compared to that previously determined for iodide.

4.2 Experimental methods

All glassware was cleaned using Nochromix dissolved in concentrated sulfuric acid and rinsed with 18.2 MΩ water (Millipore MilliQ A10). Solutions were made with 18.2 MΩ water and NaBr (Sigma-Aldrich, >99.0%) or NaCl (Sigma-Aldrich >99.0%) and further purified by

baking in a tube furnace under nitrogen at 500°C for eight hours. All samples were prepared and measured at room temperature.

The laser system and data collection have been described in detail previously.[31, 32] Briefly, home-built Ti:sapphire oscillator is used to seed a regenerative amplifier. The amplified output pumps an optical parametric amplifier (OPA). The output of the OPA is tuned to either 530 nm or 386 nm, and this light is used as the fundamental beam. Less than 10% of the fundamental is directed to a photodiode as a reference power measurement. The remaining fundamental is focused onto the sample with p-polarization at a 60º angle relative to the surface normal. The pulse energy density at the interface is less than 0.3 $J \cdot cm^{-2}$ per pulse. The SHG signal is collected in the reflection geometry and separated from the collinear fundamental by a series of dichroic mirrors and a spectrometer. The fundamental light is further rejected by using a solar-blind photomultiplier tube. The detected signal intensity is approximately 0.01 photons per pulse.

4.3 A Langmuir adsorption model

The model used here has been described in detail elsewhere[31, 8, 32] and an overview is given here. In order to extract the affinity of ions to the interface, the solution is partitioned into a surface and bulk region, and the following equilibrium exchange reaction is used to model the adsorption of ions into the surface region:

$$H_2O_S + N_B \rightleftharpoons H_2O_B + N_S \qquad [4.1]$$

Here, N_i represents a solute species, while the subscripts *S* and *B* indicate that the species in the surface region. A modified Langmuir model is used to represent N_S as a function of the bulk solute concentrations,

$$N_S = \frac{N_S^{\max}[N_B]}{[N_B] + [H_2O_B]/K}, \qquad [4.2]$$

where *K* is the equilibrium constant for the exchange reaction [4.1].

The SHG response is proportional to the square of the magnitude of the effective second-order nonlinear susceptibility, $\chi_{eff}^{(2)}$. This can be separated into a solvent and a solute contribution, where the solute contribution is proportional to N_S,

$$\left|\chi_{eff}^{(2)}\right|^2 = \left|A + (B + iC)N_S\right|^2 \qquad [4.3]$$

The phase of the solvent response, *A*, is defined to be purely real, while the complex phase of the solute response can vary relative to that of the solvent. The magnitude of the solute response, represented by *B* and *C*, can become large when in resonance with the CTTS band.

The SHG response is measured as a function of salt concentration, and a Langmuir isotherm fit weighted by the error in the data is used to determine the equilibrium constant. The Gibbs free energy, ΔG, of adsorption is extracted from the equilibrium constant.

4.4 Results and discussion

The bulk CTTS band of chloride peaks at 181 nm.[33] The SHG response of sodium chloride as a function of concentration is shown in Figure 4.1. At both 193 nm and 265 nm, the surface adsorbed chloride response and the water response initially interfere destructively, as the SHG response of the system decreases below that of the neat water surface, which is defined as unity on the normalized scale. As higher salt concentrations are probed the number of surface adsorbed chloride ions becomes large enough that the response of the system begins to increase.

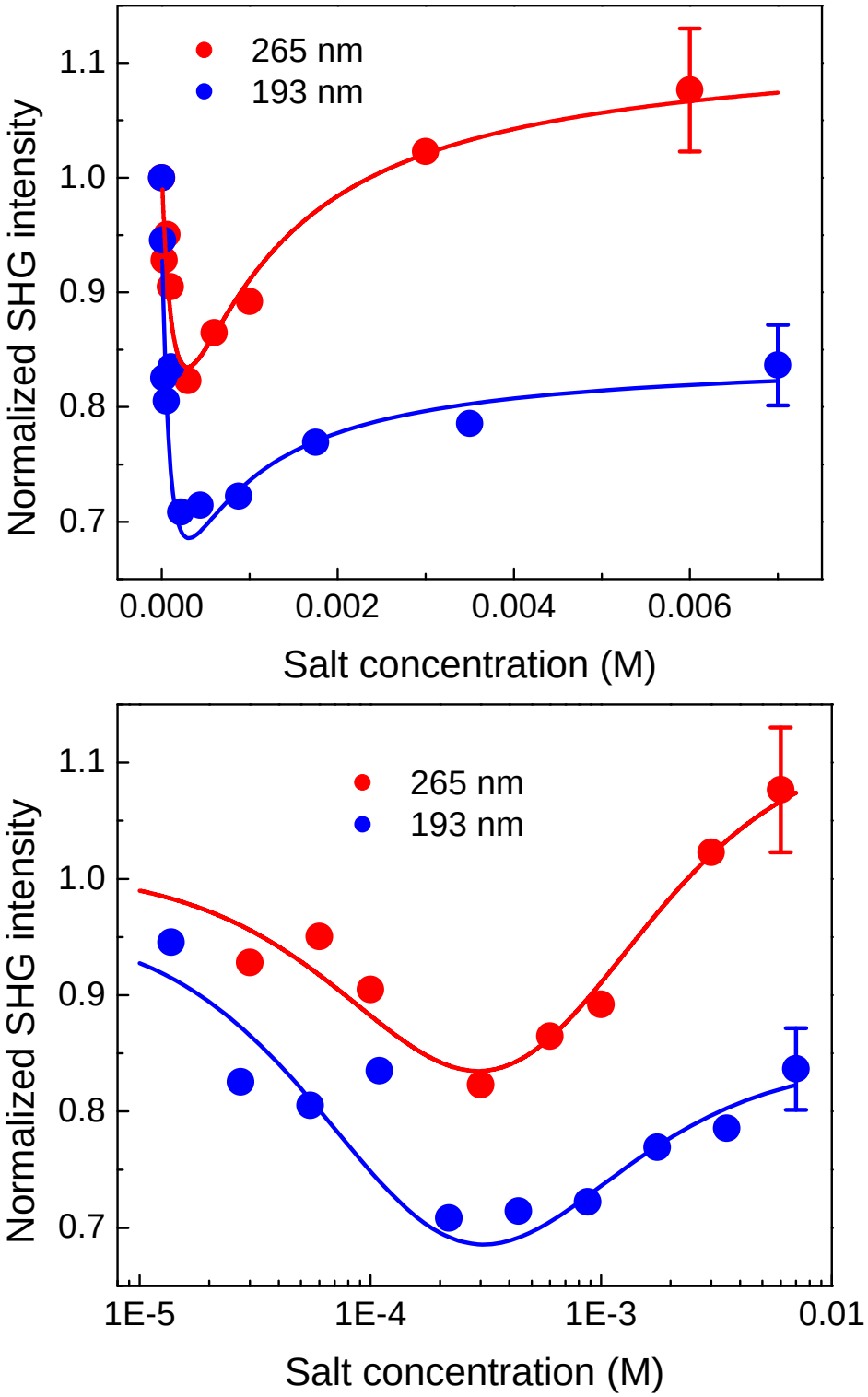

Figure 4.1. The normalized SHG of adsorbed chloride ions at 265 nm and 193 nm plotted versus bulk concentration (top panel) on a linear scale and (bottom panel) on a logarithmic scale. The response of neat water is unity.

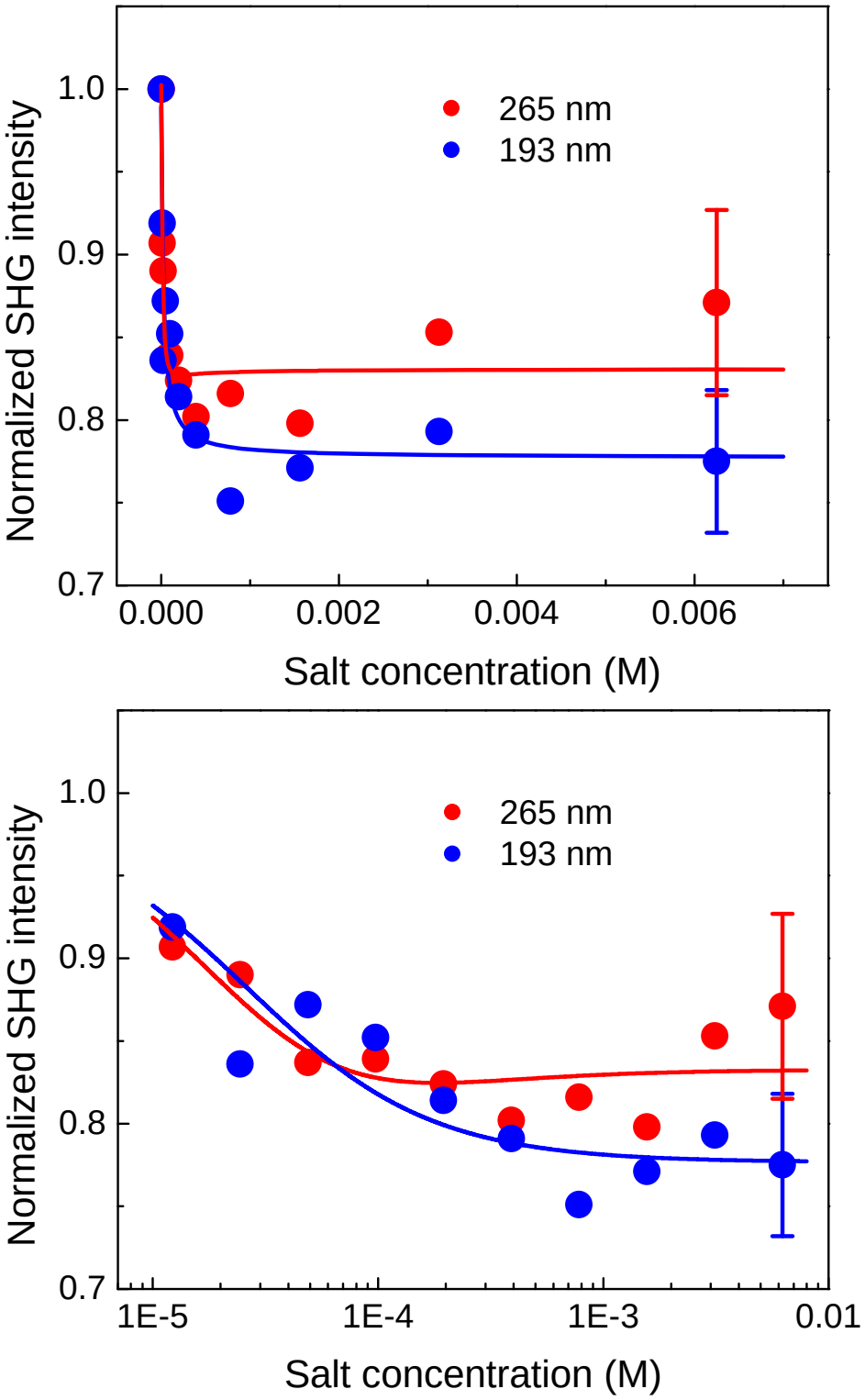

Figure 4.2. The normalized SHG of adsorbed bromide ions at 265 nm and 193 nm plotted versus bulk concentration (top panel) on a linear scale and (bottom panel) on a logarithmic scale.

The Langmuir isotherm fit to the data yields a free energy of -29.2 kJ/mol with a range defined by the error of the fit of $-29.7 \leq \Delta G \leq -28.4$ kJ/mol. Note that the error is asymmetric about the free energy because the fit parameter, the equilibrium constant, depends exponentially on the free energy.

The SHG response of bromide, with the peak of its bulk CTTS band at 200 nm,[33] is both weaker and noisier than that of chloride (see Figure 4.2). Similar to chloride, the SHG response of bromide destructively interferes with that of water in this concentration regime before leveling off as the concentration is increased. The best Langmuir isotherm fit for bromide gives a free energy of -35 kJ/mol, but because the data are noisy, the error in the free energy is large: $-36 \leq \Delta G \leq -20$ kJ/mol.

In the millimolar concentration regime the affinities of both chloride and bromide for the surface are large, greater than or equal to the strength of a hydrogen bond. It is interesting to compare these affinities to that of iodide, which was previously determined to be -25.5 ± 0.1 kJ/mol by probing millimolar sodium iodide solutions with SHG. Figure 4.3a is a bar graph showing the free energies of the three halide ions for the interface, and Figure 4.3b shows their fractional surface coverage predicted by the determined free energies. Chloride is more strongly adsorbed than iodide, but the error on the free energy of bromide is too large to conclude whether a periodic trend exists.

That chloride exhibits a greater affinity for the interface than iodide in this concentration regime is surprising. At higher concentrations halide, and more generally anion, affinity for the air/water interface generally increases with increasing ionic radii and decreasing hydration energy. This has been demonstrated by XPS measurements,[6, 9] VSFG measurements,[3] electrospray ionization mass spectrometry measurements,[7] and a surface-bulk partitioning model based on surface tension measurements.[34] The rationalization of this trend is that the larger anions are more disruptive of the hydrogen bonding network, therefore it is entropically favorable for larger ions to reside at the interface.

The contrast in relative ion affinities at millimolar and molar concentrations indicates that a different mechanism of adsorption operates in these concentration regimes. A similar conclusion was made previously due to the difference in the magnitude surface affinity of iodide at millimolar and molar concntrations.[4, 8] A similar comparison can be made with bromide. At molar concentrations, bromide affinity for the interface at most corresponds to a free energy of -4.1 kJ/mol (see Chapter 3). This is much weaker than the affinity determined here for millimolar concentrations. This serves as further evidence that there are different ion adsorption mechanisms at low and high concentrations.

4.5 Conclusions

SHG measurements of sodium chloride and sodium bromide at the air/water interface indicate that both anions are strongly adsorbed to the surface in the millimolar bulk concentration regime. A similar result was previously found for sodium iodide.[4] In contrast to molar salt solutions, chloride exhibits a larger affinity for the surface than iodide. This change in the order of ion affinity from low concentrations to molar concentrations indicates that there are multiple adsorption mechanisms dictating ion adsorption. The error in the determined free energy of adsorption for bromide prevents any meaningful conclusion about its affinity relative to chloride and iodide. However, comparison of the affinity of bromide to the surface at low and high concentrations lends further support to the existence of multiple adsorption mechanisms.

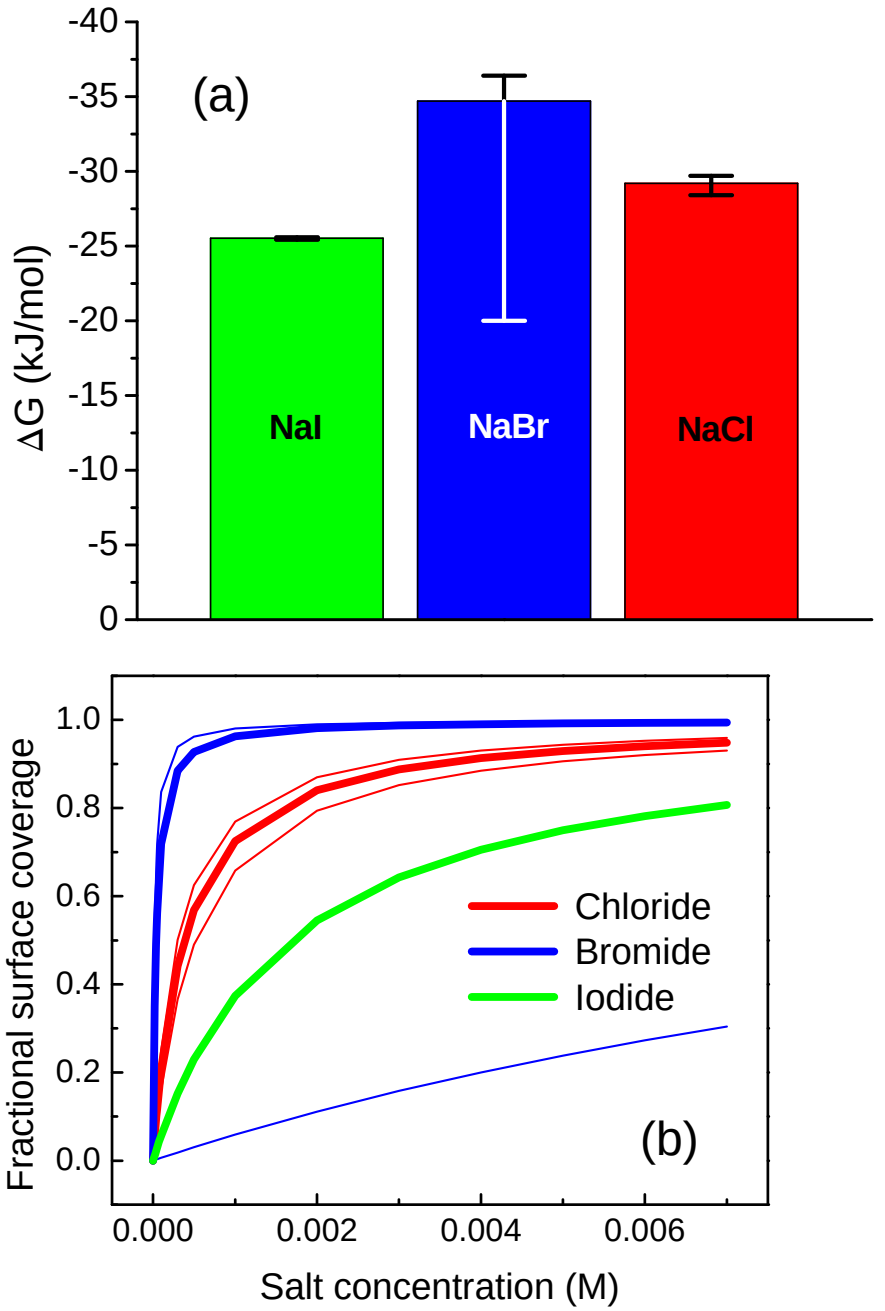

Figure 4.3. (a) a bar graph of the determined affinity of halide ions to the interface. (b) the predicted fractional surface coverage of the halides. The bold lines are the best fit, while the narrow lines represent the error. In the case of iodide the error is approximately the thickness of the line.

4.6 Future SHG work

As liquid interfaces are still not well understood, SHG can be used to address many unanswered questions. Many of these problems involve experimental modifications to extend the scope of possible work, and this section is broken down into categories based on the experimental modifications necessary to address future problems.

A. No experimental modifications. One problem that can be addressed without any changes to the experimental design is determining the effect of cations. Jones and Ray found only 13 inorganic salts with a minimum in surface tension, and these salts were highly cation specific.[11-15] In SHG studies of low concentration ion adsorption, the cation has only been varied for iodide. Both the sodium and potassium salts were tested, but no difference in affinity for the interface was found.[4] Studies involving cation effects could be valuable to understanding the mechanism of adsorption in the low concentration regime.

The pH and ionic strength of solution could also be studied without any experimental changes. These effects require a negative result; in other words, a cation and an anion that are both not surface active must be determined (e.g. Na_2SO_4 is a candidate). Without a negative result, changing the pH or the ionic strength of the solution will also cause unintended changes to the composition of the interface.

B. Extending SHG detection deeper into the UV. Many ions, especially environmentally relevant ones such as sulfate and carbonate, have CTTS bands that are not accessible with the current detection setup due to the absorption of light at these frequencies by air. Sealing the sample and detection setup and purging with gas (e.g. nitrogen) would allow for studies of these ions.

Also, this could facilitate studies addressing whether the interface is basic or acidic. The CTTS band of hydroxide peaks at 187 nm in the bulk. Petersen and Saykally probed sodium hydroxide at 200 nm, and saw a weak response, but probing closer to the resonance will provide more reliable data. Sodium hydroxide was also probed at 193 nm in the millimolar concentration regime to test if there was a greater response (see Figure 4.4). However, these measurements show only a small increase in SHG signal and were not significantly different than those made by Petersen at 200 nm.

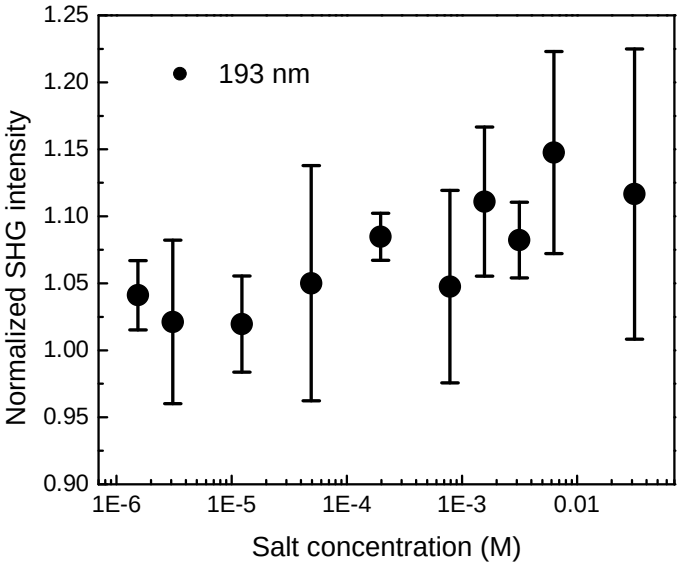

Figure 4.4. The normalized SHG of sodium hydroxide aqueous interface at 193 nm plotted versus bulk concentration on a logarithmic scale.

C. Broadband spectra. One major difficulty with using the SHG technique to determine ion affinity to the interface is the often large and sometimes indeterminate error in the derived free energies. Collecting broadband spectra would allow for a more complete characterization of the SHG response and a decrease in the associated errors. It would also allow for a more complete spectral analysis. This would allow for spectral shifts in the CTTS band from the bulk to the surface to be addressed. It would also enable for any shifts in the CTTS band with concentration to be assessed.

Unfortunately, this experimental improvement would be technically very challenging. One way to achieve a broadband spectrum would be to generate a white light continuum near 400 nm and to use this as the probe. As currently designed, on the order of one photon is detected per 10 laser pulses. In order to collect a broadband spectrum the incident power would be spread over many more frequencies decreasing the photon detection probability at each frequency.

D. Temperature dependence. Work on this experiment has already begun. The goal of a temperature dependent experiment is to be able to separate the enthalpic effects from the entropic effects. This may shed considerable light on the ion adsorption mechanism.

E. Phase-sensitive measurements. As currently designed, the complex phase of the resonant SHG response is determined through the Langmuir isotherm fit. A phase sensitive experiment would allow for the direct determination of the relative phases of neat water and the resonant response. This would decrease the number of parameters used in the fitting process, which would decrease the error in the derived free energies.

4.7 References

1. E. M. Knipping, M. J. Lakin, K. L. Foster, P. Jungwirth, D. J. Tobias, R. B. Gerber, D. Dabdub and B. J. Finlayson-Pitts, "Experiments and Simulations of Ion-Enhanced Interfacial Chemistry on Aqueous NaCl Aerosols." *Science.* **288**, 301-306, (2000).
2. S. W. Hunt, M. Roeselova, W. Wang, L. M. Wingen, E. M. Knipping, D. J. Tobias, D. Dabdub and B. J. Finlayson-Pitts, "Formation of Molecular Bromine from the Reaction of Ozone with Deliquesced NaBr Aerosol: Evidence for Interface Chemistry." *The Journal of Physical Chemistry A.* **108**, 11559-11572, (2004).
3. D. F. Liu, G. Ma, L. M. Levering and H. C. Allen, "Vibrational Spectroscopy of aqueous sodium halide solutions and air-liquid interfaces: Observation of increased interfacial depth." *Journal of Physical Chemistry B.* **108**, 2252-2260, (2004).
4. P. B. Petersen, J. C. Johnson, K. P. Knutsen and R. J. Saykally, "Direct experimental validation of the Jones-Ray effect." *Chemical Physics Letters.* **397**, 46-50, (2004).
5. E. A. Raymond and G. L. Richmond, "Probing the molecular structure and bonding of the surface of aqueous salt solutions." *Journal of Physical Chemistry B.* **108**, 5051-5059, (2004).
6. S. Ghosal, J. C. Hemminger, H. Bluhm, B. S. Mun, E. L. D. Hebenstreit, G. Ketteler, D. F. Ogletree, F. G. Requejo and M. Salmeron, "Electron spectroscopy of aqueous solution interfaces reveals surface enhancement of halides." *Science.* **307**, 563-566, (2005).
7. J. Cheng, C. D. Vecitis, M. R. Hoffmann and A. J. Colussi, "Experimental anion affinities for the air/water interface." *Journal of Physical Chemistry B.* **110**, 25598-25602, (2006).
8. P. B. Petersen and R. J. Saykally, "Probing the interfacial structure of aqueous electrolytes with femtosecond second harmonic generation spectroscopy." *Journal of Physical Chemistry B.* **110**, 14060-14073, (2006).
9. S. Ghosal, M. A. Brown, H. Bluhm, M. J. Krisch, M. Salmeron, P. Jungwirth and J. C. Hemminger, "Ion Partitioning at the Liquid/Vapor Interface of a Multicomponent Alkali Halide Solution: A Model for Aqueous Sea Salt Aerosols." *Journal of Physical Chemistry A.* **112**, 12378-12384, (2008).
10. L. Onsager and N. N. T. Samaras, "Surface tension of Debye-Huckel electrolytes." *Journal of Chemical Physics.* 528-536, (1934).
11. G. Jones and W. A. Ray, "The surface tension of solutions." *Journal of the American Chemical Society.* **57**, 957-958, (1935).
12. G. Jones and W. A. Ray, "The surface tension of solutions of electrolytes as a function of the concentration I A differential method for measuring relative surface tension." *Journal of the American Chemical Society.* **59**, 187-198, (1937).
13. G. Jones and W. A. Ray, "The Surface Tension of Solutions of Electrolytes as a Function of the Concentration II*." *Journal of the American Chemical Society.* **63**, 288-294, (1941).
14. G. Jones and W. A. Ray, "The surface tension of solutions of electrolytes as a function of the concentration. III. Sodium chloride." *Journal of the American Chemical Society.* **63**, 3262-3263, (1941).
15. G. Jones and W. A. Ray, "The surface tension of solutions of electrolytes as a function of the concentration. IV. Magnesium sulfate." *Journal of the American Chemical Society.* **64**, 2744-2745, (1942).

16. I. Langmuir, "Repulsive forces between charged surfaces in water, and the cause of the Jones-Ray effect." *Science.* **88**, 430-432, (1938).
17. M. Dole and J. A. Swartout, "A twin-ring surface tensiometer. I. The apparent surface tension of potassium chloride solutions." *Journal of the American Chemical Society.* **62**, 3039-3045, (1940).
18. J. H. Hu, Q. Shi, P. Davidovits, D. R. Worsnop, M. S. Zahniser and C. E. Kolb, "Reactive Uptake of Cl2(G) and Br2(G) by Aqueous Surfaces as a Function of Br- and I- Ion Concentration - the Effect of Chemical-Reaction at the Interface." *Journal of Physical Chemistry.* **99**, 8768-8776, (1995).
19. G. A. Impey, P. B. Shepson, D. R. Hastie, L. A. Barrie and K. G. Anlauf, "Measurements of photolyzable chlorine and bromine during the Polar sunrise experiment 1995." *Journal of Geophysical Research-Atmospheres.* **102**, 16005-16010, (1997).
20. R. R. Dickerson, K. P. Rhoads, T. P. Carsey, S. J. Oltmans, J. P. Burrows and P. J. Crutzen, "Ozone in the remote marine boundary layer: A possible role for halogens." *Journal of Geophysical Research-Atmospheres.* **104**, 21385-21395, (1999).
21. I. Nagao, K. Matsumoto and H. Tanaka, "Sunrise ozone destruction found in the sub-tropical marine boundary layer." *Geophysical Research Letters.* **26**, 3377-3380, (1999).
22. I. E. Galbally, S. T. Bentley and C. P. Meyer, "Mid-latitude marine boundary-layer ozone destruction at visible sunrise observed at Cape Grim, Tasmania, 41 degrees 5." *Geophysical Research Letters.* **27**, 3841-3844, (2000).
23. K. L. Foster, R. A. Plastridge, J. W. Bottenheim, P. B. Shepson, B. J. Finlayson-Pitts and C. W. Spicer, "The role of Br-2 and BrCl in surface ozone destruction at polar sunrise." *Science.* **291**, 471-474, (2001).
24. V. Matveev, M. Peleg, D. Rosen, D. S. Tov-Alper, K. Hebestreit, J. Stutz, U. Platt, D. Blake and M. Luria, "Bromine oxide - ozone interaction over the Dead Sea." *Journal of Geophysical Research-Atmospheres.* **106**, 10375-10387, (2001).
25. C. W. Spicer, R. A. Plastridge, K. L. Foster, B. J. Finlayson-Pitts, J. W. Bottenheim, A. M. Grannas and P. B. Shepson, "Molecular halogens before and during ozone depletion events in the Arctic at polar sunrise: concentrations and sources." *Atmospheric Environment.* **36**, 2721-2731, (2002).
26. J. Stutz, R. Ackermann, J. D. Fast and L. Barrie, "Atmospheric reactive chlorine and bromine at the Great Salt Lake, Utah." *Geophys. Res. Lett.* **29**, 1380, (2002).
27. U. Friess, J. Hollwedel, G. König-Langlo, T. Wagner and U. Platt, "Dynamics and chemistry of tropospheric bromine explosion events in the Antarctic coastal region." *J. Geophys. Res.* **109**, D06305, (2004).
28. P. B. Petersen and R. J. Saykally, "On the nature of ions at the liquid water surface." *Annual Review of Physical Chemistry.* **57**, 333-364, (2006).
29. P. Jungwirth and B. Winter, "Ions at aqueous interfaces: From water surface to hydrated proteins." *Annual Review of Physical Chemistry.* **59**, 343-366, (2008).
30. P. B. Petersen and R. J. Saykally, "Adsorption of ions to the surface of dilute electroyte solutions: The Jones-Ray effect revisited." *Journal of the American Chemical Society.* **127**, 15446-15452, (2005).
31. P. B. Petersen and R. J. Saykally, "Confirmation of enhanced anion concentration at the liquid water surface." *Chemical Physics Letters.* **397**, 51-55, (2004).

32. R. M. Onorato, D. E. Otten and R. J. Saykally, "Adsorption of thiocyanate ions to the dodecanol/water interface characterized by UV second harmonic generation." *Proceedings of the National Academy of Sciences.* **106**, 15176-15180, (2009).
33. M. J. Blandamer and M. F. Fox, "Theory and applications of charge-transfer-to-solvent spectra." *Chem. Rev.* **70**, 59-93, (1970).
34. L. M. Pegram and M. T. Record, "Hofmeister Salt Effects on Surface Tension Arise from Partitioning of Anions and Cations between Bulk Water and the Air-Water Interface." *J. Phys. Chem. B.* **111**, 5411-5417, (2007).

Chapter 5

Chirped-CARS microscopy

5.1 The CARS technique

Coherent anti-Stokes Raman scattering (CARS) is an effective chemically selective imaging technique, exploiting molecular vibrations as endogenous chromophores. A brief introduction to CARS will be given here; thorough reviews of CARS microscopy theory and technique[1-3] as well as biological applications of CARS microscopy[4] have recently been published.

CARS is a third-order nonlinear process that achieves chemical specificity through a coherence at the frequency ω_p - ω_S driven by two laser pulses at different frequencies, the pump pulse (ω_p) and the Stokes pulse (ω_S). The resulting CARS signal is generated at the frequency $2\omega_p$ - ω_S by the probe pulse interacting with the coherence as shown in Figure 5.1a. The CARS signal is proportional to the square of the third-order susceptibility $\chi^{(3)}$, which can be written as

$$\chi^{(3)} = \frac{A}{\omega_M - (\omega_p - \omega_S) - i\Gamma_M} + \chi_{NR}^{(3)} \qquad [5.1]$$

Resonant CARS occurs when the frequency difference ω_p - ω_S approaches a vibrational mode, ω_M, wherein the denominator will become small and $\chi^{(3)}$ will become large. A represents the cross section of the CARS process, Γ_M is related to the lifetime of the vibrational mode, and $\chi_{NR}^{(3)}$ is the non-resonant CARS signal. The phase matching condition also dictates the intensity of the CARS signal as can be seen in [5.2]:[5]

$$I = \frac{\pi\omega_{aS}^{\ 2}}{2n_{aS}} l^2 \left|P^{(3)}\right|^2 \mathrm{sinc}^2\left[\frac{\Delta k \cdot l}{2}\right] \qquad [5.2]$$

Here l is the thickness of the sample and Δk is the phase mismatch, $k_{aS} - (2\,k_p + k_S)$. The sinc^2 term is large when $\Delta k \cdot l << \pi/2$. Therefore, the CARS signal is highly directional, and when the pump/probe and Stokes pulses are collinear the CARS signal propagates in the forward and backward (epi) directions. All nonlinear optical spectroscopy techniques exhibit an instantaneous non-resonant wave-mixing signal. In the case of CARS it can be quite large, sometimes overwhelming any resonant response. Many different variations of CARS have been developed to minimize the non-resonant signal including epi-detection,[6] polarization control,[7, 8] and interferometry.[9-12]

CARS is a more complicated technique than fluorescence, but in instances where there is no endogenous fluorophore and labeling is difficult or will perturb the system, CARS is a useful alternative. Like CARS, both infrared absorption and traditional Raman spectroscopy probe molecular vibrations, but CARS has distinct advantages compared to the other techniques. Since CARS probes vibrational resonances at the frequency difference ω_p - ω_s, an infrared frequency can be probed using two frequencies of visible light. The diffraction limit, and therefore the lateral spatial resolution of an optical technique, is approximately equal to half the wavelength of the incident light. Since CARS uses wavelengths in the visible, the lateral spatial resolution is nearly an order of magnitude better than that of infrared absorption. Both infrared absorption and Raman scale linearly with the incident light intensity, but since CARS is a third-order nonlinear process, it scales as the third power of the incident light intensity. As a result CARS is generated

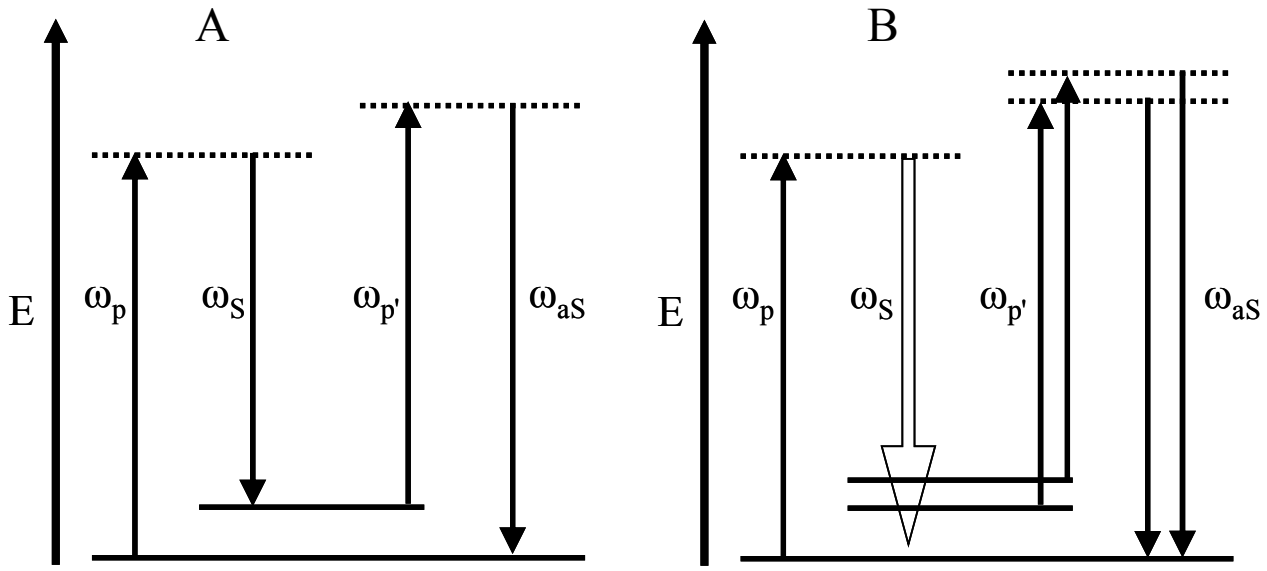

Figure 5.1. CARS single frequency (a) and multiplex (b) energy level diagrams. In (a) both the Stokes and the degenerate pump/probe frequencies are narrowband. A vibrational mode is stimulated at the frequency difference $\omega_p - \omega_S$, and the anit-Stokes signal is generated by probing the stimulated mode. In (b) a broadband ω_S can probe multiple vibrational modes simultaneously. The narrowband probe generates signal at anti-Stokes frequencies corresponding to each vibrational mode.

primarily at the focus, increasing contrast with the surrounding material, and results in a significantly improved axial spatial resolution compared to the other vibrational techniques. CARS is also a much more sensitive technique than traditional Raman spectroscopy; 10^5-10^6 times more CARS signal can be collected than traditional Raman spectroscopy in an equivalent amount of time using similar average powers. This increased sensitivity is due to resonance enhancement and the phase matching condition, which results in a directional signal. Additionally, traditional Raman often must compete with a fluorescence background. Since the Stokes shift, at a lower energy than the incident photon, is used in traditional Raman microscopy, the detected Raman signal can occur at the same wavelength as any inherent fluorescence. However, the anti-Stokes photon generated in CARS has a higher energy than any of the incident photons, so any inherent fluorescence will occur at wavelengths longer than that of the CARS signal. One consideration when deciding between using Raman spectroscopy or CARS for a particular application is whether background fluorescence or non-resonant CARS will pose a larger problem.

In this chapter the development of a novel technique, chirped-CARS (c-CARS), is detailed. C-CARS is a multiplex technique, meaning that it can probe multiple vibrational frequencies simultaneously. The original objective for c-CARS was to develop a multiplex technique with high spectral and spatial resolution for the purpose of three dimensional mapping of chemical moieties within a range of potential samples, including interstellar dust and comet particles collected during NASA's STARDUST mission, soot particles in order to determine the spatial distribution of chemicals in air pollutants, and cellular structures. In this chapter, proof-of-principle experiments using various polymer samples are demonstrated, and the unsuccessful attempts to apply this technique to more complicated systems are briefly discussed.

5.2 Chirped-CARS

One of the current challenges in CARS microscopy is the development of an effective multiplex CARS imaging technique. Multiplex CARS is achieved by exciting a range of frequencies determined by the energy difference ω_p - ω_S and is therefore able to probe multiple molecular vibrations simultaneously. This can be done by using a broadband Stokes pulse, as shown in Figure 5.1b. There are various methods currently being used to generate multiplex CARS signal, all of which utilize femtosecond lasers: synchronizing femtosecond and picosecond laser pulses in time,[13] using a photonic crystal fiber to generate a continuum that is used as the Stokes pulse,[14] using a pulse shaper,[10, 15] and chirping the probe pulse.[16] The latter three utilize a single laser pulse to generate both the degenerate pump/probe pulse and the Stokes pulse, transcending the complication of synchronizing two lasers in time.

In chirped CARS (c-CARS), the degenerate pump/probe pulse is chirped and then overlapped in time with a transform limited broadband femtosecond Stokes pulse; both pulses are generated from the same seed pulse. The overlap of the pump and Stokes pulses resonantly excites vibrational coherences at the frequencies ω_p - ω_s within a bandwidth proportional to that of the Stokes pulse. These vibrational coherences are probed by the chirped pulse, generating the c-CARS signal. Since the chirped pulse is spread out in time, an effective 'temporal slit' is created (Figure 5.2), where the c-CARS signal is primarily generated during the temporal overlap of the pulses. In the limiting case that the dephasing time of the coherence is on the order of the temporal pulsewidth of the Stokes pulse, the spectral resolution is determined by multiplying the chirp rate of the pump/probe pulse and the temporal width of the Stokes pulse.[16] Spectra exhibiting 10 cm^{-1} spectral resolution with a spectral bandwidth of 300 cm^{-1} were previously reported, with calculations from a simple model supporting the analysis.[17]

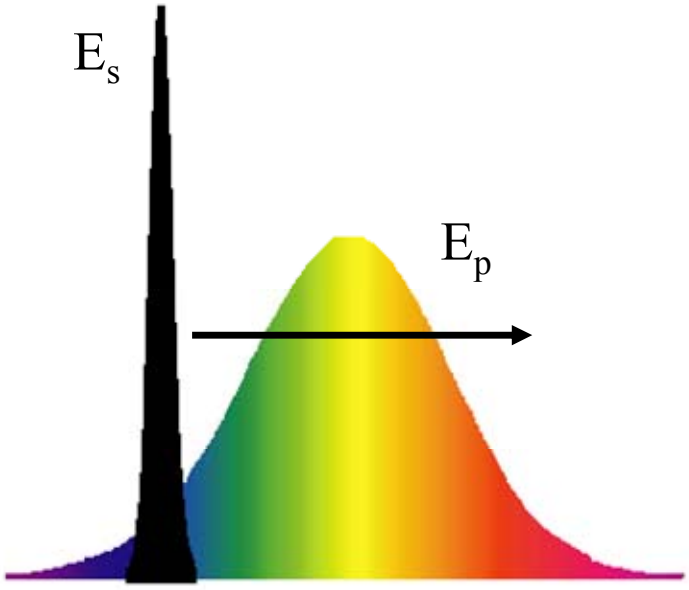

Figure 5.2. The c-CARS signal is generated primarily during the temporal overlap of the Stokes and chirped pulses. The transform limited Stokes pulse is overlapped with the chirped pulse, drawn as a rainbow to depict its chirped nature. The arrow indicates that the overlap can be controlled by independently varying the path lengths of the two pulses.

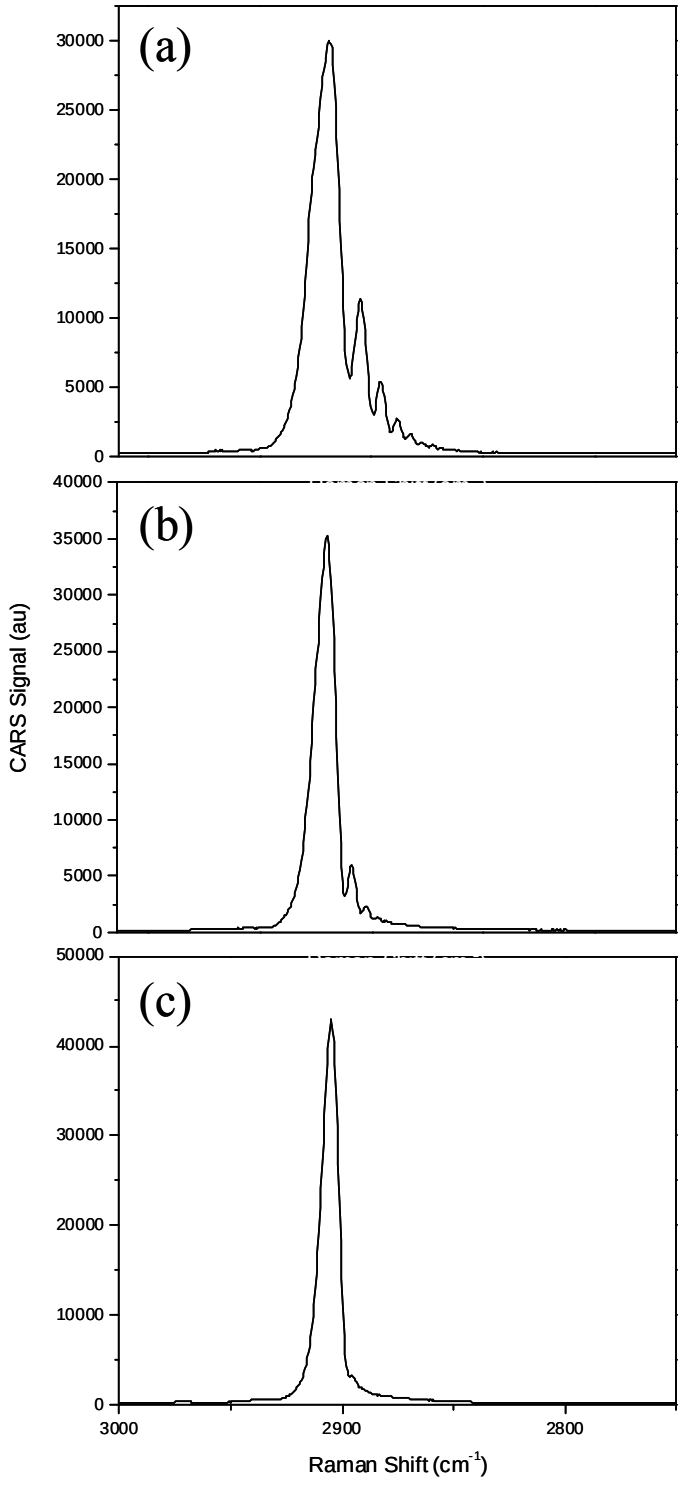

Figure 5.3. Acetonitrile c-CARS spectra of the symmetric C-H vibrational mode (T2 = 5.4 ps) for the chirped pulse temporal HWHM equal to 5ps (a), 11ps (b), and 26ps (c). The spectral distortion is most significant in (a) where the chirped pulse HWHM and the dephasing time of the vibrational mode are similar. At longer chirped pulse HWHM the distortion decreases.

The line-shape of c-CARS is not the natural line-shape of the CARS technique. Since the chirped pulse is broader in time than the Stokes pulse, it will interact with the vibrational coherence at times later than the temporal overlap of the two pulses. Since the pulse is negatively chirped, the c-CARS spectrum will exhibit a distorted line-shape on the low frequency side. When the dephasing time of the vibrational coherence is much less than the half-width half maximum (HWHM) of the chirped pulse, the effect is difficult to detect; there is interference due to the interaction of the evolving phases of the vibrational coherence and the chirped pulse. However, when the dephasing time is on the order of or larger than one half the temporal width of the chirped pulse (~5 ps for all spectra and images unless otherwise noted), there will be significant spectral distortion due to the lower frequencies of the chirped pulse interacting with the vibrational coherence, appearing as an exponential decay of the vibrational mode convoluted with an oscillation due to the interaction of the respective phases evolving in time.

The symmetric C-H stretch of acetonitrile, T2 = 5.4 ps,[18] is used to demonstrate this phenomenon. Figure 5.3 shows c-CARS spectra with chirped pulse HWHM of 5, 11, and 26 ps. In the 5 ps HWHM spectrum, the spectral distortion is the strongest since the HWHM and the dephasing time are similar. As the HWHM is increased the distortion is minimized. The 11 ps HWHM spectrum exhibits less distortion, while any level of distortion is difficult to detect in the 26 ps HWHM spectrum. For comparison, a c-CARS spectrum of the symmetric C-H stretch of methanol, T2 = 2.4 ps,[18] using a 5 ps HWHM chirped pulse is shown in Figure 5.4. There is some distortion, but it significantly less than in the case of acetonitrile due to the shorter dephasing time.

This dephasing time is generally much shorter for non-liquid samples, such as the polymer samples described in the following section, and in this case the effect is insignificant. In cases where the effect is significant it can be minimized by decreasing the chirp rate, resulting in a temporally longer pulse and a decrease in the extent of the interaction between the dephasing vibrational coherence and the lower frequencies of the chirped pulse.

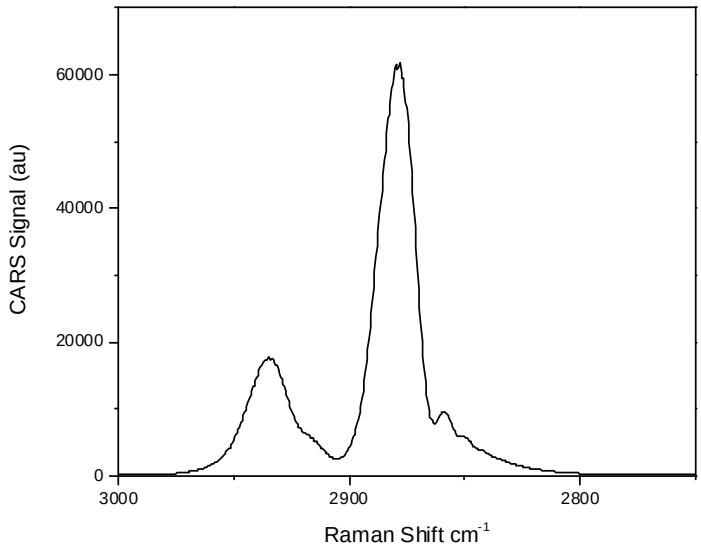

Figure 5.4. Methanol c-CARS spectrum with the chirped pulse HWHM set to 5ps. The symmetric C-H stretch centered at 2880 cm^{-1} (T2 = 2.4ps) exhibits some spectral distortion, but it is weaker than in the acetonitrile case (Figure 5.3a).

5.3 Experimental methods

Femtosecond pulses are generated in a home-built Ti:sapphire oscillator, which seeds a regenerative amplifier (Spectra Physics, Spitfire). The amplified output is split with a beam splitter; approximately 5% is sent to a pair of diffraction gratings. The first grating spreads the pulse in space, and the second grating collimates the beam, resulting in a beam that has been stretched horizontally. The beam is then retro-reflected, reflecting off both gratings again and resulting in a beam of the initial diameter. The higher frequencies travel a shorter distance than the lower frequencies during the four grating reflections, resulting in a negatively chirped pulse, as shown in Figure 5.5. A negatively chirped pulse has been stretched in time with the higher frequencies occurring at earlier times and the lower frequencies at later times. The remaining amplifier output is used to pump an optical parametric amplifier (Light Conversion, TOPAS), providing tunable infrared light, which is doubled with a BBO crystal. The chirped and tunable pulses are spatially and temporally overlapped and focused onto the sample by an objective and collected by a matched objective. The sample position is controlled with a nano-positioning stage (Physik Instrumente, P527 multi-axis piezo scanner).The CARS signal is dispersed by a spectrograph (Acton Research, SpectraPro 300i) and collected with a CCD (Roper Scientific, Spec10B-LN2) for spectra and with a photomultiplier tube (PMT) for images. The bandwidth of the signal collected by the PMT can be controlled by the exit slit-width of the spectrograph.

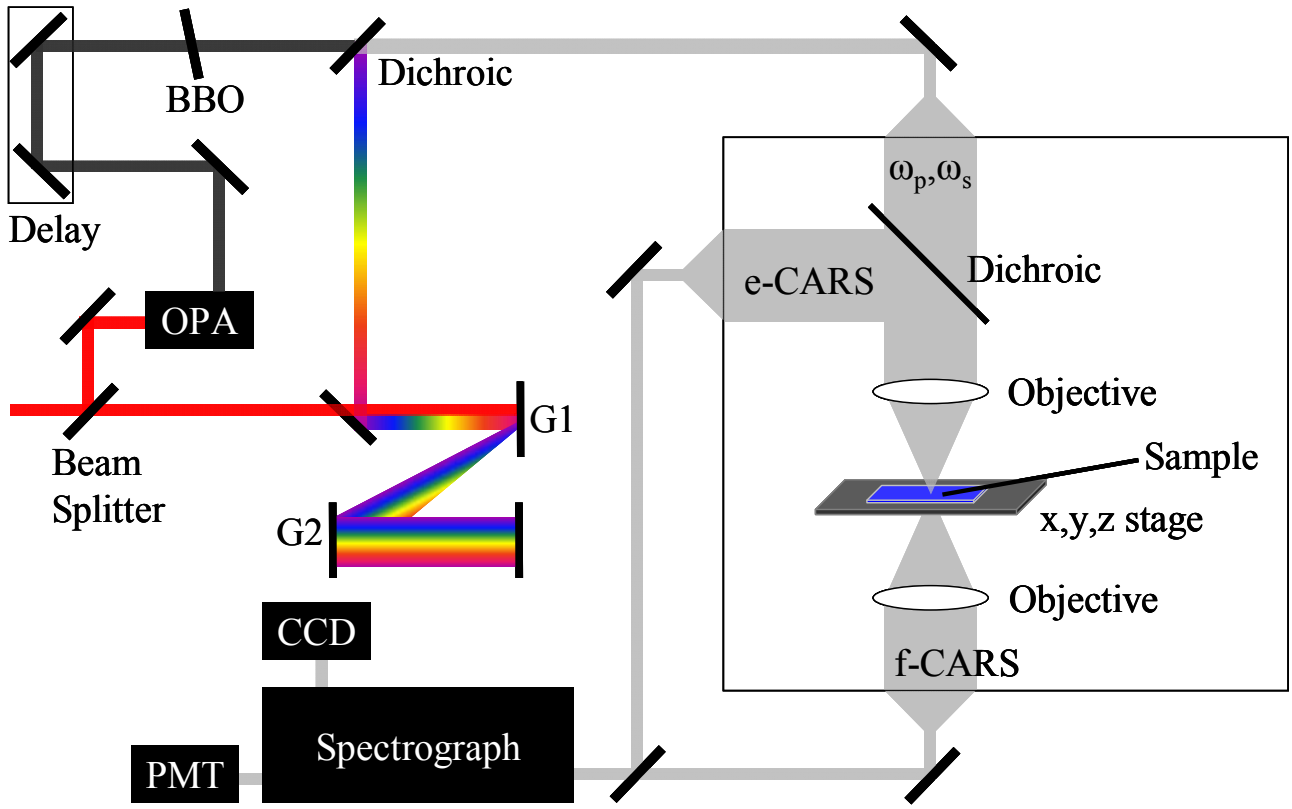

Figure 5.5. The c-CARS experimental setup. 800nm light (1KHz, 100fs) from a regenerative amplifier is split by a beam splitter. Five percent of the beam is used to generate the chirped pulse using a pair of diffraction gratings (G1 and G2). When dispersed, the lower frequency light travels farther, making the pulse negatively chirped. The rest of the 800nm light is converted to infrared light by an OPA and then frequency doubled using a BBO crystal. The two pulses are spatially and temporally overlapped using a dichroic mirror and a delay stage. The pulses are then focused onto the sample, and the signal can be collected in the forward and epi directions. The c-CARS signal is then directed through a spectrograph to a CCD for spectroscopy or a photomultiplier tube (PMT) for imaging.

5.4 Results and discussion

5.4.1 Polystyrene beads

The CARS response of polystyrene (PS) in the C-H stretching region exhibits three strong and broad peaks due to asymmetric and symmetric aliphatic stretching modes at 2901cm^{-1} and 2851cm^{-1}, respectively, and an aromatic stretching mode at 3054 cm^{-1}, as shown in the spectrum collected from a 6 μm PS bead on a glass slide Figure 5.6. Since PS beads give high signal-to-noise, they were used as a model sample for proof-of-principle imaging experiments.

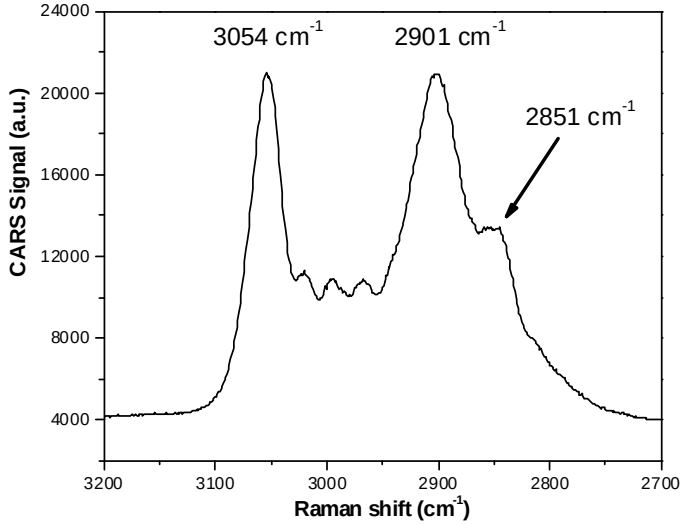

Figure 5.6. C-CARS spectrum of a 6 μm polystyrene bead in the C-H stretching region. The asymmetric and symmetric aliphatic stretching modes are at 2901cm^{-1} and 2851cm^{-1}, respectively, and the aromatic stretching mode is at 3054 cm^{-1}.

Recall from [5.2] that the sinc^2 term, and therefore the CARS intensity, is large when $\Delta k \bullet l << \pi/2$. In the case of forward CARS, the CARS signal is large, even for a think material, because Δk is small. In the case of epi-detected CARS, however, Δk is not small. As a result epi-detected CARS generates more signal from thin samples than thick samples. This can be used to enhance the contrast of resonant CARS signal, for example, from a PS bead versus non-resonant CARS signal that is generated in a thicker substrate.

The glass slide on which the PS beads were dispersed generates a considerable amount of non-resonant c-CARS signal in the forward direction. As anticipated, epi-detection was shown to exhibit better rejection of the non-resonant signal for a 3 μm PS bead with a ratio of the on-bead signal to the off-bead signal of 81:1, which is more than seven times better than forward detection (11:1). The corresponding resonant and non-resonant spectra collected by focusing on and off of the PS bead, respectively, are shown in Figure 5.7. The forward c-CARS signal, however, is more than 14 times greater than the epi-detected signal. While the non-resonant rejection of the epi-detected c-CARS signal is significantly better than in forward detection,

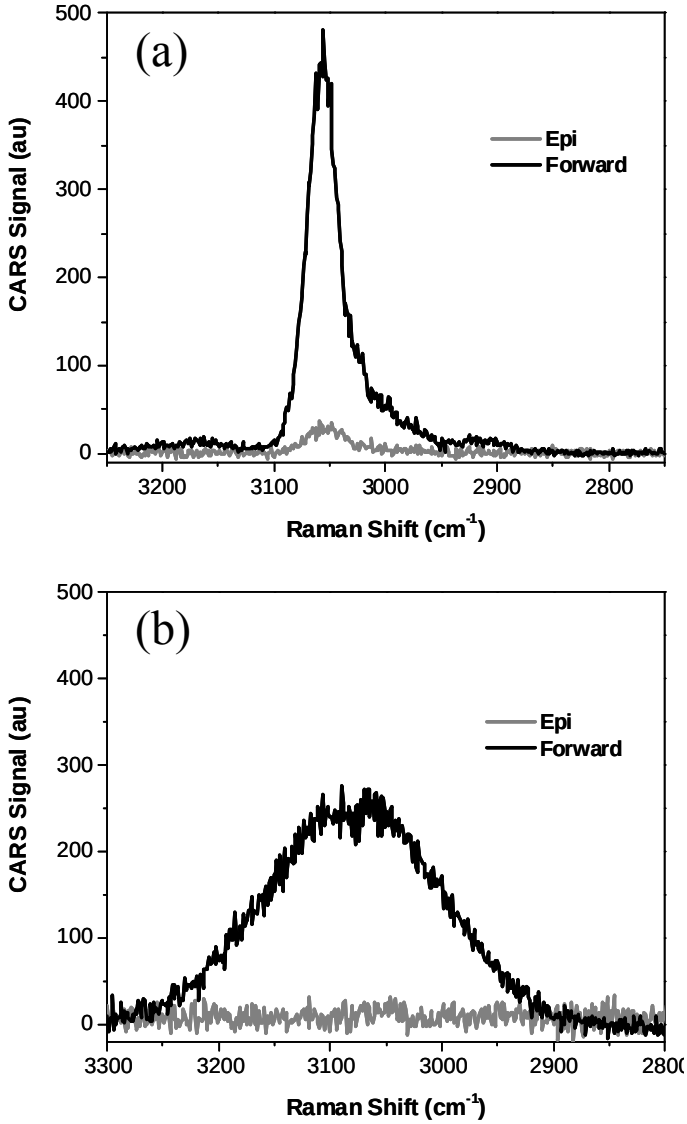

Figure 5.7. Epi-detected and forward-detected on-bead (a) and off-bead (b) c-CARS spectra of a 3 μm polystyrene bead with ω_S tuned to the aromatic C-H vibration. The resonant on-bead spectra were collected for 0.2s, while the non-resonant off-bead spectra were collected for 5s. While the forward-detected resonant signal is much greater than the epi-detected resonant signal, the ratio of resonant to non-resonant signal is greater for epi-detection than for forward-detection.

forward may still be better for systems where there is little non-resonant background and/or for systems where the signal-to-noise ratio is smaller than the resonant to non-resonant signal ratio. Forward and epi-detected images of 6 μm, 3 μm, and 1 μm PS beads are shown in Figure 5.8. For each size of PS bead the forward and epi-detected images are scans of identical regions, so that they are directly comparable. They are also plotted with the same intensity scales, so that the amount of signal from forward and epi-detection can be compared, although in the 3 μm forward detected image many of the on-bead pixels saturated the detection setup. As expected, for all of the PS bead sizes the epi-detected image exhibits a weaker non-resonant background, but the on-bead signal is less than in the forward direction. These images clearly demonstrate the

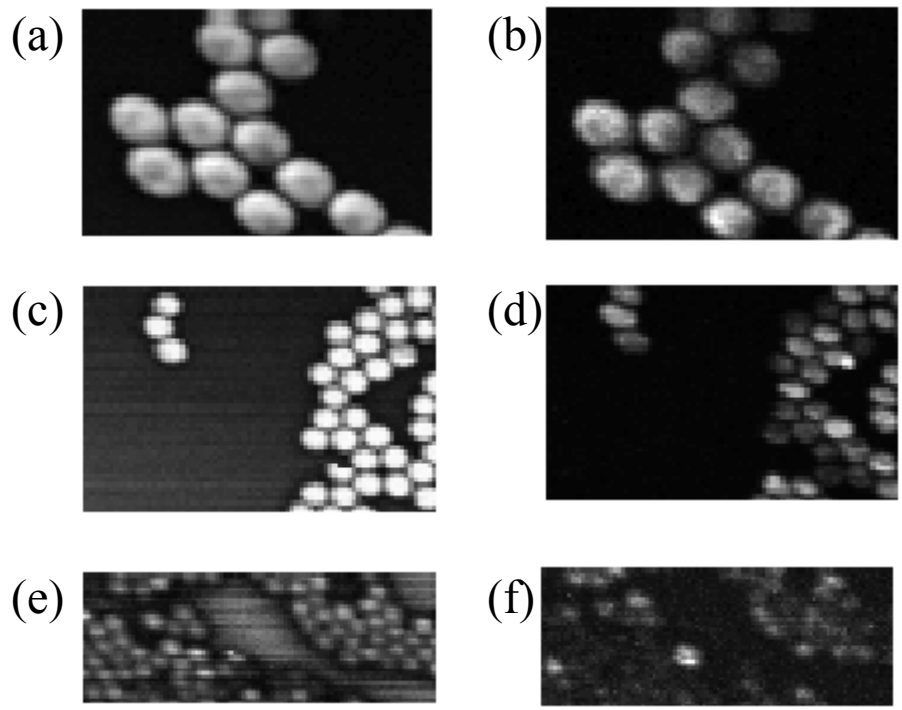

Figure 5.8. C-CARS images of 6 μm (a) and (b), 3 μm (c) and (d), and 1 μm (e) and (f) polystyrene beads in the forward (a), (c), and (e) and epi (b), (d), and (f) directions. The images were acquired with ω_S tuned to the aromatic C-H vibration, as in Figure 5.7. The intensity scales are the same for the forward- and epi-detected images of each size bead (i.e. (a) and (b) are on the same scale, but (a) and (c) are not). The forward detected 3 μm bead image signal saturated the detection setup when focused on the beads.

ability to use c-CARS as an imaging technique, but they do not define the achievable spatial resolution. Also, the number of C-H oscillators probed for these experiments is large, on the order of 10^{12}.

The image in Figure 5.9a shows clearly resolved 480 nm PS beads on a glass slide. This image was acquired by collecting the aromatic C-H signal and has a signal to noise ratio of approximately 11:1. Line scans of this image, Figure 5.9b, show that two adjacent PS beads are resolved using c-CARS. The theoretical lateral resolution was calculated using the method of Cheng et al.[19] to be 350 nm. There is further discussion of the c-CARS spatial resolution in section 5.4.2.

In order to evaluate potential applications, it is necessary to determine a detection limit for c-CARS. For the model system, PS beads on a glass slide, the resonant c-CARS signal must be differentiated from the non-resonant background due to the glass slide. A detection limit was reached for resonant c-CARS spectra acquired by detecting the entire C-H stretching region from a single 100 nm PS bead with a 1 s integration time, and at the same time avoiding any photodamage. A 100 nm PS bead has on the order of 10^7 C-H bonds. This system can act as an estimate of the detection limit for other applications, but the Raman cross section of the resonant transition as well as the non-resonant signal strength may be different in other systems.

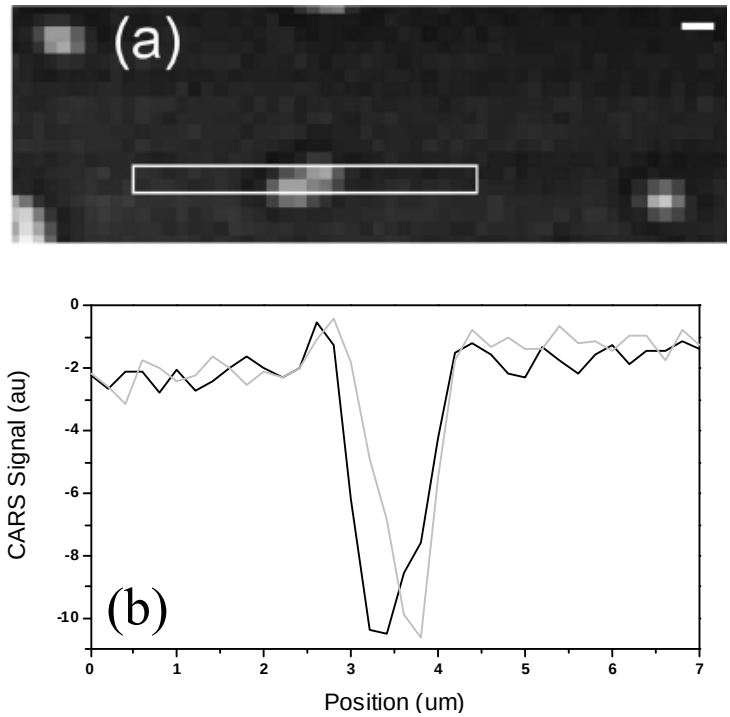

Figure 5.9. C-CARS image of 480 nm polystyrene beads (a). The scale bar is 500 nm. C-CARS line scans (b) of the region in (a) that is outlined in white. The peaks due to two adjacent polystyrene beads are clearly resolved.

5.4.2 Polymer films

Multiplex imaging is demonstrated with c-CARS, using a phase separated polymer film blend of PS and poly(vinyl methyl ether) (PVME). C-CARS lateral spatial resolution approaching the theoretical limit is also shown. Grains of PS (M_n=140,000, M_w=230,000, Sigma-Aldrich) and 50 wt. % PVME toluene solution (SP2 Inc.) were used to prepare thin films (ca. 15 μm thick) of a 1:1 blend from 10 wt. % toluene solutions by drop casting on glass slides. The film was heated in a vacuum oven at 50°C for at least three days. The homogeneous film has a lower critical solution temperature (LCST), and hence the phase separation into PS- and PVME-rich domains was thermally induced by heating at a temperature above the binodal points, 128°C, from 60 s to 240 s corresponding to domain sizes of approximately 0.1 μm to 10 μm.

C-CARS spectra of the PVME- and PS-rich domains of a film that was heated for 240 s are shown in Figure 5.10a (all polymer film images herein are obtained using forward detected c-CARS). The PVME-rich domain spectrum is dominated by the asymmetric aliphatic C-H stretch near 2900 cm^{-1}. The two smaller features are the symmetric C-H stretch near 2850 cm^{-1} and an aromatic C-H stretch near 3050 cm^{-1}, which is due to the small amount of PS in the PVME-rich domain. The PS-rich domain spectrum exhibits the same C-H vibrations, but with different intensities. The aromatic C-H signal and the asymmetric aliphatic C-H signal are of similar intensity and are both more intense than the asymmetric aliphatic C-H signal of the PVME-rich region.

The image in Figure 5.10b is a c-CARS image collecting the aromatic C-H stretching signal of a polymer film, showing a strong contrast between the PS- and PVME-rich regions. The white regions correspond to the aromatic c-CARS signal of the PS-rich domains, and the dark regions correspond to the PVME-rich regions that produce relatively little c-CARS signal in

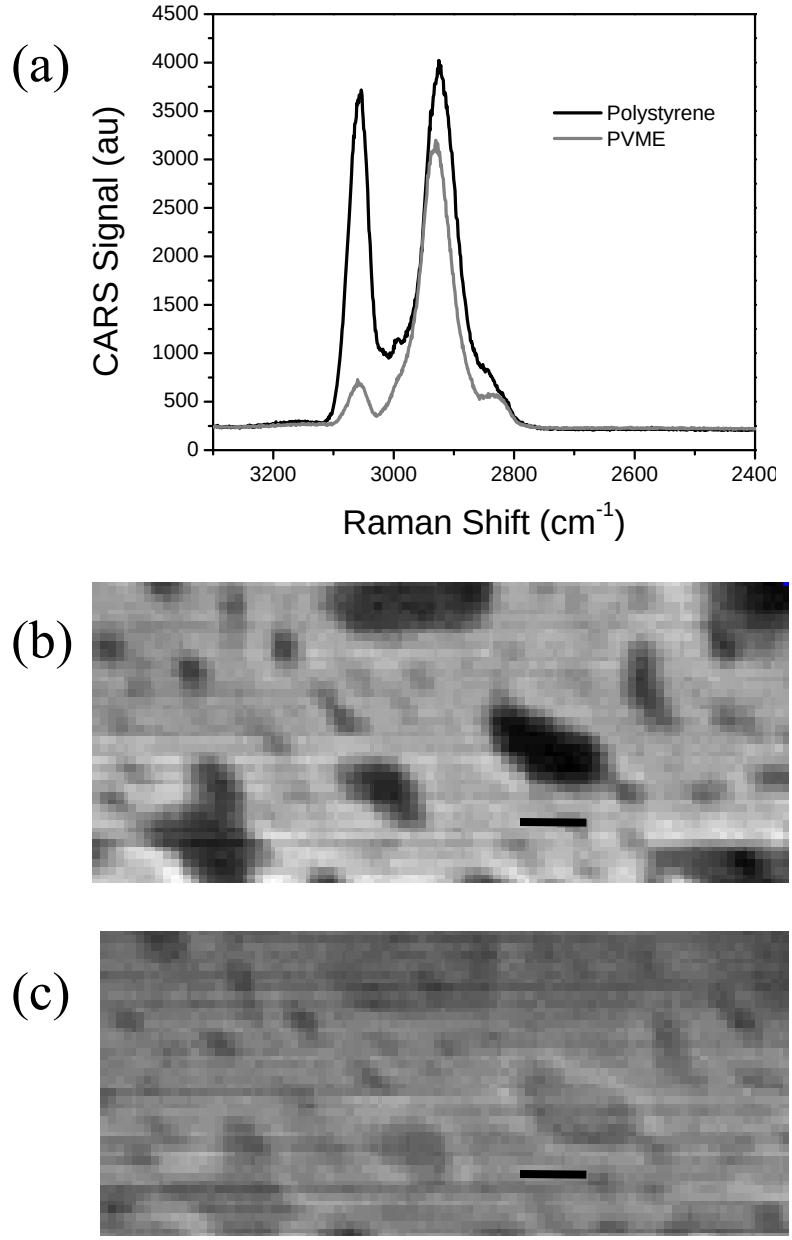

Figure 5.10. C-CARS spectra (a) of PS- and PVME-rich polymer film domains. C-CARS images of the polymer film utilizing the aromatic (b) and aliphatic (c) C-H stretching modes. The scale bars are 3 μm.

the aromatic spectral region. Figure 5.10c is an image of the same polymer film region taken by collecting the asymmetric aliphatic signal. This image shows a much weaker contrast. The PS-rich domains exhibit stronger signal than the PVME-rich domains, but the difference between the two domains is much less significant, since both regions provide a strong aliphatic C-H response. Images of another PS/PVME film that was heated for 240 s are shown in Figure 5.11 a and b. The images are at the edge of the film, as there is no polymer film in the top region that is dark in both images. In this case the PS and PVME have segregated more effectively than in Figures 5.10 b and c. PVME comprises most of the film and the aromatic image correspondingly exhibits little signal over most regions of the film; however, there are a few streaks of higher

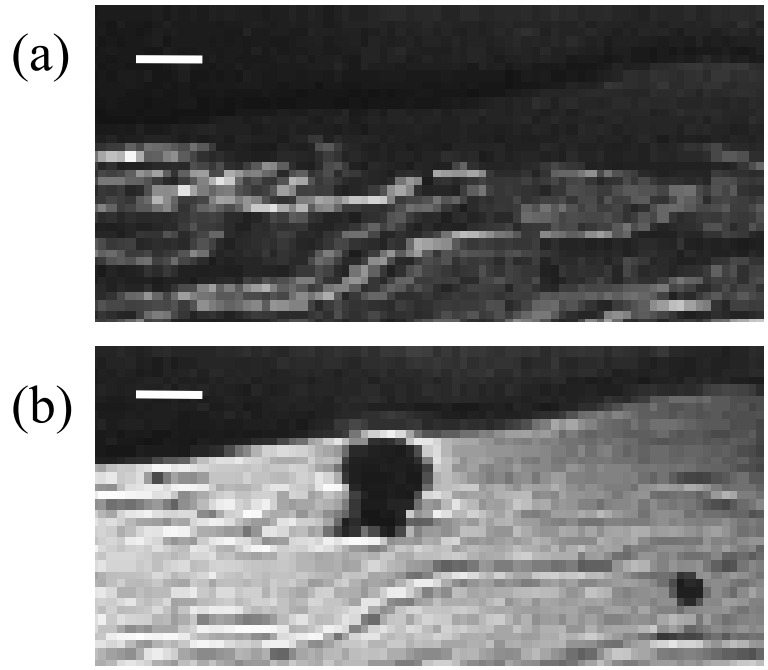

Figure 5.11. C-CARS images of PS- and PVME-rich polymer film domains utilizing the aromatic (a) and aliphatic (b) C-H stretching modes. The scale bars are 3 μm. There is no polymer film in the top region of the film that is dark in both images. The polymer film segregation is more complete when compared to Figure 5.10, as the aromatic image appears as the negative of the aliphatic image. The two dark spots in (b) that are not apparent in (a) are due to photodamage that occurred after the acquisition of (a).

signal that are due to thin strips of PS in the film. The aliphatic image exhibits a strong signal except in the strips of PS, where there was weaker aliphatic c-CARS signal. Also there are two dark spots in the aliphatic image; these are due to photodamage from the laser. These spots are not present in the aromatic image, since it was acquired first. The photodamage must have occurred either during the acquisition of the aromatic image or in between image acquisitions, which is more likely since there is no evidence of the photodamage in the aromatic image.

Figures 5.12 a and b show an aromatic C-H stretching region image and line scan, respectively, of a PS/PVME polymer film that was heated for 60 s. The error bars in the line scan represent the noise in the c-CARS signal of a PVME-rich domain of Figure 5.10b, which was acquired less than an hour earlier, and are an estimation of the noise level. Since pixel-to-pixel signal variations are often much greater than the error bars, it is clear that there are pixel-to-pixel signal variations due to the domain structures of the polymer films. Since the pixels are 220 nm, this demonstrates that the achieved c-CARS spatial resolution is consistent with the calculated resolution.

5.4.3 Other studies and future work

Interstellar dust particles: This project was a collaboration with Andrew Westphal (Space Sciences Laboratory, UC Berkeley) and the NASA STARDUST mission that collected interstellar and cometary dust particles (IDPs). The goal of this project was to search for and identify organic material using c-CARS in the returned IDPs. To evaluate c-CARS viability for

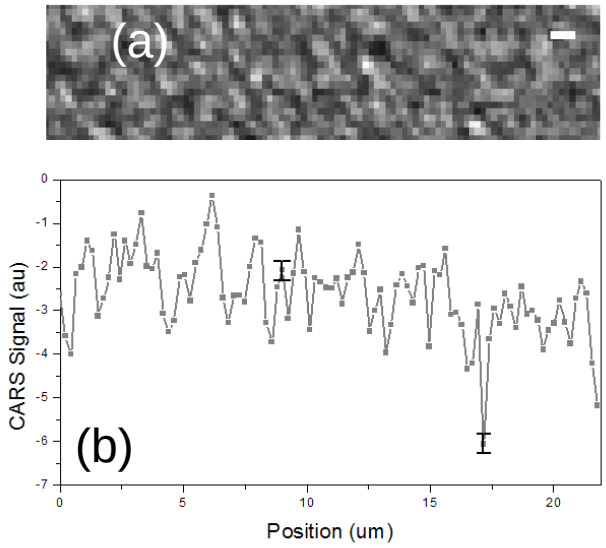

Figure 5.12. C-CARS image of PS- and PVME-rich polymer film domains (a) utilizing the aromatic C-H stretching region. Pixel size is 220 nm. The scale par is 1 μm. A representative line scan (b) of the c-CARS signal intensity. The error bars in the line scan represent the noise in the c-CARS signal of a PVME-rich domain of Figure 5.10b, which was acquired less than an hour earlier, and are an estimation of the noise level.

this application, Orgeuil particles, particles from a meteorite that fell in southern France in 1864, were used as a test sample. No resonant c-CARS spectra were acquired looking in both the C-H stretching region and the fingerprint region over a range of input powers. The most likely explanation is that there was too little material with vibrational frequencies in these regions. Sample damage was observed in many cases with incident powers of tens of μW.

Carbonaceous materials: Soot was collected on glass slides by burning various hydrocarbons. No c-CARS signal was detected. Again, this was most likely due to an inadequate amount of sample in the laser focus. The goal of these experiments was to determine whether c-CARS could be used to chemically image particulate matter. Carbon nanotubes were used as a test sample because they are robust carbonaceous samples. Raman shifts of the C=C, C-C, and C-H regions were investigated, but no resonant c-CARS spectra were acquired.

Biofilms: C-CARS and third-harmonic imaging: This project was a collaboration with Paul Wilmes and Jill Banfield (Department of Earth and Planetary Science, UC Berkeley). Biofilms were collected from an acid mine drainage site. The original goal was to search for variation in the make-up of the lipids in the different regions of the biofilm. Some images were acquired probing in the region between 1400 and 1500 cm^{-1}, and there was significant contrast. However, the contrast in the images did not correlate with the different regions within the biofilm.

A secondary project with the biofilms was to attempt third-harmonic generation (THG) imaging to determine the distribution of Fe(II) and Fe(III) in the biofilms. Fluorescently labeled PS beads were used as a test sample. The beads were designed to be excited at 441 nm and fluoresce at 486 nm. 1320 nm light was used for imaging the beads; therefore the THG was three-photon resonant. Imaging of the fluorescent beads was successful, see Figure 5.13, but the

spatial resolution is only 800 nm, significantly worse than c-CARS. This is not surprising, since the incident light is a longer wavelength. Additionally, since the objectives were not designed to transmit such long wavelengths, there is likely additional aberration. When applied to the biofilms, however, there was no contrast between the different regions.

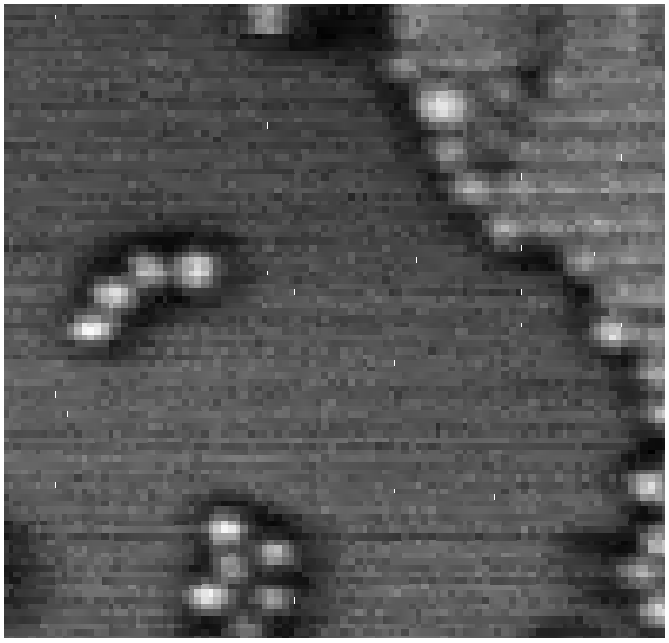

Figure 5.13. THG image of 1 μm fluorescent PS beads. The incident light was 1320 nm. The scale bar is 1 μm.

Outlook and future experiments: If the c-CARS imaging project is resumed, one potential project would be following up on the work of Justin Johnson (THESIS-unpublished) on spatially locating Photosystems I and II (PSI and PSII) in chloroplasts. He used the Soret bands to differentiate between the two structures via THG detected by near-field scanning optical microscopy. Segregation of PSI and PSII in different cellular structures was observed, but the chloroplast had to be opened to image with the near-field probe, and the results were not repeatable. Using CARS would be an improvement because it would allow a longer working distance. Additionally, this project may be more viable than the previously attempted c-CARS applications since it could be done as a doubly resonant experiment, using the Soret bands and C-H vibrations as the resonances.

Proof-of-principle experiments have demonstrated the multiplex chemically-selective imaging ability of c-CARS as well as the ability of this technique to achieve high spatial resolution. While a number of multiplex CARS techniques have demonstrated imaging on relatively simple systems, to our knowledge, there has yet to be a multiplex CARS study on a more complicated system wherein the sample is not composed primarily of the probed endogenous chromophore. The difficulty in multiplex CARS imaging arises from the balance between the decreased signal-to-noise ratio relative to single frequency CARS and remaining below the sample damage threshold. The CARS intensity is proportional to the Stokes pulse intensity, and since multiplex CARS disperses the usable pulse intensity over a broad range of frequencies, there is a decrease in the signal to noise ratio at each frequency for multiplex CARS

relative to single frequency CARS at a given Stokes intensity. The intensity at each frequency could be increased by an overall increase in the Stokes pulse intensity, but this can lead to significant photodamage of the sample. Fu et al.[20] provide a detailed account of CARS photodamage using picosecond lasers. The mechanisms of photodamage for multiplex CARS differ due to the use of femtosecond pulses,[21] and a thorough discussion of pulsed laser photodamage can be found in the context of nanosurgery of cells and tissues.[22] The challenge of multiplex CARS remains that of achieving a sufficiently high signal-to-noise ratio while the intensity of the incident pulses remains below the damage threshold.

5.5 References

1. J. X. Cheng and X. S. Xie, "Coherent anti-Stokes Raman scattering microscopy: Instrumentation, theory, and applications." *Journal of Physical Chemistry B.* **108**, 827-840, (2004).
2. A. Volkmer, "Vibrational imaging and microspectroscopies based on coherent anti-Stokes Raman scattering microscopy." *Journal of Physics D-Applied Physics.* **38**, R59-R81, (2005).
3. M. Muller and A. Zumbusch, "Coherent anti-stokes Raman scattering microscopy." *Chemphyschem.* **8**, 2157-2170, (2007).
4. C. L. Evans and X. S. Xie, "Coherent Anti-Stokes Raman Scattering Microscopy: Chemical Imaging for Biology and Medicine." *Annual Review of Analytical Chemistry.* **1**, 883-909, (2008).
5. S. Mukamel *Principles of nonlinear optical spectroscopy*; Oxford University Press: New York, 1995.
6. J. X. Cheng, A. Volkmer, L. D. Book and X. S. Xie, "An epi-detected coherent anti-Stokes Raman scattering (E-CARS) microscope with high spectral resolution and high sensitivity." *Journal of Physical Chemistry B.* **105**, 1277-1280, (2001).
7. J. J. Song, G. L. Eesley and M. D. Levenson, "Background Suppression in Coherent Raman-Spectroscopy." *Applied Physics Letters.* **29**, 567-569, (1976).
8. J. X. Cheng, L. D. Book and X. S. Xie, "Polarization coherent anti-Stokes Raman scattering microscopy." *Optics Letters.* **26**, 1341-1343, (2001).
9. C. Vinegoni, J. S. Bredfeldt, D. L. Marks and S. A. Boppart, "Nonlinear optical contrast enhancement for optical coherence tomography." *Optics Express.* **12**, 331-341, (2004).
10. S. H. Lim, A. G. Caster and S. R. Leone, "Single-pulse phase-control interferometric coherent anti-Stokes Raman scattering spectroscopy." *Physical Review A.* **72**, (2005).
11. E. O. Potma, C. L. Evans and X. S. Xie, "Heterodyne coherent anti-Stokes Raman scattering (CARS) imaging." *Optics Letters.* **31**, 241-243, (2006).
12. T. W. Kee, H. X. Zhao and M. T. Cicerone, "One-laser interferometric broadband coherent anti-Stokes Raman scattering." *Optics Express.* **14**, 3631-3640, (2006).
13. M. Muller and J. M. Schins, "Imaging the thermodynamic state of lipid membranes with multiplex CARS microscopy." *Journal of Physical Chemistry B.* **106**, 3715-3723, (2002).
14. T. W. Kee and M. T. Cicerone, "Simple approach to one-laser, broadband coherent anti-Stokes Raman scattering microscopy." *Optics Letters.* **29**, 2701-2703, (2004).
15. D. Oron, N. Dudovich, D. Yelin and Y. Silberberg, "Narrow-band coherent anti-stokes Raman signals from broad-band pulses." *Physical Review Letters.* **88**, (2002).
16. K. P. Knutsen, J. C. Johnson, A. E. Miller, P. B. Petersen and R. J. Saykally, "High spectral resolution multiplex CARS spectroscopy using chirped pulses." *Chemical Physics Letters.* **387**, 436-441, (2004).
17. K. P. Knutsen, B. M. Messer, R. M. Onorato and R. J. Saykally, "Chirped coherent anti-Stokes Raman scattering for high spectral resolution spectroscopy and chemically selective imaging." *Journal of Physical Chemistry B.* **110**, 5854-5864, (2006).
18. S. M. George, H. Auweter and C. B. Harris, "Inhomogeneous Broadening of Vibrational Linewidths in Polyatomic Liquids." *Journal of Chemical Physics.* **73**, 5573-5583, (1980).

19. J. X. Cheng, A. Volkmer and X. S. Xie, "Theoretical and experimental characterization of coherent anti-Stokes Raman scattering microscopy." *Journal of the Optical Society of America B-Optical Physics.* **19**, 1363-1375, (2002).
20. Y. Fu, H. F. Wang, R. Y. Shi and J. X. Cheng, "Characterization of photodamage in coherent anti-Stokes Raman scattering microscopy." *Optics Express.* **14**, 3942-3951, (2006).
21. H. J. Koester, D. Baur, R. Uhl and S. W. Hell, "Ca2+ fluorescence imaging with pico- and femtosecond two-photon excitation: Signal and photodamage." *Biophysical Journal.* **77**, 2226-2236, (1999).
22. A. Vogel, J. Noack, G. Huttman and G. Paltauf, "Mechanisms of femtosecond laser nanosurgery of cells and tissues." *Applied Physics B-Lasers and Optics.* **81**, 1015-1047, (2005).

Chapter 6

Nonlinear optical studies of $KNbO_3$ nanowires

6.1 Introduction

Semiconductor devices are ubiquitous in today's technology. Integrated circuits, diode lasers, light-emitting diodes, and solar cells, among many other examples are based on semiconductor technology. As the ability to synthesize and control the growth of semiconductor nanostructures has and continues to advance, current and future technologies capitalize on the uniquely powerful electrical and optical properties of nano-sized semiconductors. Due to the effects of quantum confinement, semiconductor nanostructures behave differently than their bulk counterparts, and designing nanostructures of specific compositions, sizes, and shapes provides control over their electronic properties. This is being exploited in order to build cheaper and more efficient devices.

Many devices have been designed using nanowires as the building blocks, including light-emitting diodes,[1] photodetectors,[2] as have several techniques for their integration.[3-8] One missing element of this growing field is a nano-scale source of tunable coherent light. It has been shown that single nanowires can be used as frequency converters via second harmonic generation (SHG).[9] Additionally, nanowires can be used as waveguides[10, 11] and as a gain medium for lasing with the end facets forming the optical cavity.[12-15, 8] Considering these characteristics, it is a reasonable hypothesis that a nanowire could be used as a medium for optical parametric oscillation (OPO), wherein a single pump frequency is converted into two lower frequencies: $\omega_p = \omega_{signal} + \omega_{idler}$. This requires a cavity and a nonlinear crystal. In this case the end facets of the nanowire would comprise the cavity. The frequencies of the signal and idler frequencies could potentially be controlled by changing the temperature and/or orientation of the nanowire. In this chapter individual $KNbO_3$ nanowires are employed as an efficient medium for frequency conversion via SHG and sum frequency generation (SFG), and identified as a promising material for optical parametric light conversion from a single nanowire.

6.2 Experimental design

Femtosecond pulses are generated in a home-built Ti:sapphire oscillator, which seeds a regenerative amplifier (Spectra Physics, Spitfire). The amplified output is divided with a beamsplitter. The post-amplifier experimental setup is shown in Figure 6.1. Approximately 95% is used to pump an optical parametric amplifier (Light Conversion, TOPAS), providing tunable infrared light, which is doubled with a BBO crystal. The remaining 5% bypasses the OPA and can be temporally and spatially overlapped with the other pulse for SFG experiments. Either beam path can be used without the other for SHG experiments. The polarization of the pulses can be controlled with a half-wave plate. The pulses are focused onto the nanowire by an objective and collected by a matched objective. The nanowire position is controlled with a nano-positioning stage (Physik Instrumente, P527 multi-axis piezo scanner). The signal is dispersed by a spectrograph (Acton Research, SpectraPro 300i) and spectra are collected with a CCD (Roper Scientific, Spec10B-LN2).

6.3 Results

We chose the perovskite oxide $KNbO_3$ as the nanowire material because of its low toxicity, chemical stability, large effective nonlinear optical coefficients (d_{eff} = 10.8– 27 pm/V at

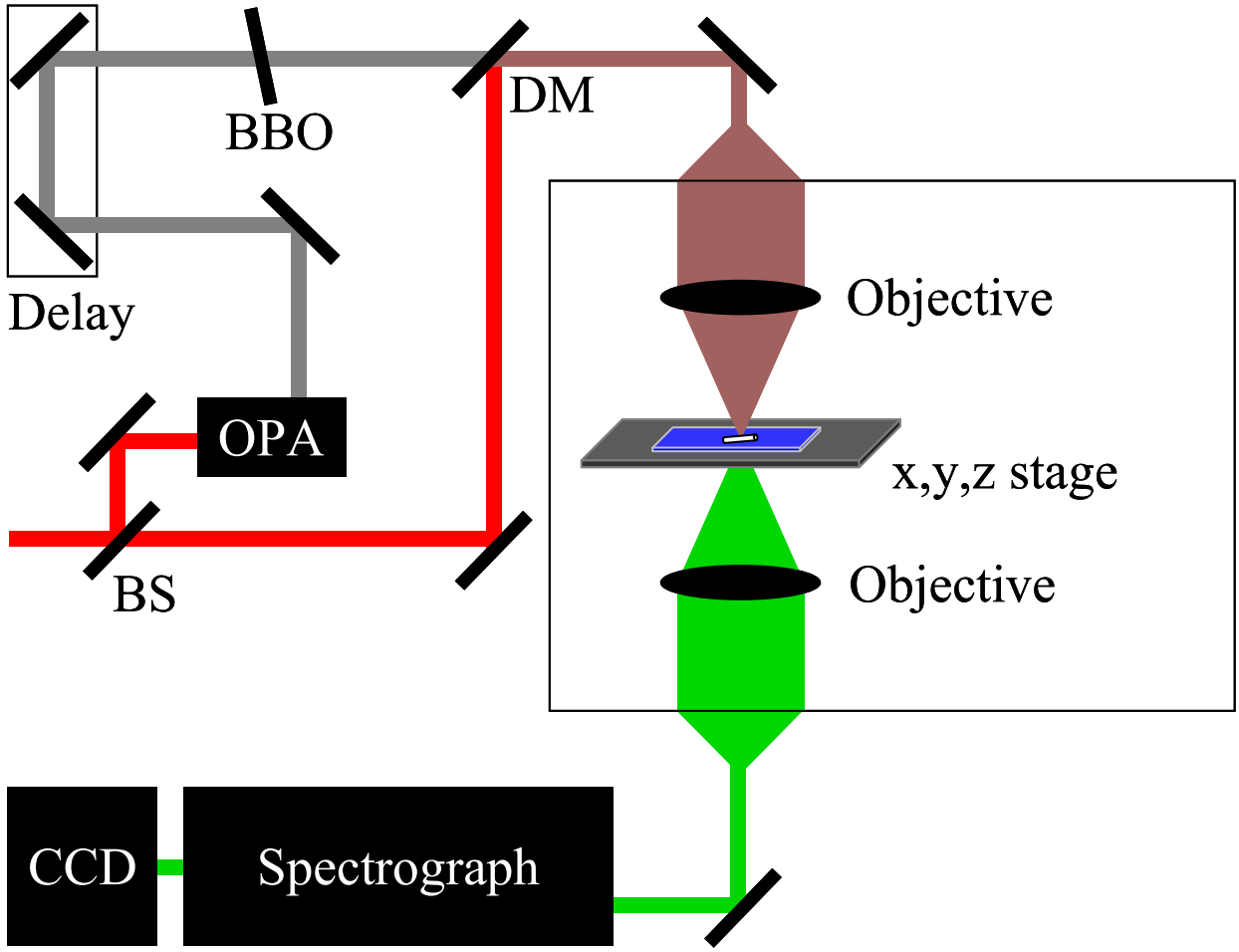

Figure 6.1. The experimental setup. 800 nm, 100 fs pulses are split with a beam-splitter (BS). 95% is used to pump the OPA. The OPA output is doubled by passing through a BBO crystal, and the temporal overlap between the doubled OPA output and the 800 nm pulses is controlled with a delay stage. The overlapped pulses are focused onto the nanowire and collected by matched objectives, and the wave-mixed light is directed to a spectrograph and a CCD detector.

λ = 1064 nm) at room temperature (298 K),[16] large refractive indices (n = 2.1–2.5),[17] as well as its transparency in a wide range of wavelengths including the visible spectral region.[18] Single-crystalline $KNbO_3$ nanowires were synthesized using a hydrothermal method,[19] and characterized as orthorhombic phase (Amm2) with the growth axis parallel to the [011] direction (see Figure 6.2 a–e). The polar c-axis[20] is therefore 45° off the nanowire growth axis.

The SHG response of single $KNbO_3$ nanowires were first characterized using femtosecond pulses and compared with measurements of ZnO nanowires, which have been studied previously.[10] The nanowires were supported on amorphous silica cover slips and aligned such that the growth axis was orthogonal to the pump beam. The maximum SHG signals for both $KNbO_3$ and ZnO nanowires (λ = 502 nm) are shown in Figure 6.3, generated by introducing the fundamental beam (λ = 1,004 nm, 18 kW/cm^2). A direct comparison of the SHG signal collected from single $KNbO_3$ and ZnO nanowires is complicated by the anisotropic scattering related to

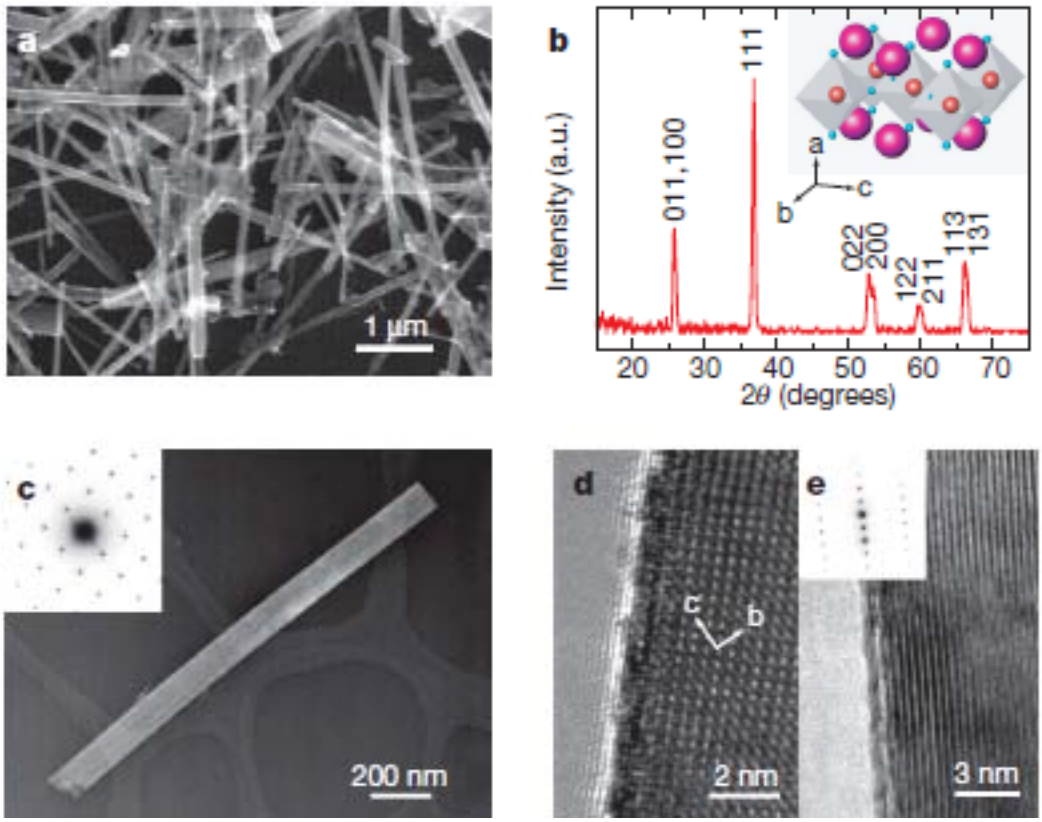

Figure 6.2. (a) Scanning electron micrsoscopy image of $KNbO_3$ nanowires. (b) X-ray powder diffraction pattern of $KNbO_3$ nanowires. The inset shows the unit cell structure of the material. The spontaneous polarization is parallel to the c-axis. (c) TEM image of a single $KNbO_3$ nanowire. The inset shows its electron diffraction pattern with [100] zone axis and [011] growth direction. (d) and (e) High resolution TEM images of single [011] growth direction nanowires. The inset in (e) is the electron diffraction pattern with the zone axis of [100].

their respective rectangular and hexagonal cross-sections. However, a rough estimate for the d_{eff} of KNbO3 nanowires based on the relative ratio of integrated signals is possible and we found it to be 9.1 pm/V. This illustrates that the nonlinear polarizability of $KNbO_3$ nanowires is larger than that for ZnO, 5.5 pm/V,[10] as expected from the consideration of bulk values.

The second key requirement for a versatile nonlinear circuit element for use in nano-photonics is wave mixing, specifically sum frequency generation (SFG) ($\omega_3 = \omega_1 + \omega_2$) and difference frequency generation ($\omega_3 = |\omega_1 - \omega_2|$). Figure 6.4 shows SFG signals (λ = 423 nm, 454 nm) and SHG signals (λ = 525 nm, 700 nm), obtained from a single $KNbO_3$ nanowire by introducing fundamental beams at a variety of different frequencies via the tunable femtosecond pump. This demonstrates the ability of nanowire frequency converters to create four different waves from two fundamental input frequencies ω_1 and ω_2: $2\omega_1$, $2\omega_2$, and $|\omega_1 \pm \omega_2|$. We did not observe the difference frequency generation signal corresponding to the SFG at 423 nm here because the expected wavelength (λ = 7200 nm) is outside current instrumental limits. The SHG signal at 400 nm was weak, owing to photoabsorption within the nanowire. This set of experiments demonstrates the ability of $KNbO_3$ nanowires to generate continuously tunable and coherent light throughout the visible spectrum via nonlinear wave mixing.

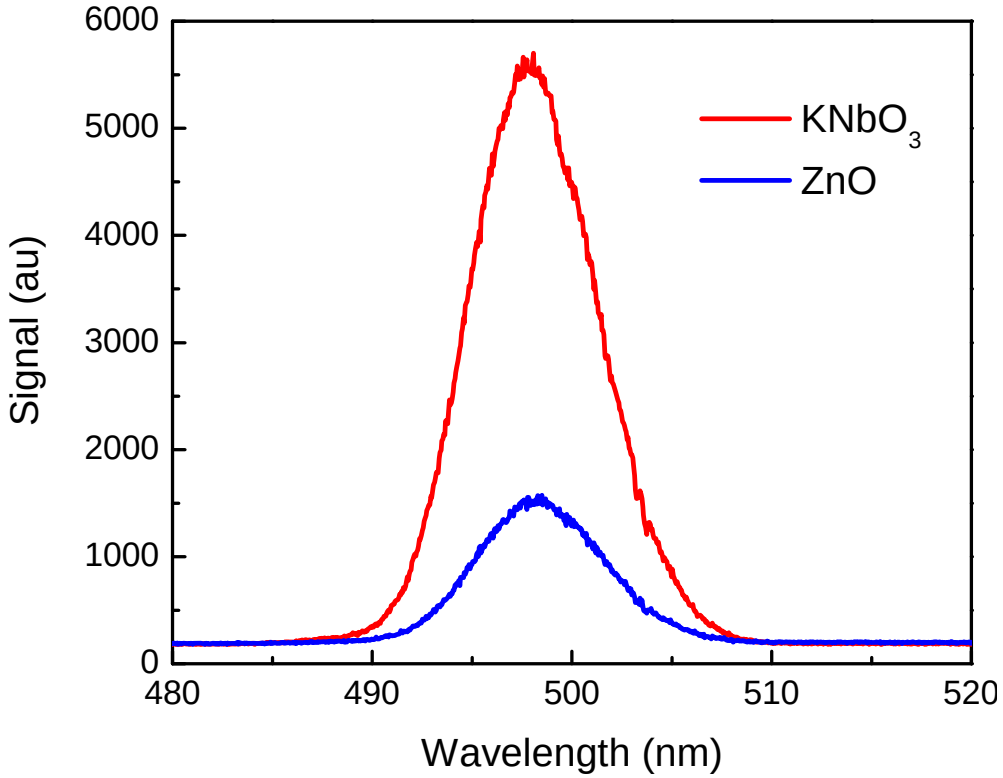

Figure 6.3. Polarization maximum SHG spectra of single $KNbO_3$ and ZnO nanowires indicating the larger nonlinear polarizability of $KNbO_3$.

$KNbO_3$ nanowires were then used as the key component to a novel sub-wavelength optical probe technique.[21] An individual nanowire was optically trapped using 1064 nm continuous wave light. Green light at 532 nm was generated via SHG in the nanowire, and the green light was emitted from the ends of the nanowire. The nanowire was then scanned across 200 nm wide gold stripes on a cover-slip, while the green light was detected in transmission mode. This technique successfully mapped out the gold stripes with spacing increments down to 200 nm below the diffraction limit of 532 nm light.

6.4 Future outlook

Given the success and strength of the different wave mixing processes in $KNbO_3$ nanowires, it was hypothesized that it is a strong candidate for observing OPO in a single nanowire. Attempts were made to find appropriate conditions for OPO, but no OPO was observed. Using OPO curves from Biaggio et al.[20] as a rough guide, wavelengths between 400 nm and 450 nm were used as a pump to induce OPO. Numerous orientations of multiple individual nanowires were used, rotating the nanowire in three dimensions to try to find the appropriate phase matching conditions, but there were no positive results.

If this collaboration is resumed, two adjustments to the nanowire preparation may prove useful. The nanowires as prepared here were sonicated to break off individual nanowires from a larger crystal, which in most cases left an end facet that was rough (see Figure 6.2c). Manually breaking the end of a single nanowire to make a cleaner break would improve the quality of the cavity comprising the nanowire. Another possible aid would be to minimize the nanowire contact with the substrate. This may decrease losses within the cavity[12] and increase the probability of

observing OPO. Contact with the substrate can be minimized can be done by propping the nanowire up on one or two other nanowires. A continued effort to induce OPO in a single nanowire world seem to merit further efforts.

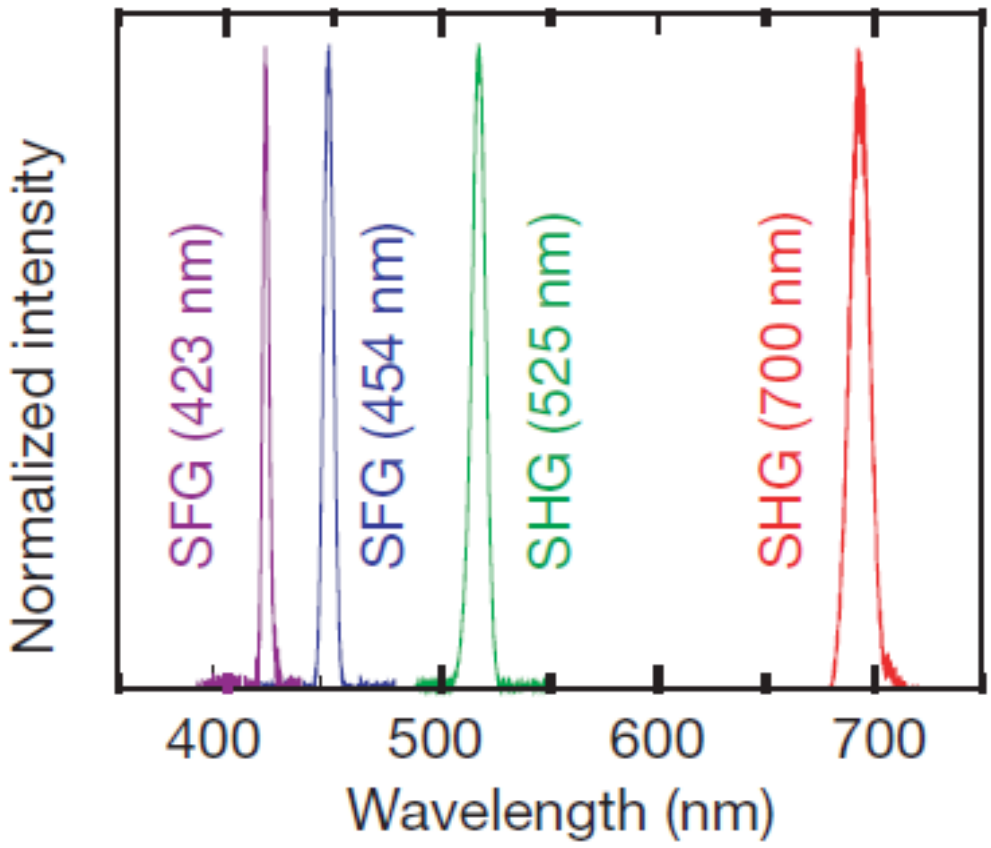

Figure 6.4. Wavelengths spanning the visible spectrum generated via second-order wave-mixing within single $KNbO_3$ nanowires.

6.5 References

1. E. L. Florin, A. Pralle, J. K. H. Horber and E. H. K. Stelzer, "Photonic force microscope based on optical tweezers and two-photon excitation for biological applications." *Journal of Structural Biology.* **119**, 202-211, (1997).
2. D. J. Sirbuly, M. Law, H. Q. Yan and P. D. Yang, "Semiconductor nanowires for subwavelength photonics integration." *Journal of Physical Chemistry B.* **109**, 15190-15213, (2005).
3. Y. Huang, X. F. Duan, Q. Q. Wei and C. M. Lieber, "Directed assembly of one-dimensional nanostructures into functional networks." *Science.* **291**, 630-633, (2001).
4. X. F. Duan, Y. Huang, R. Agarwal and C. M. Lieber, "Single-nanowire electrically driven lasers." *Nature.* **421**, 241-245, (2003).
5. J. C. Johnson, H. Q. Yan, P. D. Yang and R. J. Saykally, "Optical cavity effects in ZnO nanowire lasers and waveguides." *Journal of Physical Chemistry B.* **107**, 8816-8828, (2003).
6. F. Qian, Y. Li, S. Gradecak, D. L. Wang, C. J. Barrelet and C. M. Lieber, "Gallium nitride-based nanowire radial heterostructures for nanophotonics." *Nano Letters.* **4**, 1975-1979, (2004).
7. M. Law, L. E. Greene, J. C. Johnson, R. Saykally and P. D. Yang, "Nanowire dye-sensitized solar cells." *Nature Materials.* **4**, 455-459, (2005).
8. P. J. Pauzauskie, D. J. Sirbuly and P. D. Yang, "Semiconductor nanowire ring resonator laser." *Physical Review Letters.* **96**, (2006).
9. J. C. Johnson, K. P. Knutsen, H. Q. Yan, M. Law, Y. F. Zhang, P. D. Yang and R. J. Saykally, "Ultrafast carrier dynamics in single ZnO nanowire and nanoribbon lasers." *Nano Letters.* **4**, 197-204, (2004).
10. J. C. Johnson, H. Q. Yan, R. D. Schaller, P. B. Petersen, P. D. Yang and R. J. Saykally, "Near-field imaging of nonlinear optical mixing in single zinc oxide nanowires." *Nano Letters.* **2**, 279-283, (2002).
11. M. Law, D. J. Sirbuly, J. C. Johnson, J. Goldberger, R. J. Saykally and P. D. Yang, "Nanoribbon waveguides for subwavelength photonics integration." *Science.* **305**, 1269-1273, (2004).
12. J. C. Johnson, H. Q. Yan, R. D. Schaller, L. H. Haber, R. J. Saykally and P. D. Yang, "Single nanowire lasers." *Journal of Physical Chemistry B.* **105**, 11387-11390, (2001).
13. J. C. Johnson, H. J. Choi, K. P. Knutsen, R. D. Schaller, P. D. Yang and R. J. Saykally, "Single gallium nitride nanowire lasers." *Nature Materials.* **1**, 106-110, (2002).
14. H. J. Choi, J. C. Johnson, R. R. He, S. K. Lee, F. Kim, P. Pauzauskie, J. Goldberger, R. J. Saykally and P. D. Yang, "Self-organized GaN quantum wire UV lasers." *Journal of Physical Chemistry B.* **107**, 8721-8725, (2003).
15. P. D. Yang, "The chemistry and physics of semiconductor nanowires." *Materials Research Society Bulletin.* **30**, 85-91, (2005).
16. I. Shoji, T. Kondo, A. Kitamoto, M. Shirane and R. Ito, "Absolute scale of second-order nonlinear-optical coefficients." *Journal of the Optical Society of America B-Optical Physics.* **14**, 2268-2294, (1997).
17. B. Zysset, I. Biaggio and P. Gunter, "Refractive-Indexes of Orthorhombic Knbo3 .1. Dispersion and Temperature-Dependence." *Journal of the Optical Society of America B-Optical Physics.* **9**, 380-386, (1992).

18. K. Kudo, K. Kakiuchi, K. Mizutani and T. Fukami, "Characterization of KNbO3 crystal by traveling solvent floating zone (TSFZ) method." *Japanese Journal of Applied Physics Part 1-Regular Papers Short Notes & Review Papers.* **42**, 6099-6101, (2003).
19. A. Magrez, E. Vasco, J. W. Seo, C. Dieker, N. Setter and L. Forro, "Growth of single-crystalline KNBO3 nanostructures." *Journal of Physical Chemistry B.* **110**, 58-61, (2006).
20. I. Biaggio, P. Kerkoc, L. S. Wu, P. Gunter and B. Zysset, "Refractive-Indexes of Orthorhombic Knbo3 .2. Phase-Matching Configurations for Nonlinear-Optical Interactions." *Journal of the Optical Society of America B-Optical Physics.* **9**, 507-517, (1992).
21. Y. Nakayama, P. J. Pauzauskie, A. Radenovic, R. M. Onorato, R. J. Saykally, J. Liphardt and P. D. Yang, "Tunable nanowire nonlinear optical probe." *Nature.* **447**, 1098-U8, (2007).